1981

Single-crystal polarized electronic spectra of the compounds tetra-[Greek letter mu]-acetatodimolybdenum(II), tetrakis-[Greek letter mu]-(trifluoroacetato)-dimolybdenum(II), potassium-diaquo-tetra-[Greek letter mu]-sulfatodiplatinum(III), and the X-ray diffraction crystal structure of tetra-[Greek letter mu]-acetatodimolybdenum(II)Â·potassium chloride

Robert Alan Newman
Iowa State University

Newman, Robert Alan

SINGLE-CRYSTAL POLARIZED ELECTRONIC SPECTRA OF THE COMPOUNDS TETRA - MU - ACETATODIMOLYBDENUM(II), TETRAKIS - MU - (TRIFLUOROACETATO)DIMOLYBDENUM(II), POTASSIUM - DIAQUO - TETRA - MU - SULFATODIPLATINUM(III), AND THE X-RAY DIFFRACTION CRYSTAL STRUCTURE OF TETRA - MU - ACETATODIMOLYBDENUM(II).POTASSIUM CHLORIDE

Iowa State University PH.D. 1981

PLEASE NOTE:

In all cases this material has been filmed in the best possible way from the available copy. Problems encountered with this document have been identified here with a check mark __✓__.

1. Glossy photographs or pages _____
2. Colored illustrations, paper or print _____
3. Photographs with dark background _____
4. Illustrations are poor copy _____
5. Pages with black marks, not original copy _____
6. Print shows through as there is text on both sides of page _____
7. Indistinct, broken or small print on several pages __✓__
8. Print exceeds margin requirements _____
9. Tightly bound copy with print lost in spine _____
10. Computer printout pages with indistinct print __✓__
11. Page(s) _____ lacking when material received, and not available from school or author.
12. Page(s) _____ seem to be missing in numbering only as text follows.
13. Two pages numbered _____. Text follows.
14. Curling and wrinkled pages _____
15. Other _____

Single-crystal polarized electronic spectra of the compounds tetra-μ-acetatodimolybdenum(II), tetrakis-μ-(trifluoroacetato)-dimolybdenum(II), potassium-diaquo-tetra-μ-sulfatodiplatinum(III), and the X-ray diffraction crystal structure of tetra-μ-acetatodimolybdenum(II)·potassium chloride

by

Robert Alan Newman

A Dissertation Submitted to the
Graduate Faculty in Partial Fulfillment of the
Requirements for the Degree of
DOCTOR OF PHILOSOPHY

Department: Chemistry
Major: Inorganic Chemistry

Approved:

Signature was redacted for privacy.

In Charge of Major Work

Signature was redacted for privacy.

For the Major Department

Signature was redacted for privacy.

For the Graduate College

Members of the Committee:

Signature was redacted for privacy.

Iowa State University
Ames, Iowa

1981

TABLE OF CONTENTS

LIST OF TABLES

ABSTRACT

The polarized absorption spectra for the compounds tetra-μ-acetato-dimolybdenum(II),[1] tetrakis-μ-(trifluoroacetato)dimolybdenum(II),[2] and potassium-diaquo-tetra-μ-sulfatodiplatinum(III)[3] have been recorded at both room temperature and 6K. X-ray diffraction data were collected for the compound tetra-μ-acetatodimolybdenum(II)·potassium chloride[4] on the Ames Laboratory automated four-circle diffractometer, and the structural data were refined by utilizing standard programs written for that purpose.

The study of $Mo_2(O_2CCH_3)_4$ was greatly enhanced by our ability to examine two distinct crystallographic faces of the compound via solid-state spectroscopy. Analysis of the spectra resulted in a definite assignment for the lowest energy absorption maximum at 6K, even though the observed maximum to minimum ratio deviated considerably from the values predicted in the case of ideal D_{4h} symmetry for the $Mo_2(O_2CCH_3)_4$ molecule. The ability to record spectra for two crystal faces of the compound enabled the determination of the spatial orientation of the transition moment, with respect to the molecular axes, for the lowest energy transition. It was found that the transition moment, represented by a vector, pointed at an angle $\sim 34^{\circ}$ away from the Mo-Mo, or molecular $\underset{\sim}{z}$-axis. This led to the definite assignment of the transition at 21,700 cm^{-1} in the 6K

---

[1] $Mo_2(O_2CCH_3)_4$.

[2] $Mo_2(O_2CCF_3)_4$.

[3] $K_2[Pt_2(SO_4)_4 \cdot 2H_2O]$.

[4] $Mo_2(O_2CCH_3)_4 \cdot KCl$.

spectra of $Mo_2(O_2CCH_3)_4$ as the $\delta \rightarrow \delta^*$, $^1A_{1g} \rightarrow {}^1A_{2u}$, $\underset{\sim}{z}$-polarized, electric-dipole allowed transition. The remaining vibrational details in the low energy band are assigned as dipole forbidden, vibronically excited transitions based on this dipole allowed origin. The observed energy separation of 375 cm^{-1} for the three most intense Franck-Condon progressions is assigned to the $^1A_{1g}$ metal-metal stretching vibration of the electronic excited state, reduced in energy as expected from the value of 406 cm^{-1} determined for the ground state by Raman spectroscopy. The band observed at ~26,500 cm^{-1} is assigned as the $\delta \rightarrow \pi^*$, $^1A_{1g} - {}^1E_g$, dipole-forbidden, vibronically allowed transition, based primarily on the results of Xα calculations.

Although it was possible to examine only one crystal face of $Mo_2(O_2CCF_3)_4$ by solid-state spectroscopy, the similarity between this compound and $Mo_2(O_2CCH_3)_4$ in both their crystal structures and crystal spectra has led to the conclusion that the same effect is being observed in this case, that is, the shift of the transition moment away from the molecular $\underset{\sim}{z}$-axis. This conclusion is reinforced by the fact that a calculated transition moment vector, oriented ~22° away from $\underset{\sim}{z}$ and in the proximity of the transition moment orientation for $Mo_2(O_2CCH_3)_4$, accounts for the observed polarization ratio for the lowest energy absorption maximum at 6K. For these reasons, the 6K spectra of $Mo_2(O_2CCF_3)_4$ are being assigned consistent with the spectral assignments for $Mo_2(O_2CCH_3)_4$. The transition at 22,070 cm^{-1} at 6K is assigned as the $\delta \rightarrow \delta^*$, $^1A_{1g} \rightarrow {}^1A_{2u}$, $\underset{\sim}{z}$-polarized, electric-dipole allowed transition. Again, the vibrational details of the low energy band are assigned as

dipole forbidden, vibronically excited transitions based on the dipole allowed origin. The four most intense Franck-Condon progressions, with a measurable energy separation of $\sim$360 cm^{-1} are assigned as based on the totally symmetric metal-metal vibration of the electronic excited state. The band observed at $\sim$27,500 cm^{-1} is then assigned as the $\delta \rightarrow \pi^*$, $^1A_{1g} \rightarrow {}^1E_g$ dipole forbidden transition, also in agreement with the $Mo_2(O_2CCH_3)_4$ assignment.

It was presumed that the electronic spectra of $K_2[Pt_2(SO_4)_4 \cdot 2H_2O]$ would be comparable to the calculated and experimental spectroscopic results for $Rh_2(O_2CR)_4 \cdot 2H_2O$, since the two metals have equivalent d^7 electron configurations in these compounds. However, the considerable discrepancies between the solid-state spectra of $K_2[Pt_2(SO_4)_4 \cdot 2H_2O]$, when compared with the spectral results for $Rh_2(O_2CCH_3)_4 \cdot 2H_2O$, led to the postulation of a significantly different molecular orbital diagram compared to that for $Rh_2(O_2CH)_4 \cdot 2H_2O$. From the postulated MO diagram, the three observed $\underset{\sim}{z}$-polarized bands are assigned under D_{2h} symmetry as follows: 22,400 cm^{-1} band, $M\text{-}O\sigma^* \rightarrow M\text{-}O\sigma^*$, $^1b_{1g} \rightarrow {}^1a_u$; 26,300 cm^{-1} band, $M\text{-}M\delta \rightarrow M\text{-}M\delta^*$, $^1a_g \rightarrow {}^1b_{1u}$; 29,100 cm^{-1} band, $M\text{-}M\delta \rightarrow M\text{-}M, M\text{-}OH_2\sigma^*$, $^1a_g \rightarrow {}^1b_{1u}$. A weak, apparently $\underset{\sim}{x},\underset{\sim}{y}$-polarized band at $\sim$25,600 cm^{-1} is attributed to the $M\text{-}M\delta \rightarrow M\text{-}M, M\text{-}OH_2\sigma^*$, $^1a_g \rightarrow {}^3b_{1u}$ spin-forbidden transition.

The data collected on the automatic four-circle diffractometer for $Mo_2(O_2CCH_3)_4 \cdot KCl$ yielded the following preliminary results:

$\underset{\sim}{a}$ = 9.601(2)Å	$\alpha = 90^\circ$	Z = 4
$\underset{\sim}{b}$ = 12.799(3)Å	$\beta = 97.59(3)^\circ$	Volume = 1457.4(5)$Å^3$
$\underset{\sim}{c}$ = 11.641(2)Å	$\gamma = 90^\circ$	

Examination of extinction conditions for certain reflections led to the conclusion that the compound crystallized in a c-centered monoclinic cell; possible space groups were C2/c, C2/m, Cm, Cc, and C2. Since the cell was found to have a center of inversion, three of the space groups were eliminated, leaving only C2/m and C2/c. The fact that only $h0\ell$ reflections with $\ell = 2n$ were observed verified that the space group was C2/c. The atom positions were refined by computer least-squares fitting to an agreement factor of 3.3%. The $Mo_2(O_2CCH_3)_4$ molecules and chlorine atoms were found to sit on inversion sites, with the potassium atoms resting on two-fold axes. The structure consists of alternating molybdenum-molybdenum-chlorine endless chains across the two $\underset{\sim}{a}$ and $\underset{\sim}{b}$ axes' diagonals, with the chains stacking in the $\underset{\sim}{c}$-axis direction, and the potassium atoms lying halfway between chlorine atoms of successive stacked chains. The metal-metal distance of 2.1019Å is significantly longer than that in $Mo_2(O_2CCH_3)_4$ of 2.093Å, and the very long molybdenum-chlorine distance of 2.9507Å, when compared with the potassium-chlorine distance of 3.0078Å, suggests an ionic-type interaction.

I. INTRODUCTION

The purpose of this thesis and research is to elucidate details of the structure and bonding for dimeric metal-metal bonded systems. The technique of solid-state polarized spectroscopy has an important application in these systems, since it can in many cases provide experimental data on specific energy spacings between the various highest filled molecular orbitals and lowest unfilled molecular orbitals of these metal dimer compounds.

The first two compounds to be discussed are the quadruply-bonded metal dimers tetra-μ-acetatodimolybdenum(II), $Mo_2(O_2CCH_3)_4$, and tetrakis-μ-(trifluoroacetato)dimolybdenum(II), $Mo_2(O_2CCF_3)_4$. While the solid-state spectra for both of these compounds had been studied before (1, 2), the considerable discrepancies between the conclusions drawn in these studies, when compared to the conclusions for other quadruply bound molybdenum dimer systems (3-6) previously studied, led us to undertake a careful examination of the single crystal polarized spectra of these compounds.

The next compound to be discussed is potassium diaquo-tetra-μ-sulfatodiplatinum(III). While this was only a single metal-metal bonded dimer (7), it represented an opportunity to study a dimeric platinum compound in the rare formal oxidation state of three (7), as well as a highly symmetric platinum compound with a metal-metal bond. We were also interested in comparing the spectral results for this compound with the spectra for the isoelectronic diaquo-tetra-μ-acetatodirhodium(II), which had been studied in our research group previously (8).

The final compound to be discussed, tetra-μ-acetatodimolybdenum(II)·potassium chloride, $Mo_2(O_2CCH_3)_4 \cdot KCl$, was synthesized in order to further characterize the bonding and energy levels of the $Mo_2(O_2CCH_3)_4$ molecule by solid-state spectroscopy. However, no significant spectral data have been obtained for this compound, as it crystallized in a form unfavorable for the measurement of high resolution spectra. Therefore, only the X-ray crystal structure of this new compound will be presented.

The first formal proposal of a metal-metal quadruple bond was presented by F. A. Cotton in 1965 (9), and accompanied the solution of the X-ray crystal structure for $K_2Re_2Cl_8 \cdot 2H_2O$ (10). In the solution of this crystal structure, two striking features appeared; first, the Re-Re interatomic distance was extremely short, even shorter than the sum of the atomic radii; and secondly, the chloride ligands of the metal dimer compound were eclipsed rather than staggered. Cotton presented an explanation based on simple molecular orbital theory which would account for these observed features (9). This proposal was the existence of four bonds between the two rhenium atoms. From simple MO theory, the $6s, 6p_x, 6p_y$, and $5d_{x2-y2}$ orbitals of the Re atoms were assigned as metal-ligand bonding orbitals. The $5d_{z2}$ and $6p_z$ orbitals formed four linear combinations which were assigned as one metal-metal σ-bonding, two nonbonding, and one σ-antibonding. The $5d_{xz}$ and $5d_{yz}$ orbitals were assigned as metal-metal π-bonding, and the $5d_{xy}$ orbitals were assigned as metal-metal δ-bonding.

This bonding scheme accounted for all of the features observed in the crystal structure. The bond order of four resulted in the very

short Re-Re distance of 2.241Å. And, since both the sigma- and pi-bonds between the metals were symmetric with respect to rotation about the metal-metal axis, the delta-bond was deemed responsible for the eclipsed configuration of the chloride ligands. In order for this to be true, the stabilization energy of the delta-bond had to be greater than the increased electrostatic repulsion caused by the eclipsed geometry of the ligands. Subsequent calculations have shown this to be a valid conclusion (11). In order to verify the proposed bonding scheme, Cotton and Harris performed an extended Hückel MO[1] calculation, the results of which are shown in Figure 1. This calculation generally supported their original proposal.

The original qualitative outline of the metal-metal bonding has not been substantially altered by subsequent MO calculations, although more recent SCF-Xα-SW[2] type calculations by Mortola et al. (12) and others (13, 14, 15) for the $Re_2Cl_8^{2-}$ anion as well as various quadruply-bonded molybdenum dimers have shown that the non-bonding orbitals originally proposed by Cotton and Harris are not present in the region of the metal-metal bonding orbitals (see Figure 2).

While the SCF-Xα-SW type MO calculations have generally been accepted as an accurate method of determining the relative ordering of the molecular orbitals for quadruply bonded dimer species, they have been poor in quantitatively predicting the observed energy spacings

---

[1] Molecular Orbital.

[2] Self-Consistent Field Xα Scattered Wave.

Only orbitals with predominant metal d character are shown. Note that the symmetries assigned to the π and π^* orbitals are incorrect. The correct assignments are $E_u(\pi)$ and $E_g(\pi^*)$ under D_{4h} symmetry.

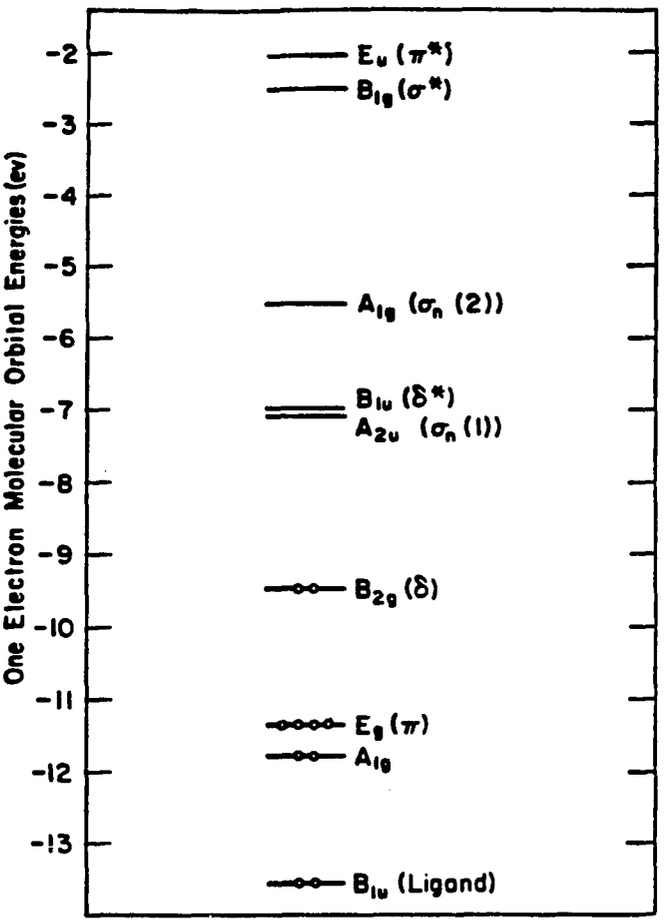

Figure 1. Partial one-electron MO[a] diagram determined from a Hückel MO calculation for $Re_2Cl_8^{2-}$ (11)

---

[a]Molecular Orbital.

Only orbitals with predominant metal d character under D_{4h} symmetry are shown.

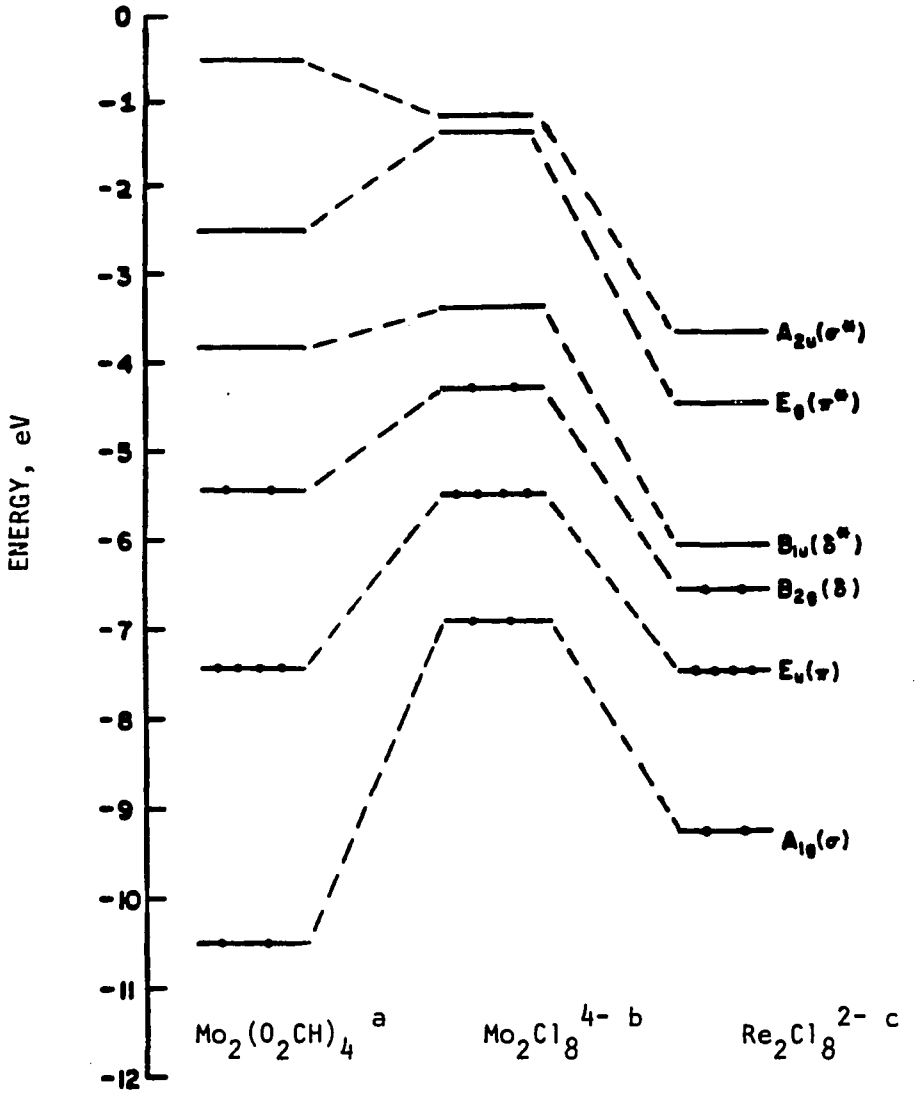

[a]Ref. 13 .

[b]Ref. 15 .

[c]Ref. 12 .

Figure 2. Partial MO diagrams for three quadruply-bonded compounds determined from SCF-Xα-SW calculations

between various molecular states, particularly the excitation of the $\delta \rightarrow \delta^*$ transition (16). It has been suggested that the Xα calculations give poor results for the energy of the $\delta \rightarrow \delta^*$ transition in the d^4-d^4 closed shell systems because they fail to take fully into account the electron repulsion contributions to the excited state energies for these species (16).

This explanation was reinforced by the accurate prediction of the $\delta \rightarrow \delta^*$ transition energy via an Xα calculation for a $Tc_2Cl_8^{3-}$ complex (17). It was noted by Gray and Trogler (16) that this is an odd-electron system, and therefore would not have an increased electron repulsion contribution to the excited state, since it has one unpaired electron in both the ground and excited states, whereas the closed shell systems have no unpaired electrons in the ground state, and would have two unpaired electrons in their triplet excited states. Clearly, there is an electron repulsion interaction in the triplet states which cannot contribute to the ground state energy.

Cotton et al. have attributed the good agreement between their spectral results (18) and the Xα calculation for the $Tc_2Cl_8^{3-}$ complex (17) to the fact that they were dealing with doublet-to-doublet excitations, and also suggested that the difficulty in estimating singlet and triplet excitation energies for closed shell species may be partly responsible for the poor agreement of calculated $\delta \rightarrow \delta^*$ transition energies with the experimentally determined energies for these systems.

Recently, Noodleman and Norman developed a new method for calculating excitation energies for cases of weak electronic coupling, such as the δ-bond in quadruply-bonded systems. The new method involves a valence

bond modification of the Xα theory (19), yielding an "Xα-VB" model which is claimed to be able to approximate the energy of δ-bonding and other weak electronic interactions much better than the original Xα-MO method. To test this new model, the authors calculated the excitation energy of the $\delta \rightarrow \delta^*$ transition for $Mo_2Cl_8^{4-}$, which had been calculated previously by the Xα-MO method to be 9,200 cm^{-1} (15). The value of 15,200 cm^{-1} calculated by the Xα-VB method is in much better agreement with the experimentally observed value of 18,800 cm^{-1} for the $\delta \rightarrow \delta^*$ transition (5). This result shows that the Xα-VB model is much better at predicting the excitation energy of the $\delta \rightarrow \delta^*$ transition in d^4-d^4 quadruply-bonded systems with non-bridging ligands. However, it remains to be seen if this method will be as accurate when applied to $Mo_2(O_2CR)_4$-type compounds.

It is convenient at this time to present the selection rules relevant to the spectra under discussion. Unless specifically indicated, all observed spectral transitions will be assigned under the assumption that the compound or ion being examined has molecular D_{4h} symmetry. Under D_{4h} symmetry, one of the electric-dipole operator components is associated with the $\underset{\sim}{z}$ molecular axis, which is the metal-metal axis in these compounds, and the other two lie in a plane containing the $\underset{\sim}{x}$ and $\underset{\sim}{y}$ molecular axes, and are equivalent in this symmetry (see Figure 3).

In order for an electronic transition to be electric-dipole allowed under D_{4h} symmetry, it must satisfy the following relationship:

$$^1A_{1g} \subset \Gamma_g \cdot \Gamma_{el} \cdot \Gamma_f \qquad (1)$$

where Γ_g = irreducible representation of initial electronic state (ground state)

This axis system is used for spectral analysis of molecules of D_{4h} symmetry. The origin of the axis system sits at the inversion center between the two metal atoms (M = metal atom, L = ligand atom).

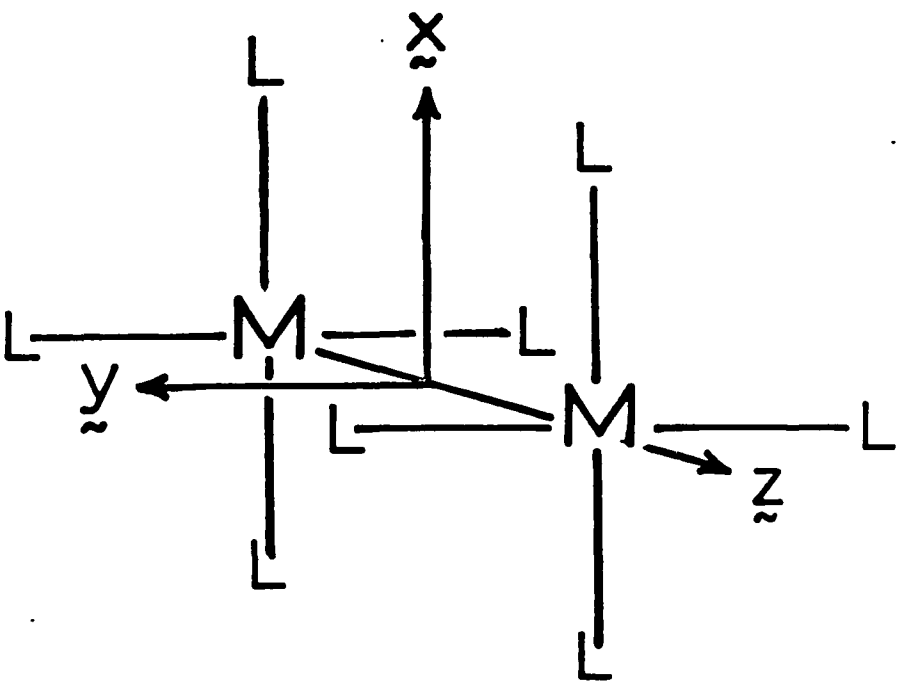

Figure 3. Molecular axis system for quadruply-bonded compounds

Γ_{el} = irreducible representation of the component of the electric dipole operator (E_u for $\underset{\sim}{x},\underset{\sim}{y}$; A_{2u} for $\underset{\sim}{z}$)

Γ_f = irreducible representation of final electronic state (excited state).

If a transition is not electric-dipole allowed, it may gain intensity through vibronic coupling, according to the following relation:

$$^1A_{1g} \subset \Gamma_g \cdot \Gamma_{el} \cdot \Gamma_f \cdot Q_i \qquad (2)$$

where Q_i is an enabling vibration of the proper symmetry to yield an $^1A_{1g}$ component in the overall product.

This type of electronic transition is said to be vibronically allowed, electric-dipole forbidden.

The first spectra recorded for a quadruply-bonded compound were reported by Cotton, et al. in 1965 (20). They measured the solution spectra of $Re_2Cl_8^{2-}$ and $Re_2Br_8^{2-}$. No spectral assignments were made in this paper, but were presented in another article also published in 1965 (9).

Only one specific assignment was made in the second paper, for the lowest energy transition observed in the solution spectra. On the basis of an estimated oscillator strength of $\sim$0.03, an assignment as the $\delta \rightarrow \delta^*$, or any other electric-dipole allowed transition, was ruled out for the 14,000 cm^{-1} band (9). Instead, this first transition was assigned as $\delta \rightarrow \sigma_n$ (see Figure 1), which was dipole forbidden under D_{4h} symmetry. It was concluded that the transition gained intensity through vibronic coupling. The $\delta \rightarrow \delta^*$ dipole allowed transition was assigned as either the

$\sim$32,000 cm^{-1} or $\sim$40,000 cm^{-1} band, both of which had estimated oscillator strengths much nearer to unity. The detailed spectral assignments for each band in the solution spectrum of the $Re_2Cl_8^{2-}$ anion were published by Cotton and Harris in 1967, and accompanied their Hückel MO calculation for $Re_2Cl_8^{2-}$ (1). The results are listed in Table 1.

The most important result was the assignment for the $\delta \rightarrow \delta^*$ transition, since the energy of this transition gave an indication of the strength of the δ-bond. Cotton and Harris also calculated a bond energy for the δ-bond by comparing the energy of the $5d_{xy}$ orbital for the hypothetical $ReCl_4^-$ ion with the energy for this orbital as determined for the $Re_2Cl_8^{2-}$ ion. Both values were obtained from a Hückel MO calculation, using the same basis set (11). The value obtained for the δ bond energy was 51 Kcal/mole, which was claimed to be a much larger stabilizing effect compared to the destabilizing Cl-Cl repulsion, which was estimated to be $\sim$7 Kcal/mole.[1]

Solution and diffuse reflectance spectra for several binuclear molybdenum(II) carboxylates were reported by Dubicki and Martin (1) in 1969. To aid in interpretation of the spectra, an SCCC-MO[2] calculation was done for $Mo_2(O_2CCH_3)_4$. It was concluded that the electronic transitions observed for the binuclear molybdenum carboxylates could be assigned in a manner consistent with the assignments for the solution spectra of $Re_2Cl_8^{2-}$ (1). Thus, for the molybdenum acetate dimer, the lowest energy

---

[1]Value obtained from the rotational barrier in C_2Cl_6, which is due to Cl-Cl repulsion.

[2]Self Consistent Charge and Configuration-Molecular Orbital.

Table 1. Calculated (11) and observed (9) electronic transitions for the solution spectrum of $Re_2Cl_8^{2-}$

	Pol.	Energy, cm^{-1} calc.	Energy, cm^{-1} obs'd.	Oscillator strength
Electric-dipole allowed				
$^1b_{2g} \rightarrow {}^1b_{1u}(\delta \rightarrow \delta^*)$	$\underset{\sim}{z}$	19,700	32,800	0.31
$^1e_g \rightarrow {}^1a_{2u}(\pi \rightarrow \sigma_n(1))^a$	$\underset{\sim}{x},\underset{\sim}{y}$	34,800	39,200	0.65
$^1e_g \rightarrow {}^1b_{1u}(\pi \rightarrow \delta^*)^a$	$\underset{\sim}{x},\underset{\sim}{y}$	35,000	--	--
$^1a_{1g} \rightarrow {}^1a_{2u}(\sigma \rightarrow \sigma_n(1))$	$\underset{\sim}{z}$	43,100	--	--
$^1b_{2g} \rightarrow {}^1e_u(\delta \rightarrow \pi^*)^a$	$\underset{\sim}{x},\underset{\sim}{y}$	59,700	--	--
Electric-dipole forbidden				
$^1b_{2g} \rightarrow {}^1a_{2u}(\delta \rightarrow \sigma_n(1))$		18,700	14,500	0.023
$^1b_{2g} \rightarrow {}^1a_{1g}(\delta \rightarrow \sigma_n(2))$		30,900	--	--
$^1e_g \rightarrow {}^1a_{1g}(\pi \rightarrow \sigma_n(2))^a$		46,100	--	--
$^1a_{1g} \rightarrow {}^1a_{1g}(\sigma \rightarrow \sigma_n(2))$		49,400	--	--

[a]These assignments are invalid, due to the incorrect irreducible representation assignments for the π and π^* orbitals (see Fig. 1).

band observed at $\sim$23,000 cm^{-1} was assigned as either ligand $\pi \rightarrow$ metal σ^* or metal $\delta \rightarrow$ metal σ^*, due to its' low intensity. Both of these possible transitions are electric-dipole forbidden, and would gain intensity through vibronic coupling. On the basis of a much higher intensity, band II, observed at $\sim$30,000 cm^{-1}, was assigned as the $\delta \rightarrow \delta^*$, $^1A_{1g} \rightarrow {}^1A_{2u}$, electric-dipole allowed transition.

It was not until 1973 that single-crystal polarized spectra were presented for a quadruple-bonded compound (21). Cowman and Gray measured spectra for a single crystal of $[(n\text{-}Bu)_4N]_2Re_2Cl_8$ at room temperature and 5K. The compound crystallized in a monoclinic cell, $P2_1/c$, and spectra were measured for the 1 0 0 face with polarizations parallel and perpendicular to the unique ($\underset{\sim}{b}$) axis.

The parallel to $\underset{\sim}{b}$ spectrum displayed the higher absorbance. The details of the spectral assignments are shown in Table 2. (Note the poor agreement between the experimental versus calculated energy for the $\delta \rightarrow \delta^*$ transition.) The most important result was the assignment of the lowest energy transition as $\delta \rightarrow \delta^*$, $^1b_{1g} \rightarrow {}^1b_{2u}$, electric-dipole allowed, which contradicted the assignment by Cotton based on solution spectra. This assignment was based on the fact that no A term[1] was observed for this transition in the MCD spectrum of $Re_2Cl_8^{2-}$, and also on the observation that the integrated intensity of this band appeared invariant to temperature, whereas a vibronic transition should decrease in intensity with decreasing temperature (21).

---

[1]An A term in an MCD spectrum is indicative of a degenerate excited state.

Table 2. Solid-state spectral assignments for $[(n\text{-}C_4H_9)_4N]_2Re_2Cl_8$ (21)

Energy, cm^{-1} observed	Energy, cm^{-1} calculated (12)	Polarization	Assignment
14,140	4,488	$\underset{\sim}{z}$	$^1A_{1g} \rightarrow {}^1A_{2u}(\delta \rightarrow \delta^*)$ [a]
17,675(w) (22) [b]		$\underset{\sim}{x}, \underset{\sim}{y}, \underset{\sim}{z}$ [c]	$^1A_{1g} \rightarrow {}^1E_g(\delta \rightarrow \pi^*)$
20,940 (22)		$\underset{\sim}{x}, \underset{\sim}{y}$ [c]	
23,645 (22)		$\underset{\sim}{x}, \underset{\sim}{y}$ [c]	$^1A_{1g} \rightarrow {}^1A_{1u}(\delta \rightarrow d_{x^2-y^2})$
27,000(w) (22)		$\underset{\sim}{z}$	$^1A_{1g} \rightarrow {}^1A_{2u}(L\pi \rightarrow \delta^*)$ [d]
30,870	21,722	$\underset{\sim}{x}, \underset{\sim}{y}$	$^1A_{1g} \rightarrow {}^1E_u(L \rightarrow \sigma^*)$
31,750(w)		$\underset{\sim}{x}, \underset{\sim}{y}$	
34,480(w)		— [c]	
35,700(w)		— [c]	
39,215	24,702	$\underset{\sim}{z}$	$^1A_{1g} \rightarrow {}^1A_{2u}(\pi \rightarrow \pi^*)$
39,840(w)		$\underset{\sim}{x}, \underset{\sim}{y}$ [c]	
42,000(w)		$\underset{\sim}{x}, \underset{\sim}{y}$ [c]	

[a] For the $\delta \rightarrow \delta^*$ transition, $^1A_{1g}$ and $^1A_{2u}$ refer to the overall electronic states; $^1b_{1g}$ and $^1b_{2u}$ refer to the molecular states (see text, page 12).

[b] (w) = weak peak.

[c] Electric dipole forbidden, vibronically allowed transition.

[d] $L\pi$ = ligand π, e_g.

At 5K, the 14,000 cm^{-1} band showed rich vibrational structure which was assigned as a Franck-Condon progression, based on the totally symmetric stretching frequency in the excited state. From the spacing of the maxima, the excited state metal-metal stretching frequency was reported to be 245 cm^{-1}. This was significantly lower than the metal-metal stretching frequency of the ground state, which was found to be 273 cm^{-1} by Raman spectroscopy (23). The frequency shift was attributed to a weakening of the metal-metal bond, caused by the excitation of an electron from the δ to the δ^* molecular orbital.

However, this assignment was not conclusive, since Cowman and Gray did not prove that the transition assigned as $\delta \rightarrow \delta^*$ was polarized along the molecular $\underset{\sim}{z}$ axis, which it must have been, according to D_{4h} selection rules, if it was in fact the $\delta \rightarrow \delta^*$ transition.

In order to relate the single-crystal polarizations[1] to the molecular axes, it is necessary to know the X-ray crystal structure of the compound, and the crystal face on which the incoming plane-polarized light wave impinges. From the angles between the crystal vibration directions and the molecular $\underset{\sim}{z}$ axis, the expected polarization ratio for a molecular $\underset{\sim}{z}$-polarized transition can easily be calculated (24).

However, since the crystal structure for $[(n\text{-}C_4H_9)_4N]_2Re_2Cl_8$ was unknown at the time of Cowman and Gray's publication (21), they could not

---

[1]The vibration directions (polarizations) for a crystal face can be pictured as two perpendicular planes, passing through the crystal in the direction of light transmission. Any light wave which impinges on the crystal face passes through the crystal only along these two vibration directions, in the absence of absorption.

calculate polarization ratios, since they could not determine the molecular axes' orientation with respect to the vibration directions of the crystal. However, their assignment was later confirmed by Cotton et al. (25). In the solution of the X-ray crystal structure of $[(n\text{-}C_4H_9)_4N]_2Re_2Cl_8$, Cotton et al. were able to show that the polarization ratio observed by Cowman and Gray for the lowest energy transition (see Table 2) was equal to the ratio expected for a $\underset{\sim}{z}$-polarized transition. The cell parameters $\underset{\sim}{a} = 10.933(5)\text{Å}$, $\underset{\sim}{b} = 15.412(6)\text{Å}$, $\underset{\sim}{c} = 16.435(5)\text{Å}$, $\beta = 122.27(3)^\circ$ were in good agreement with the previous unit cell parameters reported by Cowman and Gray (21). It was by no means a trivial problem to determine the calculated polarization ratio, because the $Re_2Cl_8^{2-}$ anions were found to be in two different orientations in the crystal. ∿74% of the ions were oriented with the metal-metal bond parallel to the $\underset{\sim}{b}$ axis, and the remaining 26% had their metal-metal bond aligned ∿ along the $\underset{\sim}{ac}$ diagonal. The calculated polarization ratio of 2.158 for a $\underset{\sim}{z}$-polarized transition agreed well with the value of 2.203 observed experimentally. This result, coupled with the fact that the integrated intensity of the band at ∿14,000 cm^{-1} was invariant to temperature, confirmed the assignment of this transition as $\delta \rightarrow \delta^*$.

Since the results of the single-crystal polarized spectra for $Re_2Cl_8^{2-}$ were published, several rhenium and molybdenum dimer compounds, as well as chromium, tungsten, and technetium dimers have been studied by polarized spectroscopy, and a recent review article by Templeton has thoroughly discussed the background and more recent developments, both theoretical and experimental, for quadruply-bonded compounds (26).

Since the primary result of interest in the present study has been the assignment of the lowest energy electronic transition observed in the polarized spectra, a review including assignments for higher energy transitions will not be undertaken. However, a discussion of assignments for the lowest energy transition for various quadruply-bonded dimers is in order. A summary of assigments reported prior to our investigation of $Mo_2(O_2CCH_3)_4$ is shown in Table 3. One very important point to note about the compounds listed in the table is that all of the metal dimers can be assumed to have D_{4h} molecular symmetry, in the ideal case. This is not a coincidence; it is necessary that a compound being examined by polarized spectroscopy have sufficiently high molecular symmetry, as this generates electric-dipole operator components of different symmetries. This separation of dipole operator components is a prerequisite to the assignment of specific electronic transitions to the absorption bands observed for the single-crystal polarized spectra of these compounds.

We can see from Table 3 that the M_2X_8-type compounds (M = Re, Mo, Tc and X = Cl, Br), and the $Mo_2(SO_4)_4^{X-}$ compounds follow the trend in which the lowest energy transition clearly behaves as a $\underset{\sim}{z}$-polarized, dipole allowed transition. However, for the $Mo_2(O_2CR)_4$-type compounds, this is not the case. For the first carboxylate-bridged compound examined by polarized spectroscopy, $Mo_2(O_2CCH_2NH_3)_4(SO_4)_2 \cdot 4H_2O$, the lowest energy progression, which originates at 20,570 cm^{-1}, is $\underset{\sim}{z}$-polarized, but is roughly an order of magnitude weaker than the Franck-Condon progression which originates at 21,510 cm^{-1} and also is $\underset{\sim}{z}$-polarized (see Figure 4).

Table 3. Assignment for the lowest energy transition observed for quadruply-bonded compounds (16)

Compound	Sample condition[a]	$\bar{\nu}_{max}$, cm^{-1}
$[(n\text{-}C_4H_9)_4N]_2Re_2Cl_8$	crystal, 5K	14,654 (21, 22)
$[(n\text{-}C_4H_9)_4N]_2Re_2Br_8$	crystal, 5K	14,104 (27)
$Mo_2(O_2CCH_2NH_3)_4(SO_4)_2\cdot 4H_2O$	crystal, 15K	22,790 (28)
$K_4Mo_2(SO_4)_4\cdot 2H_2O$	crystal, 15K	19,400 (3)
$[(n\text{-}C_4H_9)_4N]_2Tc_2Cl_8$	polycrystalline (diffuse reflectance)	14,290 (30)
$K_3Mo_2(SO_4)_4\cdot 3.5H_2O$	KBr disk, 15K crystal, 6K	7,100[d] (4) 6,311, 6,418 (32)
$Mo_2(O_2CCH_3)_4$	thin film, 15K	22,436 (2)
$Mo_2(O_2CCD_3)_4$	"	22,472 (2)
$Mo_2(O_2CCF_3)_4$	"	22,791 (2)
$Mo_2(O_2CH)_4$	" crystal, 15K	22,653 (2) 21,870 (3)
$K_3Tc_2Cl_8\cdot 2H_2O$	CsI disk, 5K	6,300[d] (18)
$K_4Mo_2Cl_8\cdot 2H_2O$	crystal, 4K	19,128 (5)

[a]These conditions refer only to the measurement of $\bar{\nu}_{max}$ and the excited state M-M stretching frequency.

[b]$\delta\rightarrow\delta^*$ is an electric dipole allowed, z-polarized transition; $\delta\rightarrow\pi^*$ is electric dipole forbidden, vibronically allowed.

[c]Ground state stretching frequencies were determined from Raman spectra; excited state frequencies were obtained from the spacings of Franck-Condon vibrational progressions observed for the lowest energy transition at low temperature ($\leq$15K).

[d]The transition is $^2b_{2g}\rightarrow{}^2b_{1u}$, $(\delta\rightarrow\delta^*)$.

[e]X and X* refer to molecular orbitals with substantial carboxyl p-π contributions.

Year	Transition[b] assignment	M-M stretching frequency, cm^{-1} [c] ground state	excited state
1973	$\delta \rightarrow \delta^*$	272 (23)	248 (22)
1978	$\delta \rightarrow \delta^*$	275 (23)	255 (27)
1976	$\delta \rightarrow L^*$, $\delta \rightarrow \pi^*$	393 (29)	345 (28)
1976	$\delta \rightarrow \delta^*$	--	--
1977	$\delta \rightarrow \delta^*$	--	--
1977	$\delta \rightarrow \delta^*$	373, 386 (31)	350, 357 (4)
1978	$\delta \rightarrow \delta^*$	--	346 (32)
1977	$\delta \rightarrow \pi^*$	406 (23)	370 (2)
1977	$\delta \rightarrow \pi^*$	--	370 (2)
1977	$\delta \rightarrow \pi^*$	397 (5)	355 (2)
1977	$\delta \rightarrow \pi^*$	406 (33)	360 (2)
1976	$\delta \rightarrow X^*$, $X \rightarrow \delta^*$ [e]	--	350 (3)
1977	$\delta \rightarrow \delta^*$	--	320 (18)
1978	$\delta \rightarrow \delta^*$	346 (33)	336 (5)

The assignment made by Cotton et al. was that the lowest energy transition was dipole forbidden in D_{4h} symmetry, but was weakly allowed by a molecular symmetry-lowering effect to S_4 in the solid state (28). The remaining three vibrational progressions which originated at 21,510 cm^{-1} ($\underset{\sim}{z}$), 21,790 cm^{-1} ($\underset{\sim}{x},\underset{\sim}{y}$) and 21,930 cm^{-1} ($\underset{\sim}{x},\underset{\sim}{y}$), as shown in Figure 4, were assigned as vibronic transitions based on enabling vibrations of 940 cm^{-1}, 1220 cm^{-1}, and 1360 cm^{-1}, respectively. The vibrations were not specifically identified. The vibrational spacing between the lines in each of the progressions was 340-345 cm^{-1}, and was assigned as the totally symmetric metal-metal stretching vibration in the excited state (28). The next compound to be examined by single-crystal polarized spectroscopy was $Mo_2(O_2CH)_4$. The 5K polarized spectra are shown in Figure 5 for light polarized along the $\underset{\sim}{a}$ and $\underset{\sim}{c}$ crystallographic axes. From the X-ray structural data, the Mo-Mo, or $\underset{\sim}{z}$-axis, was found to be oriented $\sim 33^{\circ}$ away from the $\underset{\sim}{c}$ axis. The calculated $\underset{\sim}{c}:\underset{\sim}{a}$ intensity ratio for a $\underset{\sim}{z}$-polarized transition was 4.3, and for an $\underset{\sim}{x},\underset{\sim}{y}$-polarized transition .36 (3). As shown in Figure 5, the 15K spectra exhibited a Franck-Condon vibrational progression with an origin at 21,870 cm^{-1}, and an $\underset{\sim}{a}:\underset{\sim}{c}$ intensity ratio of 0.2. The conclusion, based on the polarization ratio, was that this lowest energy transition was definitely not the $\delta \rightarrow \delta^*$, but was an $\underset{\sim}{x},\underset{\sim}{y}$-polarized transition, possibly $\delta \rightarrow X^*$ or $X \rightarrow \delta^*$, where X is an MO with substantial carboxyl $p\pi$ character (3). The deviation of the spectra for $Mo_2(O_2CR)_4$ compounds from the trend observed for other metal dimers was attributed to a unique interaction between the carboxylate ligands and the metal atoms in these compounds. Subsequent spectral examinations of other $Mo_2(O_2CR)_4$ compounds in thin sublimed films (2) yielded results which

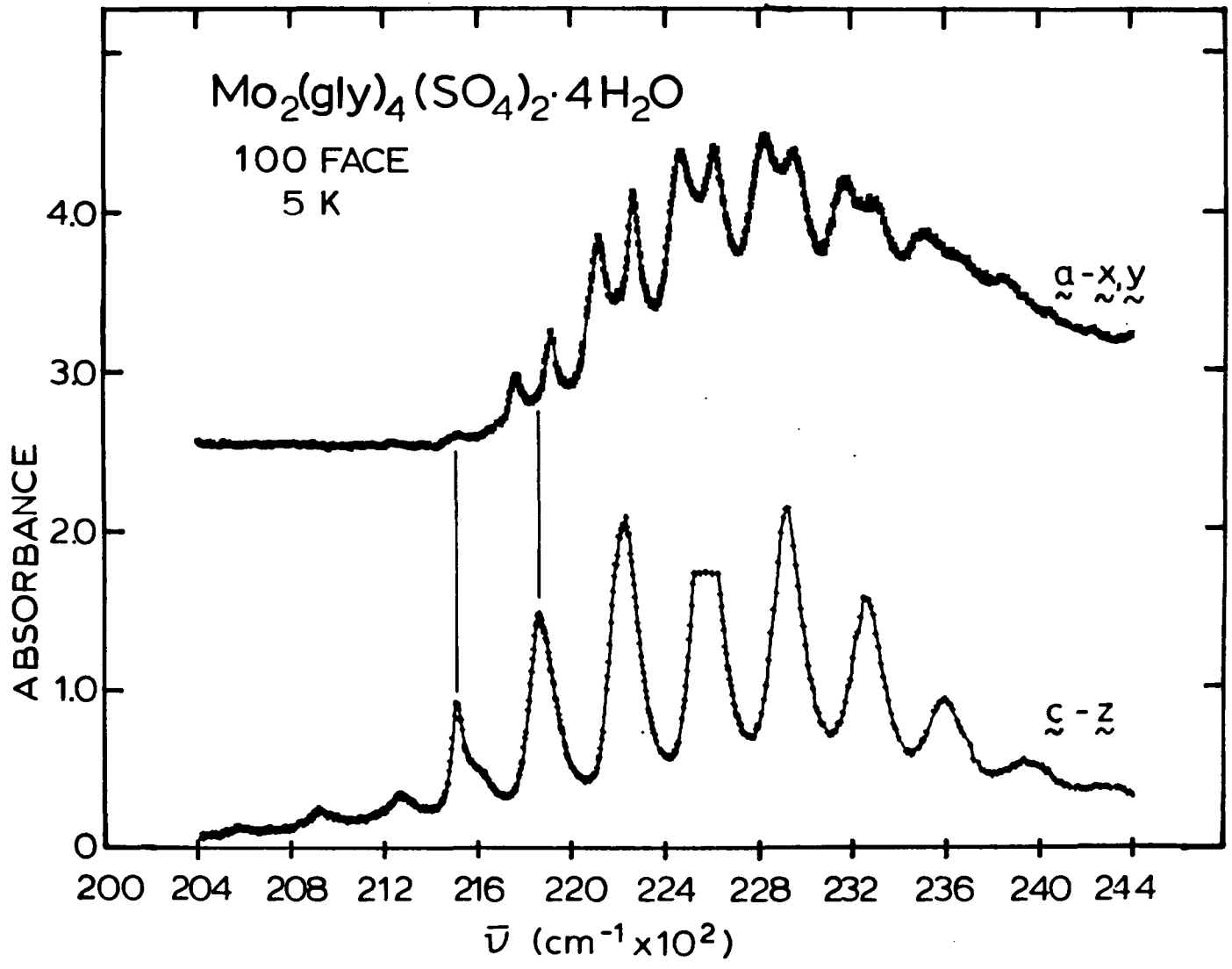

Figure 4. Low-temperature polarized spectra for a single crystal of $Mo_2(O_2CCH_2NH_3)_4(SO_4)_4 \cdot 4H_2O$ (28)

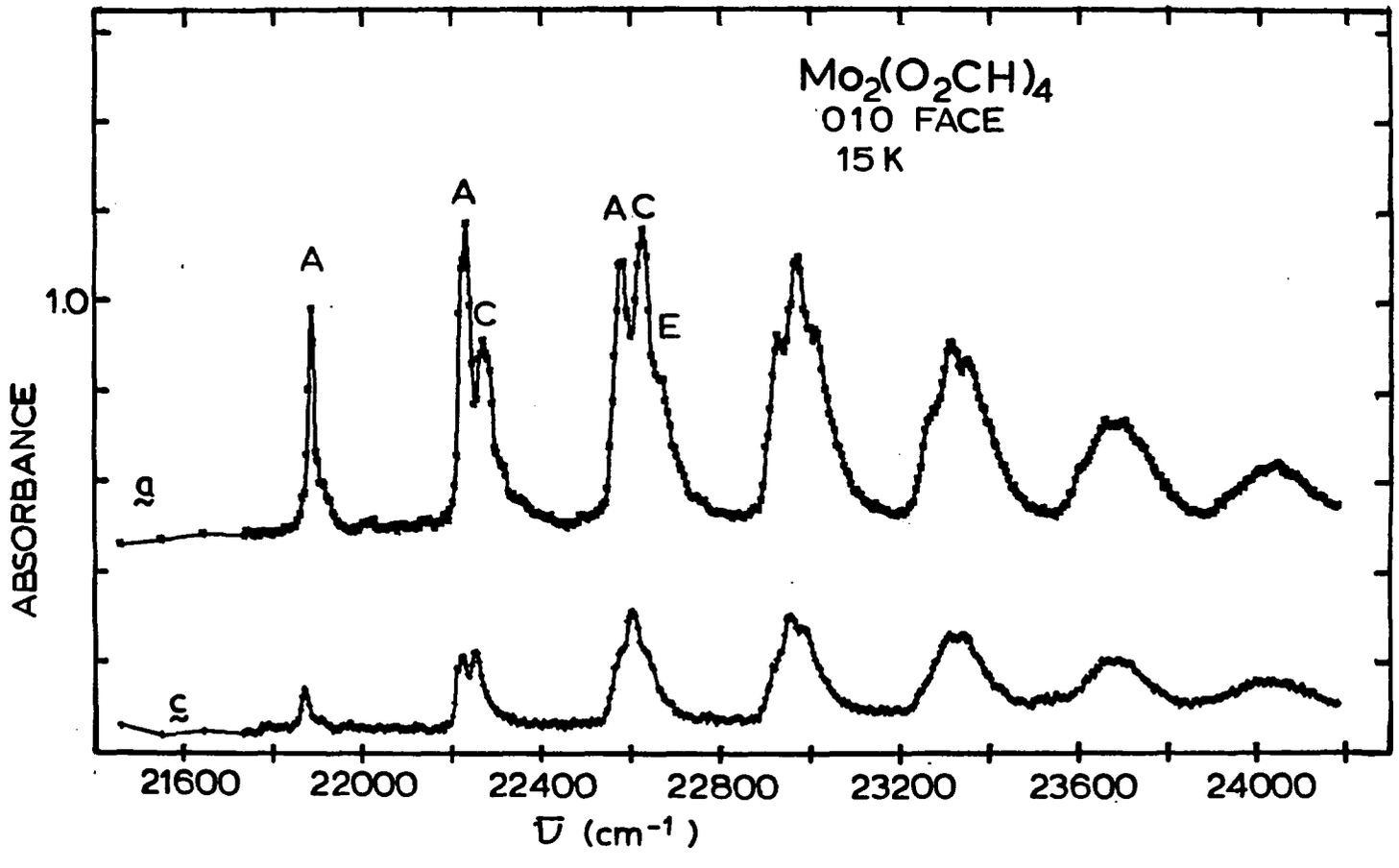

Figure 5. Low-temperature polarized spectra for a single crystal of $Mo_2(O_2CH)_4$ (3)

were similar to those seen for $Mo_2(O_2CH)_4$, although no polarization ratios could be observed. Nevertheless, based on the similarity of the spectra, the lowest energy transition was assigned as $\underset{\sim}{x},\underset{\sim}{y}$-polarized $\delta \rightarrow \pi^*$, vibronically allowed (2).

Preliminary examination of single crystals of $Mo_2(O_2CCH_3)_4$ and $Mo_2(O_2CCF_3)_4$ by our research group yielded results which, while somewhat similar to those observed for $Mo_2(O_2CH)_4$, also indicated that the assignment of the first observed transition may not be so straightforward. Therefore, a thorough and careful spectral examination of several crystals of $Mo_2(O_2CR)_4$ compounds (R = H, CH_3, CF_3) was undertaken, in order to better characterize the lowest energy transition observed.

Of the many spectral studies of single metal-metal bonded compounds, the most relevant to the study of $K_2[Pt_2(SO_4)_4 \cdot 2H_2O]$ are those of $Rh_2(O_2CR)_4 \cdot 2H_2O$. The rhodium compounds have been examined both theoretically (34, 37) and experimentally (8, 35-37). The rhodium carboxylates are isoelectronic with the platinum sulfate complex, so it was assumed that their spectral properties would be closely related to those of the dimeric platinum compound. For this reason, only the results of studies of $Rh_2(O_2CR)_4$ compounds will be presented here.

The solution of the X-ray crystal structure of $Rh_2(O_2CCH_3)_4 \cdot 2H_2O$ was published by Cotton et al. in 1971. On the basis of a bond length of 2.386Å, Cotton proposed that there was a Rh-Rh triple bond in this compound (35), since simple Rh-Rh single bonds were known to be from 0.3-0.4Å longer, in agreement with covalent radii predictions (35, 38). However, this conclusion contradicted an earlier SCCC-MO calculation by Dubicki and Martin, which supported an assignment of a Rh-Rh single bond,

and also accounted for the variation observed in electronic spectra as the axial ligands were varied (37). Several years later, Norman and Kolari presented the results of an SCF-Xα-SW calculation (34) for both $Rh_2(O_2CH)_4$ and $Rh_2(O_2CH)_4 \cdot 2H_2O$ (see Figure 6). These results essentially confirmed the presence of a Rh-Rh single bond in $Rh_2(O_2CR)_4$ compounds.

Obviously, the types of electronic transitions observable for the single metal-metal bonded rhodium carboxylates are much different than those observed for the quadruply-bonded dimer compounds. The highest occupied and lowest unoccupied orbitals for the $Rh_2(O_2CR)_4 \cdot 2H_2O$ compounds can be seen in Figure 6. Notice that the dihydrate is considered to have D_{2h} symmetry; that is because the hydrogens of the axial water ligands are considered to be fixed in space in the solid state, so the planar H_2O molecules bisect the angle between ligand planes. Another point to notice is the energy of the δ^* orbital, which was found to be higher than that of the π^* orbital(s).

Since the group-theoretical determination of dipole allowed transitions has been discussed previously, only the electric-dipole operator components under the D_{2h} symmetry group will be introduced at this time. The D_{2h} symmetry group has three unequal electric-dipole operator components, because the $\underset{\sim}{x}$ and $\underset{\sim}{y}$ molecular axes are no longer equivalent. The irreducible representations for the operator components are: $\underset{\sim}{z} = b_{1u}$; $\underset{\sim}{y} = b_{2u}$, and $\underset{\sim}{x} = b_{3u}$.

It is therefore possible to observe three different polarization ratios in the spectra of compounds which have rigorous D_{2h} molecular symmetry. The three lowest energy dipole allowed transitions, based on

Note that the x and y axes were placed in the planes which bisect the angles between the bridging ligand planes for this treatment, i.e., they were rotated 45° from the orientation shown in Figure 3

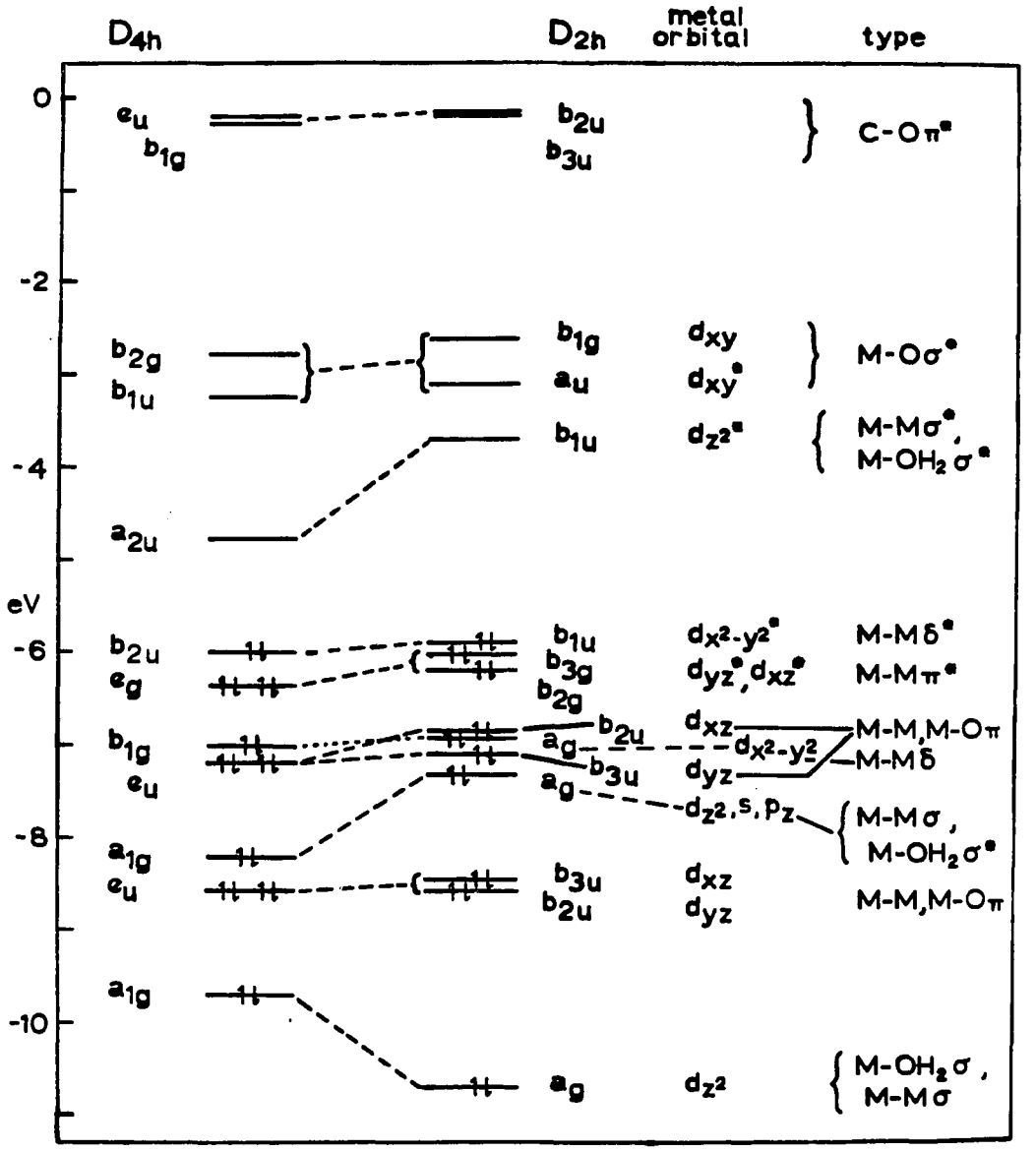

Figure 6. Molecular orbital energy diagram for $Rh_2(O_2CH)_4$ (D_{4h}) and $Rh_2(O_2CH)_4 \cdot 2H_2O$ (D_{2h}) from SCF-Xα-SW calculations (34)

the energies shown under D_{2h} in Figure 6 are: $^1(B_{3g},B_{2g}) \rightarrow {}^1a_u$, M-M$\pi^*$ → M-Oσ^*; $^1a_g \rightarrow {}^1b_{1u}$, M-M$\delta$ → M-Mσ^*; and $^1a_g \rightarrow {}^1(B_{2u},B_{3u})$, M-M$\delta$ → C-Oπ^*. It is important to note that the calculation by Norman and Kolari (34), from which Figure 6 was derived, predicted a splitting of ∿1000-2000 cm^{-1} for the Rh-Rhπ and π^* orbitals. A splitting of this magnitude should be observable in the solid-state spectra.

Solution spectra were reported by Johnson et al. in 1963 for $Rh_2(O_2CCH_3)_4$ in a variety of solvents (36). They reported two bands at ∿17,000 cm^{-1} and ∿22,300 cm^{-1}. The maximum of the first band varied as the solvent was changed, with the transition energy increasing with the electron-donor capability of the solvent. No assignments for the two transitions were reported. Dubicki and Martin presented the results of their diffuse reflectance study of $Rh_2(O_2CCH_3)_4 \cdot 2py$[1] and $Rh_2(O_2CC_4H_9)_4$ in 1970 (37). On the basis of the strong wavelength dependence of the low energy band to axial electron donors, and the results of their SCCC-MO calculation for $Rh_2(O_2CCH_3)_4 \cdot 2H_2O$, the authors assigned the 17,000 cm^{-1} band as $^1e_g \rightarrow {}^1a_{2u}(D_{4h})$, M-M$\pi^*$ → M-Mσ^*. They then assigned the second band as either π or $\pi^* \rightarrow d_{x^2-y^2}^*$, based on their D_{4h} MO-diagram for $Rh_2(O_2CCH_3)_4 \cdot 2H_2O$. The results of the single crystal spectral study of $Rh_2(O_2CCH_3)_4 \cdot 2H_2O$ were reported by Martin et al. in 1979 (8). They concluded that the crystal spectra could be assigned consistent with the assignments proposed by Norman and Kolari, based on SCF-Xα-SW calculations and the solution spectra for this compound. The 17,000 cm^{-1}

---

[1] py = pyridine.

band was assigned as $M\text{-}M\pi^* \rightarrow M\text{-}M\sigma^*$, which is dipole-allowed under both D_{4h} and D_{2h}.

However, where only one band was observed in solution, two bands were observed for the crystal spectra in the region from 22,000-24,000 cm^{-1}. Both bands had the temperature-independent intensity properties of electric-dipole allowed transitions. The higher energy band of the two was assigned as $M\text{-}M\pi^* \rightarrow M\text{-}O\sigma^*$, which is consistent with the previous assignment (34). The lower energy band in the 22,000-24,000 cm^{-1} region was then tentatively assigned as $M\text{-}M\delta \rightarrow M\text{-}M\sigma^*$, which would be dipole forbidden under D_{4h}, but dipole allowed under D_{2h} symmetry. The splitting of the π^* orbital degeneracy predicted by the Xα calculations was not observed in the crystal spectra. A Franck-Condon vibrational progression was observed at 15K for the 17,000 cm^{-1} band, with a spacing of 297 cm^{-1}, which was attributed to the Rh-Rh stretching frequency in the excited state. The observed transition energies were in very good agreement with those predicted by the SCF-Xα-SW calculation, as shown in Table 4.

Table 4. Observed vs. calculated electronic transition energies for $Rh_2(O_2CCH_3)_4 \cdot 2H_2O$

	Energy, cm^{-1} obs'd. (8)	calc. (34)	Transition[a]
Band I	16,800	17,100	$M\text{-}M\pi^* \rightarrow M\text{-}M\sigma^*$
Band II	22,000	--	$M\text{-}M\delta \rightarrow M\text{-}M\sigma^*$
Band III	23,500	22,700	$M\text{-}M\pi^* \rightarrow M\text{-}O\sigma^*$

[a] See Figure 6.

Based on these results, it appeared that we should have an accurate energy diagram which could be utilized to analyze the polarized spectra of $K_2[Pt_2(SO_4)_4 \cdot 2H_2O]$.

The synthesis and solution spectra of several $Pt_2(SO_4)_4X_2^{n-}$ species were reported by Orlova et al. (39) in 1975. The solution spectrum of the dihydrate exhibited a strong band at ∿29,500 cm^{-1}, a weaker shoulder at ∿23,000 cm^{-1}, and what appeared to be a very weak band at ∿19,000 cm^{-1}. The X-ray crystal structure of $K_2[Pt_2(SO_4)_4 \cdot 2H_2O]$ was reported by Muraveiskaya et al. in the following year. The compound was identified as containing platinum(III), based on the presence of a single metal-metal bond in this compound, proposed because of the short metal-metal distance (Pt-Pt, 2.466Å), the lack of a signal in the ESR spectrum[1], and the results of a potentiometric titration (7). No discussion and/or assignment for the absorption spectrum of this compound was reported.

The synthesis of the compound $Mo_2(O_2CCH_3)_4 \cdot KCl$ was the result of the knowledge that other molybdenum dimer compounds had formed axial adducts which had been crystallized and characterized (40-43), and the recent preparation and characterization of $Mo_2(O_2CH)_4 \cdot KCl$ by our research group (44).

The synthesis was also attempted with the hope that it would enable further spectroscopic characterization of the $Mo_2(O_2CCH_3)_4$ molecule, and provide more evidence for the identification of the lowest energy transition.

---

[1]The lack of a signal in an ESR spectrum indicates that all metal atom electrons are paired.

II. EXPERIMENTAL

A. Characterization of Crystals

1. Crystal optics

In order to undertake a detailed discussion of polarized spectroscopy, it is necessary to understand the behavior of light in crystals.

In an anisotropic crystal face, there are two mutually perpendicular directions along which the electric vector of an incoming plane-polarized light wave will be transmitted, in the absence of absorption. When absorption occurs, it is recognized that the plane-polarized light may pass through the crystal as two independent elliptically-polarized waves (45), the major axis of one wave being aligned with the minor axis of the other wave. It is generally satisfactory when transmitted light is measured to consider the ellipticity of the transmitted waves sufficiently high that they are effectively plane-polarized. The two perpendicular directions along which light is transmitted can then be pictured as two planes passing through the crystal in the direction of light transmission. Any arbitrary plane-polarized light wave whose electric vector is not aligned with one of these vibration directions will be split into two components which will then exit the crystal (see Figure 7). However, the net polarization angle and intensity of the incident wave may be altered, dependent upon the difference in absorption and indices of refraction for the two directions. From equation 3

$$\lambda = v/\nu = c/n\nu \qquad (3)$$

where λ is the wavelength of the light wave,

n is the index of refraction,

c is the speed of light in a vacuum,

v is the velocity of the light wave in the medium, and

ν is the frequency of the light wave (which must remain constant)

it is evident that the wavelength of light for the two polarizations of the crystal may be different, and may be out of phase upon exiting the crystal. The degree of phase change is dependent upon the birefringence[1] of the crystal.

It is possible to observe these effects under a polarizing microscope. This type of microscope consists of a polarizer which sends a plane-polarized light beam to a rotatable stage, with a vernier calibration to 3 seconds. Above the stage is a second polarizer, called an analyzer, which is oriented perpendicular to the lower polarizer, and which may be removed from the light beam. The net result with both polarizers in the beam and no sample on the stage is that no light passes through to the eyepiece, which then produces a dark field. When an anisotropic crystal face is placed in the light beam, several different effects may be observed. The crystal will not appear dark until it is rotated to the point where one of the wave vibration directions is aligned perfectly with the lower polarizer. When this happens, the polarized light will pass through the crystal with only this polarization, and will impinge on the analyzer perpendicular to its' vibration direction, resulting in the sample darkening, described as an extinction. For this reason, the two perpendicular vibration directions of a crystal

---

[1]The difference between the indices of refraction for the two vibration directions.

The randomly oriented plane-polarized wave is split into two components, which are transmitted through the crystal along the two perpendicular vibration directions for the anisotropic crystal face

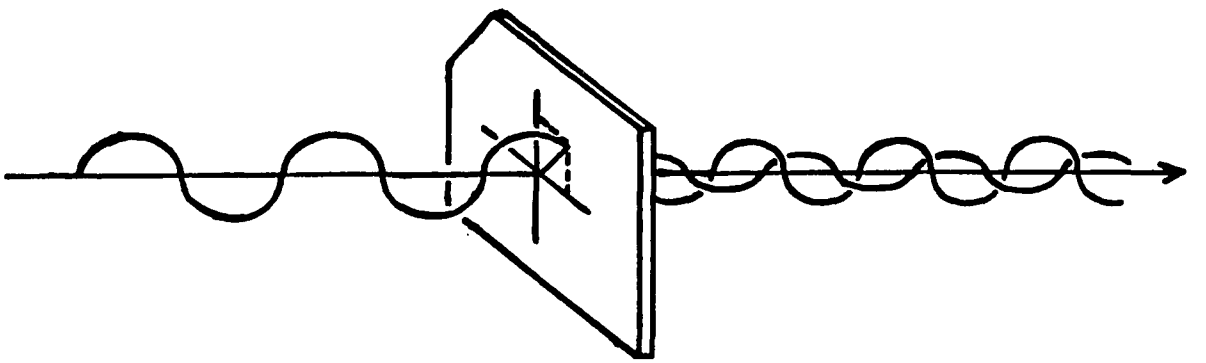

Figure 7. The behavior of a plane-polarized light wave incident on an anisotropic crystal face

are usually referred to as "extinction" directions. The crystal will transmit some light at all orientations which do not align the lower polarizer with an extinction. This is because of the birefringence, which results in a net rotation of the plane of polarization of the light beam after it passes through an anisotropic crystal face, and yields a component of light intensity along the vibration direction of the analyzer.

As the crystal is rotated on the stage, extinctions will be observed four times during a 360° rotation, or once every 90°. For some crystals, instead of a sudden dark appearance under white light, the crystal may pass through a range of different colors, and never appear to be completely dark. This is caused by the presence of a wavelength-dependent extinction, which is a property of any general face of a biaxial crystal. All crystals of orthorhombic or lower symmetry are biaxial. For orthorhombic crystals, any face which contains a crystal axis[1] is <u>not</u> a general face, cannot exhibit a wavelength dependence, and must have one extinction aligned with this crystal axis. For a monoclinic crystal, having the unique ($\underset{\sim}{b}$) axis in the crystal face precludes a wavelength-dependent extinction, and again one of the extinctions must lie parallel to this axis. For a triclinic crystal, all faces are general faces, and as such must exhibit wavelength-dependent extinctions. In any case, the wavelength dependence may be so small as to be unobservable.

---

[1] "... contains a crystal axis ..." -- this should be interpreted as having the crystal axis lie in the plane of the crystal face.

2. Polarization ratios

For any spectral wavelength, the maximum and minimum intensities will be measured only when the polarized light wave travels through the crystal aligned with the extinction directions. For the vast majority of D_{4h} dimeric compounds, the molecular $\underset{\sim}{z}$-axis is significantly closer to one of the observed extinctions than the other.

It is very important to be able to relate the extinction directions, measured with respect to crystal axes, to the molecular axes within the crystal. This relation allows the calculation of a polarization ratio, or a ratio of absorbance in the two extinction directions, for a molecular $\underset{\sim}{z}$- or $\underset{\sim}{x},\underset{\sim}{y}$-polarized transition. Obviously, the presence of an extinction which has a considerable wavelength dependence seriously complicates this determination. Technically, it should be possible to measure an extinction direction for each electronic transition observed, by illuminating a crystal with the wavelength of light at which each particular band maximizes. In practice, this would be very difficult. Instead, in cases where a wavelength-dependent extinction has been observed, polarized spectra have been recorded for 10° increments through 180° of polarizer angle.

For any crystal axis system of lower symmetry than orthorhombic, it is convenient to generate an orthogonal axis system from the crystallographic axis system, in order to determine the orientation of the molecular axes with respect to the crystal axes. This then allows the calculation of polarization ratios for molecular $\underset{\sim}{z}$- or $\underset{\sim}{x},\underset{\sim}{y}$-polarized transitions. For a monoclinic unit cell, either of the following axis systems may be used:

$$\hat{a} = \hat{i},\ \hat{b} = \hat{j},\ \hat{c} = \hat{i}(\cos\beta) + \hat{k}(\sin\beta) \tag{4}$$

or

$$\hat{a} = \hat{i}(\cos\beta) + \hat{k}(\sin\beta),\ \hat{b} = \hat{j},\ \hat{c} = \hat{k}^{1} \tag{5}$$

Generally, the axis set most convenient for a particular crystal face is used. For a triclinic crystal, the relationship is slightly more complex. Since there are no right angles, only one crystallographic axis, or crystal axis, can be made collinear with an orthogonal axis. Suppose, for instance, that spectra were recorded for the 0 0 1 face of a triclinic crystal. The indices 0 0 1 indicate that the $\underset{\sim}{a}$ and $\underset{\sim}{b}$ crystal axes lie in the plane of the crystal face, with the $\underset{\sim}{c}$ axis pointing "out" of the face. In this case, the $\hat{a}$ axis would be assigned as the $\hat{i}$ axis, then $\hat{b}$ would lie in the $\hat{i}\hat{j}$ plane, i.e., $\hat{a} = \hat{i}$, $\hat{b} = \hat{i}\cos\gamma + \hat{j}\sin\gamma$.

To convert c into the orthogonal system, a dot product is taken with the first two axes: let $\hat{c} = c_1\hat{i} + c_2\hat{j} + c_3\hat{k}$, then $\hat{c}\cdot\hat{a} = |\hat{c}||\hat{a}|\cos\beta = \cos\beta = c_1$, $\hat{c}\cdot\hat{b} = |\hat{c}||\hat{b}|\cos\alpha = \cos\beta\cos\gamma + \sin\gamma c_2$ and $c_2 = \dfrac{\cos\alpha - \cos\beta\cos\gamma}{\sin\gamma}$. Finally, $\hat{c}\cdot\hat{c} \equiv 1 = (\cos\beta)^2 + (c_2)^2 + c_3^{\,2}$, $c_3 = +\sqrt{1 - (\cos^2\beta) - (c_2)^2}$.

In matrix notation, the result is:

$$\begin{pmatrix} \hat{a} \\ \hat{b} \\ \hat{c} \end{pmatrix} = \begin{pmatrix} a_1 & a_2 & a_3 \\ b_1 & b_2 & b_3 \\ c_1 & c_2 & c_3 \end{pmatrix} \begin{pmatrix} \hat{i} \\ \hat{j} \\ \hat{k} \end{pmatrix} \tag{6}$$

---

[1] The symbol $\hat{c}$ represents a unit vector, while $\underset{\sim}{c}$ represents a crystallographic unit cell axis.

This matrix can be used to convert any (x,y,z) coordinates in the crystal axis system into the orthogonal $\hat{i}\hat{j}\hat{k}$ axis system. To locate this position in the orthogonal system, we first must multiply by the crystal axis lengths:

$$(A,B,C) = (x|\underset{\sim}{a}|,\ y|\underset{\sim}{b}|,\ z|\underset{\sim}{c}|) \tag{7}$$

The following matrix multiplication is then performed accordingly:

$$(A,B,C)\begin{pmatrix} a_1 & a_2 & a_3 \\ b_1 & b_2 & b_3 \\ c_1 & c_2 & c_3 \end{pmatrix}\begin{pmatrix} \hat{i} \\ \hat{j} \\ \hat{k} \end{pmatrix} \tag{8}$$

The following result is obtained:

$$A(a_1\hat{i} + a_2\hat{j} + a_3\hat{k}),\ B(b_1\hat{i} + b_2\hat{j} + b_3\hat{k}),\ C(c_1\hat{i} + c_2\hat{j} + c_3\hat{k}) \tag{9}$$

These expressions are rearranged to yield:

$$(a_1A + b_1B + c_1C)\hat{i},\ (a_2A + b_2B + c_2C)\hat{j},\ (a_3A + b_3B + c_3C)\hat{k} \tag{10}$$

Since the desired result is the position $(I\hat{i},\ J\hat{j},\ K\hat{k})$ in the orthogonal system, it can easily be shown from equations 8-10 that:

$$(I,J,K) = (A,B,C)\begin{pmatrix} a_1 & a_2 & a_3 \\ b_1 & b_2 & b_3 \\ c_1 & c_2 & c_3 \end{pmatrix} \tag{11}$$

Vectors of interest can now be converted to an orthogonal axis system. Dot products and cross products can be taken conveniently between vectors along the molecular axes and the crystal axes. And, polarization

ratios can be calculated for molecular $\underset{\sim}{z}$- or $\underset{\sim}{x},\underset{\sim}{y}$-polarized transitions. Actually, in some cases it is possible to have three polarization ratios, resulting from transitions polarized along either the $\underset{\sim}{x}$, the $\underset{\sim}{y}$, or the $\underset{\sim}{z}$ molecular axis. However, for molecules which possess a C_3 or higher symmetry axis, two of the axes are degenerate, usually $\underset{\sim}{x}$ and $\underset{\sim}{y}$. This is the case we are dealing with, since a molecule with D_{4h} symmetry has a C_4 symmetry axis.

To calculate a polarization ratio for a transition, it is necessary to know the component of the electric vector for the incoming plane-polarized light wave, projected onto the transition moment, for both extinction directions. In reality, it is impossible to determine the orientation or the transition moment (represented by a vector) with respect to the extinction directions, through analysis of polarized spectral measurements of a transition for only one face of a crystal. However, in the case of idealized D_{4h} molecular symmetry, the transition moment for a $\underset{\sim}{z}$-polarized transition will lie along the molecular $\underset{\sim}{z}$-axis, and the transition moments for an $\underset{\sim}{x},\underset{\sim}{y}$ polarized transition will be equal, orthogonal and lie in the molecular $\underset{\sim}{x},\underset{\sim}{y}$ plane. Therefore, in order to interpret polarized spectra for these compounds, the assumption of idealized D_{4h} molecular symmetry in the crystal is made.

Since the intensity of any wave is proportional to its amplitude squared, and the component of the electric vector amplitude ε_o projected on the molecular $\underset{\sim}{z}$-axis is $\varepsilon_o \cos\theta$, where θ is the angle between the $\underset{\sim}{z}$-axis and the extinction, it follows that the intensity of a wave along the $\underset{\sim}{z}$-axis is directly proportional to $\cos^2\theta$.

The method for calculation of polarization ratios in cases where two molecular axes are equivalent has been treated by Piper (24). The following equations can be derived from this treatment:

$$A_1 = \cos^2\theta A_{\underset{\sim}{z}} + \sin^2 A_{\underset{\sim\sim}{xy}} \tag{12}$$

$$A_2 = \sin^2\theta \cos^2\phi A_{\underset{\sim}{z}} + (1 - \sin^2\theta \cos^2\phi) A_{\underset{\sim\sim}{xy}} \tag{13}$$

or

$$A_2 = \cos^2\chi A_{\underset{\sim}{z}} + \sin^2\chi A_{\underset{\sim\sim}{xy}} \tag{14}$$

where A_1 and A_2 represent the absorbances parallel and perpendicular to the extinction direction nearest the molecular $\underset{\sim}{z}$-axis, respectively, and $A_{\underset{\sim}{z}}$ and $A'_{\underset{\sim\sim}{xy}}$ are the absorbances for light polarized along the molecular $\underset{\sim}{z}$ and $\underset{\sim}{x},\underset{\sim}{y}$ directions. The angle θ is the polar angle between $\underset{\sim}{z}$ and the nearest extinction, ϕ is the azimuthal angle measured from $\underset{\sim}{x}$, and χ is the angle between the $\underset{\sim}{z}$ axis and the farther extinction, A_2.

Polarization ratios are calculated by using values of one and zero for $A_{\underset{\sim}{z}}$ and $A_{\underset{\sim\sim}{xy}}$, and vice versa.

3. Refractive index

The indices of refraction for the two perpendicular vibration directions associated with a face of anisotropic crystals were measured by the Becke' line method (46). The measurements involved the examination of crystals immersed in refractive index standards under a polarizing microscope. The standards, which were purchased from the Cargille Company, were calibrated for three discrete wavelengths in the visible region, and their refractive indices could be interpolated for other wavelengths.

The standards allowed an accurate measurement of refractive indices to be made in the approximate range from 1.400 to 1.700, dependent on the wavelength of light used for measurement.

4. Determination of retardation

Once the indices of refraction were known for a particular crystal face, the path length (or thickness) could be determined, if an accurate value for the retardation[1] was available. Accurate values for the retardation were obtained by utilizing a Berek, or tilting compensator manufactured by Leitz-Wetlar (47). The measurements were made at a wavelength of 5461Å by utilizing an interference filter and a white light source. To make a measurement, the low index of refraction of the crystal being examined was aligned with the high index of refraction of the compensator.[2]

The compensator was then rotated until the crystal "extinguished", i.e., the light emerging from the crystal was minimized. Several readings of the rotation angle were taken, and an average value was used to calculate the retardation in microns from a calibration chart supplied with the compensator. Once a retardation value was found, the crystal thickness (in microns) could be determined by dividing the retardation by the difference between the two indices of refraction for the crystal face in question, i.e.,

---

[1]The phase difference between the light waves traveling in the two vibration directions, after they exit a crystal.

[2]The compensator consisted of a calcite crystal with its' high index of refraction aligned with the rotation axis of the compensator.

$$d = \frac{R}{\Delta n_{5461}} \qquad (15)$$

where R = the retardation in microns measured at a wavelength of 5461 Å.

Δn = the difference between the indices of refraction, measured at 5893Å and interpolated to 5461Å.

d = the path difference or crystal thickness in microns.

5. Crystal thickness

While the previously outlined method for measuring refractive indices and retardation values yielded accurate results for crystal thickness, it required optical quality crystal faces, and was a tedious procedure to follow. Accordingly, a much simpler alternative was sometimes utilized, which, though perhaps not as accurate, allowed a direct measurement of crystal thickness. This method involved the use of a microscope eyepiece which contained a scale on one of the cross-hairs. The eyepiece scale was calibrated by examining the millimeter scale of a set of calipers, using the three different objectives of the microscope. The calibration factors were determined to be 41.3 microns/division, 20 μm/div., and 4.4 μm/div. for the low (5.1X), medium (10X), and high (45X) power objectives, respectively. Once these calibration factors were known, the thickness of a crystal could, in favorable cases, be measured by placing the crystal on a glass slide, then observing the crystal under the microscope, using the scaled eyepiece and the appropriate objective. To accomplish this, it was necessary to balance the crystal on its thin edge under the microscope objective. This required a well-formed crystal with a smooth, fairly long edge. For very thin

crystals, this measurement was apparently facilitated when a static electric charge could be transferred to the crystal. The electrostatic forces would then cause the crystals to "stand" on one edge on the microscope slide, thus allowing the thin dimension to be measured under the microscope. Single crystals from 4 to 50 μm thick were successfully measured by this method.

6. Determination of molar absorptivity

It was possible to determine molar absorptivity values from the absorbance spectra recorded for a crystal of a particular compound through the use of Beer's law,

$$A = \varepsilon \cdot \ell \cdot c \tag{16}$$

where A = absorbance

ε = molar absorptivity, $cm^{-1}\ M^{-1}$

ℓ = path length in cm

c = molar concentration of sample.

However, since the spectra were recorded for a crystalline sample on which plane-polarized light impinged, the resultant ε values were only valid for the particular molecular orientation to the plane-polarized light wave as it traversed the crystal, not for any random molecular orientation to an incident unpolarized light wave, as the definition of molar absorptivity implies. Perhaps in this case the values should be referred to as 'specific molar absorptivities'.

In order to calculate these ε values, it was necessary that the crystal thickness (path length) be known for the crystal spectra which were being analyzed.

The molar concentration of the sample was also required. This value could be obtained either from the molecular weight and density, or from the crystallographic unit cell parameters.

It was necessary to calculate the molar absorptivity for only one wavelength, since it was possible to determine ε values for other wavelengths from the ratio of their absorbance values with the absorbance for which the calculation was performed.

7. Solid-state spectra

Once a crystal that appeared suitable for spectroscopy was found, it was examined to determine if it was a single crystal. This was shown by the crystal's extinction between crossed polarizers of a polarizing microscope. A single crystal would extinguish uniformly throughout its entire illuminated area, whereas a twin or multiple crystal would show different extinctions for various sections of the illuminated area. When a crystal was found to be single, it was then carefully sketched, and an extinction (or vibration direction) was characterized by measuring the angle between it and some reproducible feature of the crystal, such as the long (needle) axis or an edge. It was necessary to characterize only one extinction, since the two observable extinctions are required to be perpendicular to one another.

Prior to mounting on a metal plate, the thickness of the crystal was determined by one of the method described previously. The crystal was

then mounted over a hole from ∿30 to 200 μm in diameter (dependent on crystal size), centered on a 1 cm x 2 cm x 3 mil brass or platinum plate. Silicone vacuum grease was used to hold the crystal in place on the metal plate. This plate could then be put in a brass sample holder which was designed for use in the cryostat made by Andonian Cryogenics.

A sketch was then made in order to relate the angular orientation of the crystal and one extinction to the vertical axis of this sample holder (see Figure 8). The orientation of the extinction determined the angle at which the polarizer was set for the spectroscopic measurement, and the second polarizer angle could then be set by adding or subtracting 90^{o} from the first angle setting. It was of utmost importance that these angles be measured accurately and the polarizers be turned to these angles carefully and consistently, since the spectral data were analyzed under the assumption that the electric vector of the incoming plane-polarized light wave was coincident with one of the vibration directions (extinctions) of the crystal. As the polarizer angle is varied, the absorption of polarized light by a crystal is a maximum or a minimum, as mentioned previously, only when the polarizer is aligned with one of the vibration directions of the crystal. Consequently, for transitions with high polarization ratios, the settings of the polarizers were checked by determining the angle setting which produced the highest absorption.

Once the extinction angle had been determined, the brass holder could be screwed in place firmly on the end of the sample holding assembly. This basically was a ∿90 cm long shaft equipped with a sample

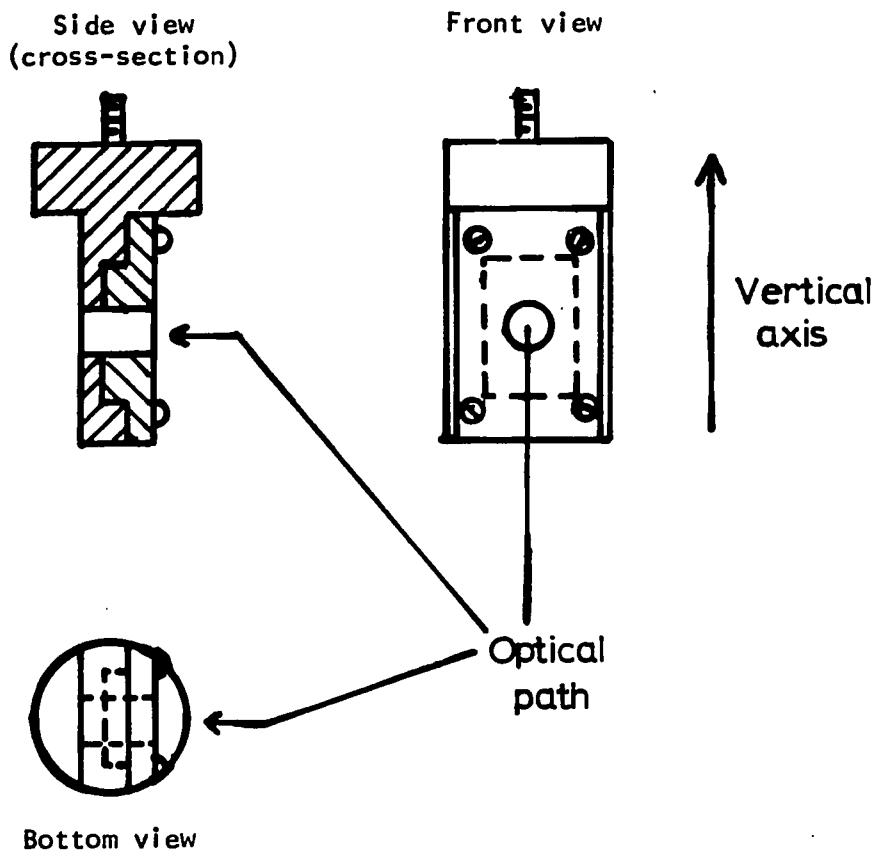

Figure 8. Solid brass sample holder for low temperature spectroscopy

heater and two temperature dependent resistance thermometers (see Figure 9). The germanium resistor allowed accurate temperature measurement in the range from ∿25K to 3K, whereas the platinum resistor had a nearly linear resistance vs. temperature correlation from >300K to 25K, and therefore yielded accurate temperatures in this range. The resistors were powered by a 100 microampere constant current source built by the research group. A switch on this power supply allowed us to select the most accurate resistor for a given temperature. Since the current was held constant, the temperature of the sample was monitored by recording voltage in millivolts on a Sargent model MR recorder. The voltage readings were easily converted to resistance values, which had been calibrated to a temperature scale, by utilization of Ohms' law.

Temperatures in the range from ∿50K to 300K could be maintained constant by utilization of the sample heater (see Figure 9). The sample-holding assembly also allowed for vertical and rotational adjustments of the sample in the light beam, in order to orient the thin dimension of the crystal perpendicular to the beam, and to maximize the light intensity passing through the crystal.

To measure spectra at 5K, the following procedure was used. First, the vacuum space of the Andonian Cryostat (see Figure 10) was pumped to a vacuum on the order of 5×10^{-5} torr by means of an oil diffusion pump. Once this vacuum was attained, the liquid nitrogen dewar of the cryostat was filled. The liquid helium dewar was evacuated and flushed with dry helium gas, to insure that no vapor was present that might freeze the throttle valve. After the liquid helium dewar was filled and a flow of liquid helium into the base of the sample chamber had been

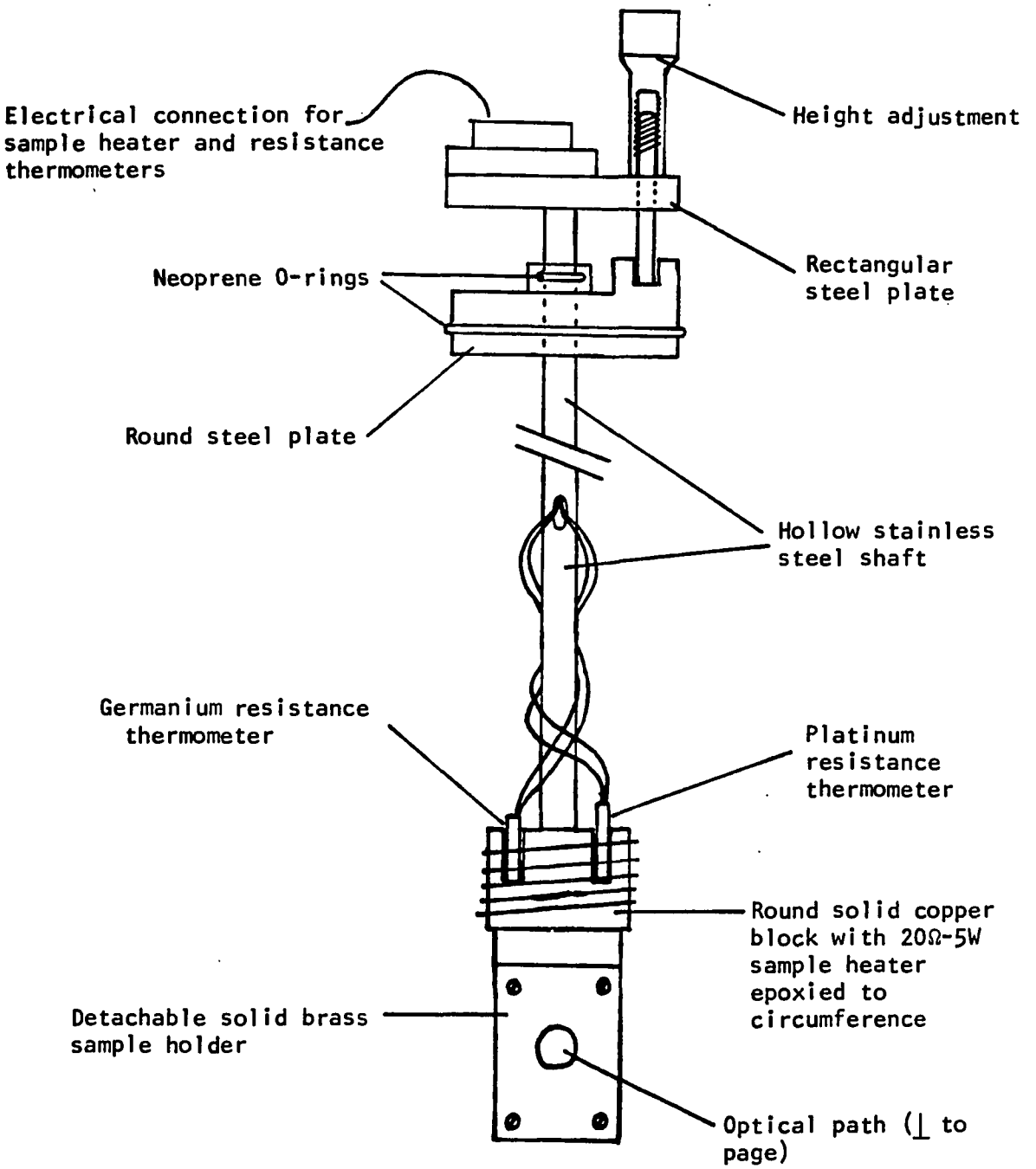

Figure 9. Sample holding assembly for Andonian Cryostat

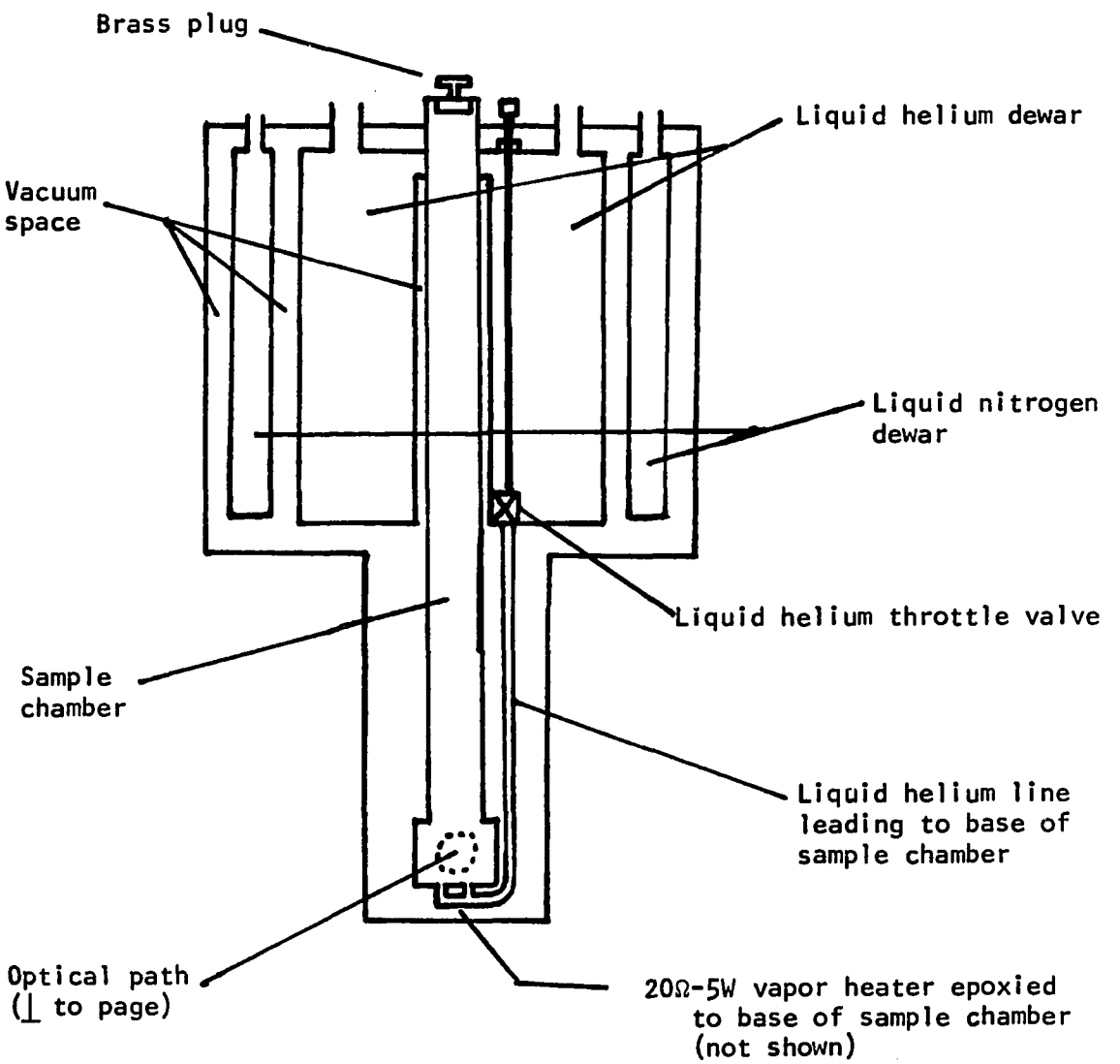

Figure 10. Simplified cross-section of the Andonian Cryogenics Cryostat

established, the top plug of the cryostat was removed, and the sample holding assembly lowered into the sample chamber (see Figure 10).

Once a temperature of ∿10K was attained, the helium flow and heater were monitored and controlled to stabilize the temperature at 5-6K. The cryostat was mounted on a metal frame which supported its weight and centered the optical path of the cryostat in the sample beam of the spectrophotometer. The support also allowed the cryostat to be adjusted horizontally, in order to fully optimize the light intensity passing through a sample.

The spectrophotometer used to record all spectra was a Cary model 14 equipped with a model 1471200 high intensity tungsten-halogen light source and a special product number 50-025-000 Range Modifier. These modifications, and the use of various neutral density screens to attenuate the reference beam, allowed the measurement of a range of ∿3 absorbance units for most crystals, if necessary. Spectra could be recorded in the visible mode from 810 nm to 300 nm through the use of a Varian model R928HA phototube, which was sensitive at long wavelengths (>650 nm). However, for the spectra to be reported here, a Cary model 1460215 phototube was used, which was limited to the range from 600 to 230 nm. This phototube was used because it was more sensitive to wavelengths below 500 nm, which resulted in smaller slit widths, and yielded higher resolution. Plane-polarization of the light beam was effected by two Glan-type calcite polarizers. One polarizer was mounted in the sample compartment and could be rotated by means of an external crank. Under the UV-visible mode, the monochromatic light was polarized before it reached the sample. The polarizer in the reference beam was

rotated by hand to match the sample polarizer, in order to balance absorption due to calcite and cancel out systematic polarization from the spectrophotometer optics.

The use of neutral density screens to attenuate the reference beam was of mixed value. While the attenuation of the reference beam yielded a lower absorbance value on the recorder chart, it also caused the slit width to increase, thus decreasing the resolution. In general, 5K spectra with slit widths larger than ~0.1 mm were rejected as inaccurate because of low resolution.

Baselines were obtained by using a blank pinhole and recording baseline spectra in the cryostat with the same polarizer settings and reference attenuation as the original spectra. All spectral data were automatically punched on cards by an IBM model 29 keypunch, which was interfaced to the Cary 14 via a Cary-Datex digitalization system. The spectra were assembled, baselines subtracted and the finished spectra plotted on a Calcomp plotter by a program developed by previous members of the research group.

B. X-ray Crystallographic Indexing of Crystals

Crystals were routinely indexed on the automatic diffractometer for the following reasons:

(1) to confirm the identity of crystalline material,

(2) to determine which crystal face was being examined spectroscopically, and

(3) to relate the axes of the unit cell to some reproducible morphological feature of a crystal, such as a needle axis.

Any crystal deemed suitable for X-ray analysis was cemented to a glass fiber with a small amount of epoxy, and mounted on a goniometer head. Careful drawings were made to show the relationship between the face(s) and/or long axis of a crystal with respect to the two horizontal adjustment axes of the goniometer head. The alignment of a crystal face with a macroscopic feature of the goniometer head allowed the identification of crystal faces to be more positively made during indexing. The crystals were mounted on the Ames Lab automated four-circle diffractometer, which was interfaced to a PDP-15 computer in a time-sharing mode. Automatic indexing was accomplished by using the interactive program ALICE (48) developed by Dr. R. A. Jacobson. Omega-oscillation photographs were taken for phi values from 0^{o} to 180^{o}, usually in increments of 30^{o}. Several diffraction spots were measured from the photographs and entered into the computerized indexing program. From a set of ten or more diffraction peaks, the crystal was indexed according to the standard guidelines published in Crystal Data (49). When the unit cell parameters were considered to be reasonably accurate, various crystallographic faces could be called (via the computer) into diffracting position, and the crystallographic axes could be placed in a vertical orientation for oscillation photographs. In this way, the observed face(s) and axes of a crystal could be identified. The identity of a compound and the accuracy of the indexed unit cell parameters were determined by comparison with the values from original X-ray crystal structure determinations for the compounds. If the crystal represented a material for which no crystallographic data were available, no

conclusions could be drawn from its spectra until a full X-ray structural determination was completed, either by our group or by other workers.

Positive identification of the crystal face of a compound being examined spectroscopically is essential. If the crystal structure of the material had been previously described, crystal face identification enabled the determination of the molecular axes' orientation with respect to the incident plane-polarized light beam. Accurate results from this analysis were necessary for the proper interpretation of solid-state spectral data for a compound.

C. Synthesis and Characterization of Compounds

1. Tetra-μ-acetatodimolybdenum(II), $Mo_2(O_2CCH_3)_4$

The compound $Mo_2(O_2CCH_3)_4$ was made in high purity by refluxing molybdenum hexacarboxyl, excess glacial acetic acid, and a small amount of acetic anhydride for 12-18 hours at 140-160°C under an atmosphere of dry nitrogen, with O-dichlorobenzene as a solvent. After refluxing, the reaction mixture was allowed to cool in the flask overnight in contact with the oil bath. A mixture of yellow powder and bright yellow crystals formed on the bottom of the flask as it cooled. The product was filtered, then washed with ethanol and ether, and stored in a vacuum desiccator. Crystals would deteriorate in air over a period of several weeks, but could be kept in a vacuum for many months without serious deterioration. The crystals slowly turned a pale green in air, and it was later discovered that high quality crystals of $Mo_2(O_2CCH_3)_4$ could be obtained from the deteriorated material, and from the non-crystalline original product, by subliming them at ca. 270°C under a slow dry nitrogen flow.

The crystals were needle-like prisms which exhibited two clearly distinguishable faces parallel to the needle axis, as Trogler et al. observed (2). In one crystal face, the extinction between crossed polarizers was parallel (within $\pm 2^{\circ}$) to the needle axis, while for the other crystal face the extinction was 11-13° away from the needle axis. It was observed under white light, however, that the extinctions were not sharp for either face. Instead, as the crystal was rotated through "extinction", the color would pass from red to violet to blue, or vice versa, which is indicative of a considerable wavelength dependence for the extinction direction. This effect was more pronounced for the face with the extinction 11 to 13° off-axis. As noted before, such behavior is recognized as a property of a general face of a biaxial crystal.

Several well-formed crystals were cemented to fibers and mounted for indexing on the automated X-ray diffractometer. The cell parameters were refined from a set of reflections and were invariably in good agreement with the values reported by Cotton et al. (50), viz., $\underset{\sim}{a} = 8.418(2)\text{Å}$, $\underset{\sim}{b} = 5.500(1)\text{Å}$, $\underset{\sim}{c} = 7.529(1)\text{Å}$ and $\alpha = 84.13(2)^{\circ}$, $\beta = 105.24(2)^{\circ}$, $\gamma = 106.00(2)^{\circ}$. The needle axis was found to be the $\underset{\sim}{b}$ axis, again in agreement with Trogler et al. It was observed that the faces with extinctions nearly parallel to the needle ($\underset{\sim}{b}$) axis were 0 0 1 or 0 0 $\bar{1}$ faces, whereas the faces with extinctions 11-13° away from the $\underset{\sim}{b}$ axis were 1 0 0 or $\bar{1}$ 0 0. These assignments were verified for several crystals on the automatic diffractometer.

Although the crystals were mostly needles, upon closer examination several large, well-formed crystals were found which had very thin sections projecting off both faces at one end of the crystal in the needle

direction. Whereas the main part of the crystal was 100-200 μm thick, these projections were usually less than 5 μm thick. Examination of these crystals under a polarizing microscope showed that the optical extinctions and absorptions of these thin sections were perfectly aligned with those of the large crystal, which indicated that both the thick and thin sections were part of a single crystal.

Some of these crystals, after spectra were recorded, were mounted on glass fibers for face identification on the diffractometer, in order to confirm absolutely our spectroscopic face assignments. The thickness of large crystal sections was measured by using a calibrated scale in the eyepiece of a microscope. The thickness of thin crystal sections was determined by methods described previously.

The birefringence was obtained from the indices of refraction as determined by the Becke' line method. These indices were as follows: 1 0 0 face, 1.672 and 1.634; 0 0 1 face, 1.671 and 1.631. In each face, the high index of refraction was for the extinction direction near the $\underset{\sim}{b}$ axis. Once the birefringence and the phase difference had been determined, the path length (or crystal thickness) could be easily obtained, as previously described.

2. Tetrakis-μ-(trifluoroacetato)dimolybdenum(II), $Mo_2(O_2CCF_3)_4$

The synthesis of the compound $Mo_2(O_2CCF_3)_4$ was similar to that for $Mo_2(O_2CCH_3)_4$, except that trifluoroacetic acid and trifluoroacetic anhydride were substituted for acetic acid and acetic anhydride, and the reflux was at 100-120°C. The resulting product was more air sensitive, and showed serious deterioration in air within 2-4 days. $Mo_2(O_2CCF_3)_4$ was

recrystallized in high purity by sublimation at ca. 180°C under slow dry nitrogen flow. This compound invariably exhibited only one well-developed crystal face suitable for spectroscopy. The identification of the spectroscopic face, and the verification that the compound was $Mo_2(O_2CCF_3)_4$ were accomplished by examining crystals of the compound on the X-ray diffractometer as previously described. The investigation of several crystals on the X-ray diffractometer yielded results which agreed well with those found by Cotton and Norman (51), viz., $\underset{\sim}{a} = 8.382(8)\text{Å}$, $\underset{\sim}{b} = 9.209(9)\text{Å}$, $\underset{\sim}{c} = 5.568(5)\text{Å}$ and $\alpha = 91.18(4)^\circ$, $\beta = 100.561(7)^\circ$, $\gamma = 89.670(7)^\circ$. The spectroscopic face was invariably 0 1 0 or 0 $\bar{1}$ 0. Despite an extensive search, no thin crystals of this compound were found with a face suitable for spectroscopy, and which could be confirmed by X-ray diffraction, other than the 0 1 0 face.

The $\underset{\sim}{c}$ crystallographic axis is the needle axis for this compound. The extinction was found to be 7-10° off the needle axis, and also exhibited a wavelength-dependence, though not as pronounced as for $Mo_2(O_2CCH_3)_4$. The indices of refraction for $Mo_2(O_2CCF_3)_4$ were not determined, since the compound disintegrated in the refractive index standards. The thickness of thin (<10 μm) crystal sections of this compound were measured reasonably well with the aid of the calibrated eyepiece for a microscope.

3. Potassium diaquo-tetra-μ-sulfatodiplatinum(III), $K_2[Pt_2(SO_4)_4 \cdot 2H_2O]$

The preparation of $K_2[Pt_2(SO_4)_4 \cdot 2H_2O]$ by Muraveiskaya et al. was followed (52). 5.0 g of $K_2Pt(NO_2)_4$ was dissolved in 50 ml of 50% sulfuric acid in a 250 ml beaker. The solution acquired a pale blue

color, which was attributed to the formation of nitrosyl complexes (52). The solution was heated, and the color changed first to dark blue, then dark blue-green, followed by a vigorous effervescent stage during which a brown gas (NO_2) was evolved. The beaker was covered and the solution allowed to heat at $\sim$115°C for about 75 minutes. As the evolution of gas abated, the solution became pale green in color. The cover was removed, in order to reduce the volume of solution to 50 ml. After heating the uncovered solution for 15 minutes at 110°C, the volume was reduced to $\sim$60 ml, the solution had turned brown, and a yellow precipitate had formed.

The solution was heated an additional 15 minutes to insure a good yield of the yellow product, then was cooled to $\sim$60°C and diluted with 25 ml of distilled water. The yellow solid was suction filtered, then washed with cold water, acetone and ether. The yellow powder, identified as $K_2(H_3O)[Pt_2(SO_4)_4(OH)(H_2O)]$ by Muraveiskaya et al. (52), was recrystallized by dissolving a small amount in a minimum quantity of hot distilled water in a crystallizing dish, followed by slow evaporation of the solution. A small amount (5-10 ml) of 0.1N sulfuric acid was added to inhibit dissociation of the product.

It was claimed by Orlova et al. (39) that recrystallization of $K_2(H_3O[Pt_2(SO_4)_4(OH)(H_2O)])$ from hot distilled water yielded the compound $K_2[Pt_2(SO_4)_4 \cdot 2H_2O]$, so it has been assumed that our recrystallized product had this identity. Muraveiskaya et al. proposed that the complex was formed via the following reaction sequence (52):

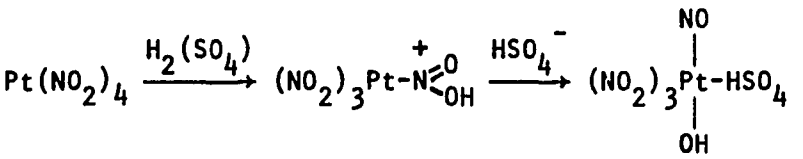

(A) (B)

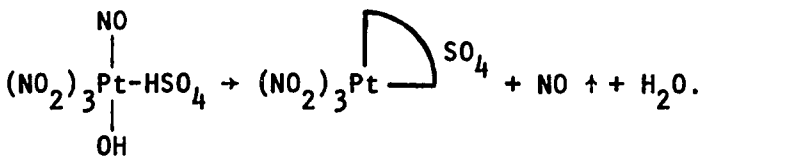

They identified the blue color of the starting solution as due to the intermediate species (B). The remainder of the observed color changes may then be attributed to a continuously changing ratio of the blue species and the yellow-brown end product. The X-ray crystal structure of this compound was solved by Muraveiskaya et al. (7). They reported interatomic distances, but without standard deviations, and they did not include the atomic positions in the unit cell. Their published cell parameters were as follows: a = 7.471(3)Å, b = 9.523(3)Å, c = 7.621(3)Å and $\alpha = 50.75(2)^{\circ}$, $\beta = 69.20(2)^{\circ}$, $\gamma = 64.80(2)^{\circ}$; space group $P\bar{1}$, cell volume = 375.8(4)Å^3, Z = 1.

It should be noted that this is a non-standard unit cell, according to the guidelines published in Crystal Data (49), which are used by the majority of X-ray crystallographers, as well as by Professor R. A. Jacobson's X-ray crystallography group at Iowa State University.

A well-formed crystal of $K_2[Pt_2(SO_4)_4 \cdot 2H_2O]$ was cemented to a glass fiber and mounted on a goniometer head for indexing on the Ames Laboratory four-circle diffractometer. From a set of diffraction peaks, the platinum

sulfate compound was indexed to a unit cell, according to the standard guidelines previously mentioned. The following unit cell parameters were found: $\underset{\sim}{a} = 7.539(2)\text{Å}$, $\underset{\sim}{b} = 7.621(2)\text{Å}$, $\underset{\sim}{c} = 7.458(3)\text{Å}$ and $\alpha = 110.85(3)^{\circ}$, $\beta = 100.22(3)^{\circ}$, $\gamma = 102.27(3)^{\circ}$. Space group = $P\bar{1}$, cell volume = $375.9(2)\text{A}^3$. These cell parameters could be converted to the original parameters published by Muraveiskaya et al. via multiplication of the axes by the following matrix:

$$\begin{pmatrix} 0 & 0 & 1 \\ -1 & -1 & 0 \\ 0 & -1 & 0 \end{pmatrix}$$

The fact that our unit cell could be converted to the original published cell parameters proved that our unit cell was valid for $K_2[Pt_2(SO_4)_4 \cdot 2H_2O]$, and that we indeed had the same compound for which the X-ray crystal structure had been determined by the original workers.

Since no atom positions were published, it was necessary to collect a set of X-ray diffraction data for a crystal of $K_2[Pt_2(SO_4)_4 \cdot 2H_2O]$. Once again, a crystal of this compound was cemented to a glass fiber and mounted on a goniometer head, then indexed to a standard unit cell as described previously. Data were collected at room temperature on the Ames Laboratory automated four-circle diffractometer, which is equipped with a scintillation counter. Graphite monochromated Molybdenum-Kα X-radiation ($\lambda = 0.71034\text{Å}$) was used for data collection with a take-off angle of 4.5°. A scan rate of 0.5 sec/step of 0.01° in omega was employed, with the scan range dependent on peak width. Peaks were scanned until background was encountered, as determined by the criterion

count $\leq$ background + σ (background). Stationary crystal, stationary counter background counts were taken at the beginning and end of each scan.

All data within a 2θ sphere of 50^{o} ($\sin\theta/\lambda = 0.595$) in the $hk\ell$, $hk\bar{\ell}$, $h\bar{k}\ell$, and $\bar{h}k\bar{\ell}$ octants were measured by this technique. Of the 1652 measured reflections, 1367 were considered observed ($|F_o| > 3\sigma_{F_o}$),[1] and from these 825 independent reflections were obtained. As a monitor of crystal and instrument stability, the intensities of three standard reflections were remeasured after every 75 reflections. If the intensities of the standard reflections decreased significantly ($>6\sigma_{F_o}$), the diffractometer would automatically re-optimize the positions of these reflections to maximize the intensities. The intensities of the standard reflections did not vary significantly throughout data collection. The intensity data were collected for Lorentz polarization effects, but no absorption correction was applied.

The estimated error in each intensity was calculated by the equation:

$$\sigma_I^2 = C_T + K_t C_B + (0.03\ C_T)^2 + (0.03\ C_B)^2 \qquad (17)$$

where C_T = Total Count

K_t = counting time factor

C_B = background count

The factor 0.03 represents an estimate of non-statistical errors inherent in the measuring process. The estimated deviations in the structure

---

[1] F_o = observed structure factor, σ_{F_o} = estimated standard deviation for F_o.

factors were calculated by the finite difference method (53). Data reduction and averaging was accomplished by using the program FDATA (54). The space group was assumed to be $P\bar{1}$, based on results of the Howells, Phillips and Rogers test (55) for a center of symmetry. The position of the unique platinum atom was obtained from a computer generated three-dimensional Patterson function.

The position of the unique platinum atom was subjected to block-diagonal least-squares refinement, as it was only necessary to refine one platinum atom position to define the molecular z-axis (Pt-Pt bond axis) orientation in the unit cell. Fourier synthesis for three-dimensional Patterson maps and electron density maps were performed through use of the computer program FOUR (56).

4. Tetra-μ-acetatodimolybdenum(II)·potassium chloride, $Mo_2(O_2CCH_3)_4 \cdot KCl$

This synthesis was very similar to the $Mo_2(O_2CCH_3)_4$ synthesis. A mixture consisting of 5 g molybdenum hexacarbonyl, 4.5 g potassium chloride, 200 ml of 75% acetic acid and 80 ml of O-dichlorobenzene was refluxed overnight at ~150°C under a nitrogen atmosphere. After the refluxing, the reaction mixture was allowed to cool in the flask, in contact with the oil bath. Upon cooling, a mixture of powder and crystals formed. Two types of crystals were found to be growing in the solution; one type were small, yellow and needle-like (the normal $Mo_2(O_2CCH_3)_4$), while the second type were large, gold-yellow polyhedra. The mixed product was filtered, washed with methanol and stored in a vacuum desiccator.

A portion of this mixed product has been exposed to air for over a year. While most of the new compound and all of the $Mo_2(O_2CCH_3)_4$ had

deteriorated after a year, some undeteriorated crystals of the new compound could be found in this sample. No recrystallization or purification of the new compound was attempted, since many large, single crystals could easily be obtained from the original product. A high quality, trigonal-antiprismatic shaped crystal of this new product was cemented to a glass fiber and mounted on a goniometer head for indexing on the automated diffractometer. From several oscillation photographs, standard programs were utilized to index the crystal to a standard set of monoclinic axes, which yielded the following preliminary unit cell parameters: $\underset{\sim}{a} = 9.56\text{Å}$, $\underset{\sim}{b} = 12.74\text{Å}$, $\underset{\sim}{c} = 11.92\text{Å}$ and $\alpha = 90.1^{\circ}$, $\beta = 97.7^{\circ}$, $\gamma = 90.0^{\circ}$; cell volume = 1440Å^3, $Z = 4$.

The details of X-ray diffraction data collection have already been described. Data for the $hk\ell$, $\bar{h}k\ell$, $\bar{h}k\bar{\ell}$, and $h\bar{k}\ell$ octants within a 2θ sphere of 50° ($\sin\theta/\lambda = 0.595$) were collected. From a total of 4577 reflections, 2913 were considered observed, and from these 1289 independent reflections were obtained. As a monitor of crystal and instrumental stability, the intensities of three standard reflections were remeasured after every 75 reflections. The standard reflections did not vary significantly in intensity throughout data collection. After data collection, 19 moderately intense reflections were entered into the program LATT (57) on the automatic diffractometer. This program remeasured and retuned the reflections to yield the following refined unit cell parameters and standard deviations: $\underset{\sim}{a} = 9.601(2)\text{Å}$, $\underset{\sim}{b} = 12.799(3)\text{Å}$, $\underset{\sim}{c} = 11.964(2)\text{Å}$ and $\alpha = 90.00^{\circ}$, $\beta = 97.59(3)^{\circ}$, $\gamma = 90.00^{\circ}$. Cell volume = $1457.4(5)\text{Å}^3$

These parameters were used in the subsequent steps in the solution of the crystal structure. The intensity data were corrected for Lorentz

polarization effects, and an absorption correction (58) was applied with a calculated absorption coefficient, (μ), of 21.9 cm^{-1}. The estimated errors in intensities and the deviations of the structure factors were determined as in the previous section.

a. Solution and refinement of structure The space group was assumed to be centric, on the basis of results from the Howells, Phillips and Rogers test (55). Examination of extinction conditions for certain reflections led to the conclusion that the space group must be C-centered, monoclinic. Possible space groups to consider were C2/c, C2/m, Cm, Cc, and C2. Since the statistical test indicated a center of inversion, three of the space groups were eliminated, leaving only C2/m and C2/c.

The fact that only $h0\ell$ reflections with $\ell = 2n$ were observed verified that the space group was C2/c. The position of the unique molybdenum atom was obtained from this Patterson map. The positions of the potassium atom, chlorine atom and remaining non-hydrogen atoms were obtained from successive structure factor and electron density map calculations. In addition to positional parameters for the eleven unique atoms in the unit cell, the anisotropic thermal parameters for all non-hydrogen atoms were refined by a full-matrix least-squares procedure (55), minimizing the function $\Sigma\omega(|F_o|-|F_c|)^2$ where $\omega = 1/\sigma_{F_o}{}^2$.[1] Statistical adjustment of the weights (ω) was performed, utilizing the requirement that $\omega(|F_o|-|F_c|)^2$ should be a constant function of $|F_o|$ and $(\sin\theta)/\lambda$ (59). Successive iterations of refinement on the 1289 independent reflections produced

---

[1] F_o = observed structure factors, F_c = calculated structure factors, and σF_o = estimated standard deviations of the observed structure factors.

final discrepancy factors of $R_u = 0.033$ and $R_w = 0.053$, as defined by the following equations:

$$R_u = \Sigma||F_o|-|F_c||/\Sigma F_o \quad (18)$$

$$R_w = [\Sigma\omega(|F_o|-|F_x|)^2/\Sigma\omega|F_o|^2]^{\frac{1}{2}} \quad (19)$$

The scattering factors used for non-hydrogen atoms were those of Hanson et al. (60), modified for the real and imaginary parts of anomalous dispersion (61). The final positional and thermal parameters are listed in Table 5. The standard deviations were calculated from the inverse matrix of the final least-squares cycle, and the final observed and calculated structure factors are listed in the Appendix.

Table 5. Final non-hydrogen atom positional[a] and thermal[b] parameters and their estimated standard deviations[c]

Atom	x	y	z	B_{11}
Mo(1)	0.31313(2)	0.68336(2)	0.49609(2)	2.03(2)
Cl(1)	0.5000	0.5000	0.5000	4.31(6)
K(1)	0.5000	0.5248(1)	0.2500	5.32(6)
O(1)	0.3463(2)	0.7178(2)	0.3277(2)	2.61(9)
O(2)	0.2112(2)	0.8584(2)	0.3346(2)	2.90(9)
O(3)	0.4962(2)	0.7669(2)	0.5594(2)	2.3(1)
O(4)	0.3625(2)	0.9075(2)	0.5702(2)	2.75(9)
C(1)	0.2887(4)	0.7997(3)	0.2827(3)	2.3(1)
C(2)	0.3107(4)	0.8284(3)	0.1644(3)	3.3(2)
C(3)	0.4812(4)	0.8631(3)	0.5844(3)	2.8(1)
C(4)	0.6104(4)	0.9245(3)	0.6304(3)	3.2(2)

[a] In fractional coordinates.

[b] The B_{ij} are defined by the equation $T = \exp[-\frac{1}{4}(B_{11}h^2a^{*2} + B_{22}k^2b^{*2} + B_{22}\ell^2c^{*2} + 2B_{12}hka^*b^* + 2B_{13}h\ell a^*c^* + 2B_{23}k\ell b^*c^*]$.

[c] In parentheses for the least significant figure.

B_{22}	B_{33}	B_{12}	B_{13}	B_{23}
1.15(2)	1.69(2)	0.0121(6)	0.18(1)	0.053(5)
2.28(5)	2.06(5)	1.58(4)	0.34(4)	0.07(3)
4.69(6)	2.22(5)	0	0.42(4)	0
2.0(1)	2.25(9)	-0.0(1)	0.27(6)	-0.30(6)
2.4(1)	2.20(9)	-0.15(8)	0.50(7)	0.12(6)
2.4(1)	3.0(1)	0.05(7)	-0.05(7)	0.06(7)
2.23(8)	2.25(9)	-0.19(7)	0.05(7)	-0.18(6)
2.6(1)	1.8(1)	-0.5(1)	-0.1(1)	0.0(3)
3.7(2)	2.1(1)	-0.4(1)	0.7(1)	0.4(1)
2.2(1)	1.9(1)	-0.5(1)	0.2(1)	0.4(1)
2.8(1)	3.8(2)	-0.9(1)	-0.3(1)	-0.0(1)

III. RESULTS AND DISCUSSION

A. $Mo_2(O_2CCH_3)_4$ and $Mo_2(O_2CCF_3)_4$

Single crystal absorption spectra are usually treated on the basis of the well-known phenomenon that in the absence of optical activity for non-absorbing crystals, light of any wavelength is transmitted through the crystal as two independent plane waves polarized in orthogonal planes. As mentioned before, if the two waves are absorbed differently, the maximum and minimum in the absorption will occur with the polarizers aligned with these extinction directions. It is usually convenient, if possible, to set the polarizer angle where maximum absorption of a strongly dichroic[1] band is observed, and at 90° to this angle, for recording spectra. This check was considered especially important for $Mo_2(O_2CCH_3)_4$, since the microscopic observations indicated an observable wavelength dependence of the extinction direction. When the intensity of individual vibration lines in the low temperature spectra were measured as a function of polarizer angle, it was found that the line intensities maximized a considerable angle away from the extinction observed under the polarizing microscope.

Spectra for the low energy region of the band were therefore recorded at a temperature of 5K for a series of polarizer angles with increments no larger than 10° through 180°. Several of these spectra are shown for the 0 0 1 face and the 1 0 0 face in Figures 11 and 12, respectively. A number of vibrational progressions are evident from the spectra, and important

---

[1] Dichroism is the unequal absorption of plane-polarized light for the two vibration directions observed for an anisotropic crystal face.

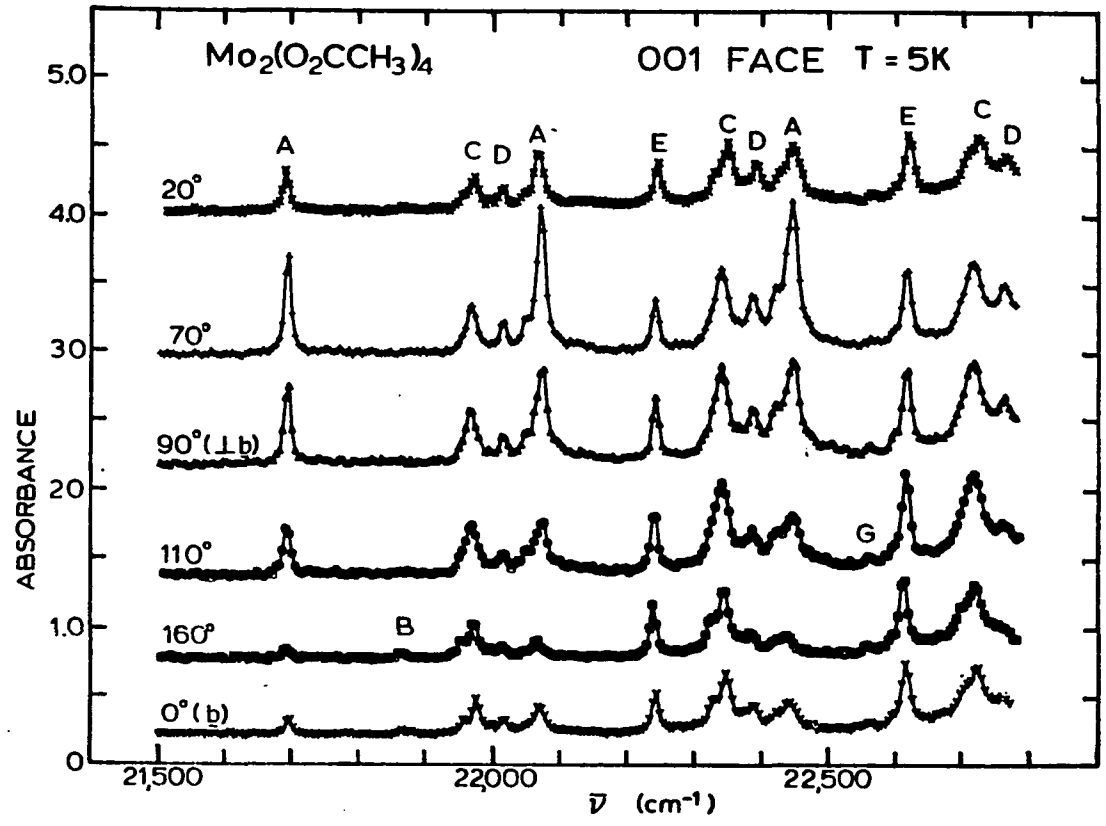

Figure 11. Absorption spectra at various polarization angles for the 0 0 1 face of $Mo_2(O_2CCH_3)_4$. The crystal was 4.2 μ thick, and absorbances can be converted to molar absorptivities by multiplying the absorbance by 463 M^{-1} cm^{-1}. 70° and 160° are the closest spectra to A_{max} and A_{min}, and 110° and 20° are the closest spectra to E_{max} and E_{min}, respectively

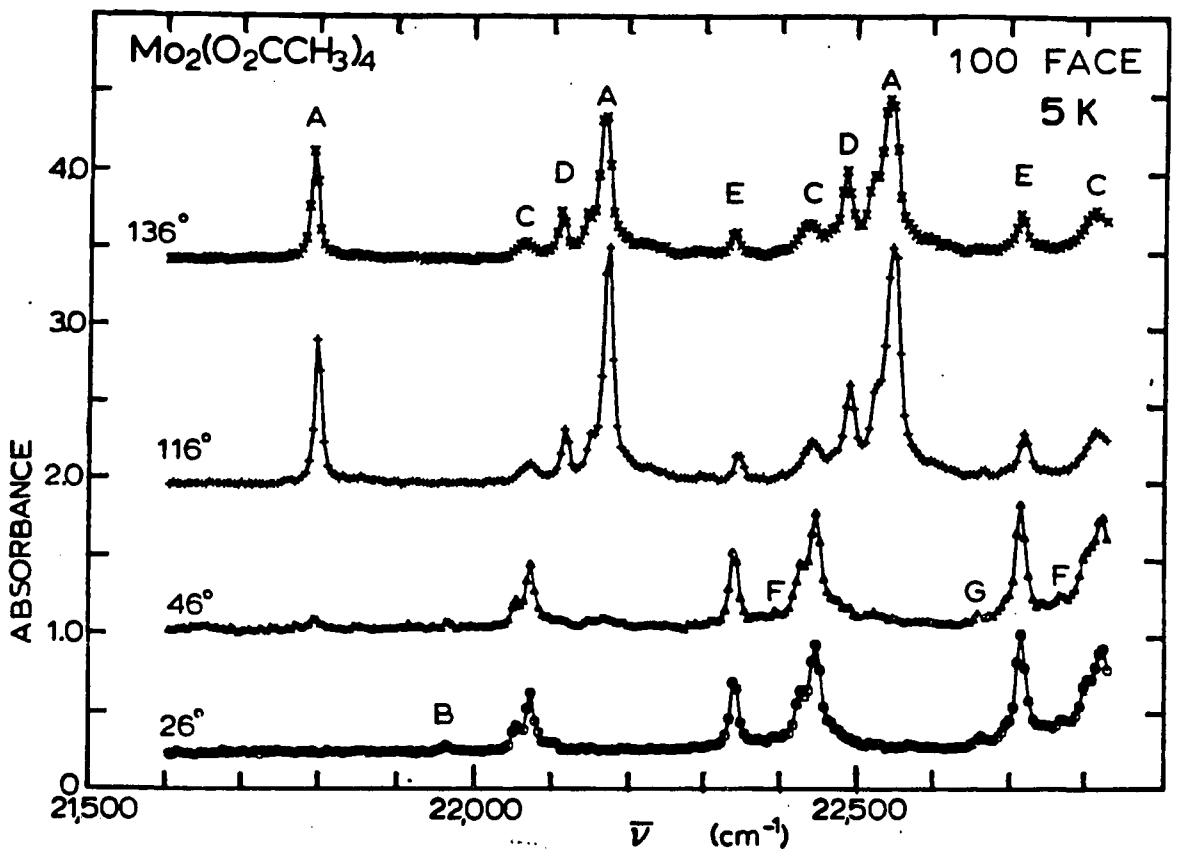

Figure 12. Absorption spectra at various polarization angles for the 100 face of $Mo_2(O_2CCH_3)_4$. The crystal was 3.8 μ thick, and absorbances can be converted to molar absorptivities by multiplying by 490 M^{-1} cm^{-1}. 116° and 26° are the closest spectra to A_{max} and A_{min}, while 46° and 136° are the closest to E_{max} and E_{min} respectively

lines have been labeled. These spectra, which contain many highly resolved vibrational features, were recorded with the slowest available scan speed of 0.05 nm/sec. Absorbance values were punched each 0.1 nm on cards to be plotted as shown. Wavenumbers of resolvable vibrational peaks and shoulders have been recorded in Table 6. The lowest energy feature in the spectra is a line at 21,700 cm^{-1}, (A0 in Table 6 which is the origin of a progression for which 5 additional terms are also listed). Other strong progressions, labeled C and E, have origins at 275 and 545 cm^{-1}, respectively, above A0. In addition, there were a number of weaker progressions, only some of which are labeled in Figures 11 and 12.

Polarizer angles in the figures have been shown as the angle in degrees measured in a clockwise direction, as observed from the direction of the entering light beam on the 1 0 0 or the 0 0 1 faces. For the $\bar{1}$ 0 0 or 0 0 $\bar{1}$ faces rotation would be in the opposite directions. This convention has been followed for all crystal spectra to be presented, unless otherwise stated. Trogler et al. (2) apparently recorded spectra for the 0 0 1 face. The 0^{o}-$\underset{\sim}{b}$ and 90^{o}-$\perp\underset{\sim}{b}$ spectra in Figure 11 appear to agree very well with their spectra, although some additional features can be recognized in the present plots. It is evident in Figure 11 that the A peak at 70^{o} is clearly higher than that at 90^{o}, and accordingly the A peak is smaller at 160^{o} than at 0^{o}. On the other hand, although not so clearly evident, the E peak was higher at 110^{o} than at 70^{o} or 90^{o}, and lower at 20^{o} than at 0^{o} or 160^{o}. Thus, it was observed that the A peaks and the E peaks attained maxima and minima at well separated polarization

Table 6. Vibrational details in the absorption spectra of $Mo_2(O_2CCH_3)_4$

Progression	$\bar{\nu}$, cm^{-1}	$\Delta\bar{\nu}$,[a] cm^{-1}
A-1	21,300	-400
C'	21,405	(-295)
C-1	21,575	-400
A0	21,700	--
	21,725 (sh)	(25)
	21,760 (vw)	(60)
	21,780 (vw)	(80)
	21,830 (vw)	(130)
B0	21,875 (w)	(175)
	21,955 (w)	(255)
C0	21,975	(275)
D0	22,020	(320)
	22,055	(355)
A1	22,075	375
E0	22,245	(545)
F0	22,290 (vw)	(590)
	22,325	370
C1	22,345	370
D1	22,390	370
	22,425	370
A2	22,445	370

[a]Values in parentheses give the difference $\Delta\bar{\nu}$ from the A0 line. Values without parentheses give the difference $\Delta\bar{\nu}$ from the preceding line in the progression.

Table 6. Continued

Progression	$\bar{\nu}$, cm^{-1}	$\Delta\bar{\nu}$,[a] cm^{-1}
G0	22,565	(865)
	22,600 (sh)	(900)
E1	22,620	375
F1	22,665 (vw)	375
	22,700 (w)	375
C2	22,720	375
D2	22,765	375
A3	22,830	375
G1	22,935 (w)	370
E2	22,985	360
C3	23,085	365
D3	23,135	370
A4	23,185	365
G2	23,310 (w)	375
E3	23,360	375
C4	23,455	370
D4	22,495	360
A5	23,550	365
G3	23,680 (w)	370
E4	23,735	375

angles for both the 0 0 1 and the 1 0 0 faces, and the polarization angles for these maxima and minima were significantly removed from the optical extinctions measured at room temperature between crossed polarizers.

The preceding observations suggested that perhaps the assumption of plane polarization for the traversing light waves should be questioned. The deviation from plane polarization to elliptical polarization would be more serious in a region of high absorption. The A peaks are some of the most intense absorption features in the $Mo_2(O_2CCH_3)_4$ spectra. It can be seen from Figure 12 that the A intensity virtually disappears at 26^o; therefore it can be concluded that ellipticity of the light at the wavelength of this band must be sufficiently great that it can be considered essentially a plane wave. The rotation of the vibration planes evident from the spectra must therefore result from variations in the real part of the refractive indices, which are recognized to fluctuate in the vicinity of absorption regions.

The A0 and E0 peaks were well-separated from other strong absorption lines. Hence the height of these peaks above the level of recorded absorbance in their proximity has been plotted in Figure 13 for the two faces. A procedure utilized by Stewart and Davidson (62) served to evaluate the intensity of absorption and the orientation of the plane waves at each of these peaks. The absorbance, Ab, is related to polarization angle, ϕ, by the expression,

$$10^{-Ab} = 10^{-Ab_{max}} \cos^2(\phi-\theta) + 10^{-Ab_{min}} \sin^2(\phi-\theta) \qquad (20)$$

where Ab_{max} and Ab_{min} are the absorption intensities of the two plane waves, and θ is the polarization angle for the wave with the higher absorption, Ab_{max}.

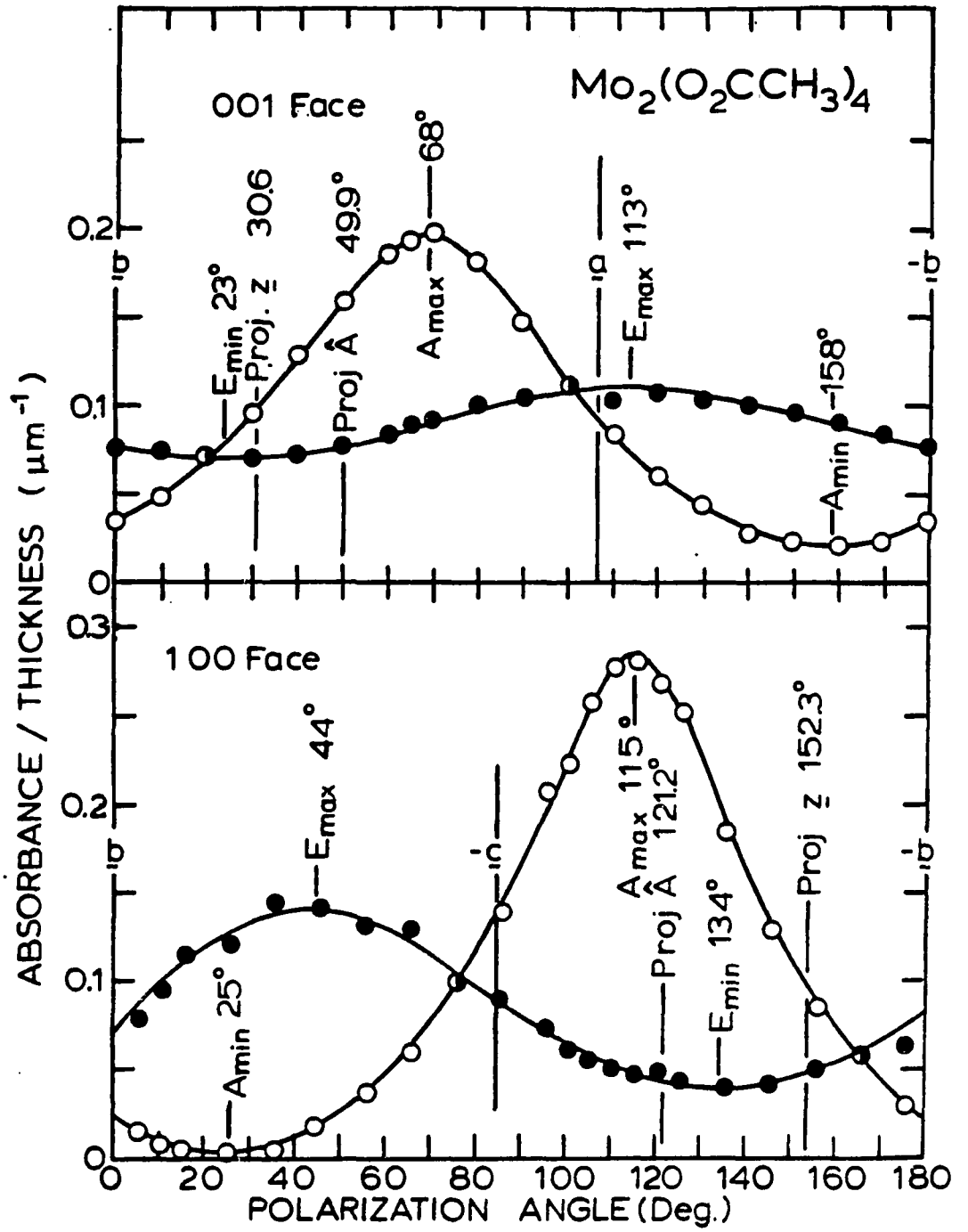

Figure 13. Peak heights recorded for the A0 and E0 peaks for the 0 0 1 and 1 0 0 faces as a function of polarizer angle. Open circles are for the A0 peak and solid circles are for the E0 peak. Curves are least squares fit

Values for Ab_{max}, Ab_{min} and θ were then determined by a non-linear least squares treatment of the data. In Table 7 are presented values for A_{max}/L, A_{min}/L and θ (where L is the crystal thickness) from the least squares computation for the A0 and E0 peaks of each face. For the A0 peaks, which have very high polarization ratios, the orientation of the vibration planes was determined with an uncertainty of only $\pm 1^{o}$. The planes for the E peak with much lower polarization ratios are given with the larger uncertainty of $\pm 3\text{-}5^{o}$.

a. Orientation of transition moments A transition moment may be assigned to the absorption of radiation from the $\underline{v}^{o}$-th vibration level of a ground state (g) to the $\underline{v}'$-th vibrational level of an excited state (f). Within the Born-Oppenheimer approximation this transition moment is given by the expression:

$$\underset{\sim}{M}_{gv^{o},fv'} = \langle \chi_{v^{o}}(..Q_i..)\ \psi_g(..x_j..Q_i..)\ |\Sigma \underset{\sim}{er}|\ \psi_f(..x_j..Q_i..)\ \chi_{v'}(..Q_i..) \rangle \qquad (21)$$

where the $...x_j...$ are electron coordinates, $...Q_i...$ are normal vibrational coordinates of the nuclei, and $\Sigma \underset{\sim}{er}$ is the usual dipole operator, a function of the electron coordinates. $\underset{\sim}{M}_{gv^{o},fv'}$ is a vector quantity, and the intensity of the absorption is proportional to the square of the length of this vector.

For the absorption of a face, the following equation has been derived from equations 14 and 16:

$$\frac{Ab_{max}}{Ab_{min}} = \frac{\cos^2\theta_1}{\cos^2\theta_2} = \frac{\cos^2\theta'_1}{\cos^2\theta'_2} \qquad (22)$$

where θ_1 and θ_2 are the angles between $\underset{\sim}{M}_{gv^{o},fv'}$ and the direction of the maximum and minimum polarizations, respectively. θ'_1 and θ'_2

Table 7. Least squares values of absorption parameters for the A and E origin peaks of $(Mo_2(O_2CCH_3)_4$

Peak	A0(1 0 0)	E0(1 0 0)	A0(0 0 1)	E0(0 0 1)
Ab_{max}/L (μ^{-1})	0.284 ± .008	0.142 ± .007	0.196 ± .004	0.109 ± .005
Ab_{min}/L (μ^{-1})	0.003 ± .004	0.041 ± .005	0.021 ± .002	0.071 ± .005
θ (deg.)	115 ± 1	134 ± 3	68 ± 1	113 ± 5
Ab_{max}/Ab_{min}	83.1	3.38	9.36	1.51

are the angles between the projection of $M_{\sim gv^o,fv'}$ in the crystal face and the directions of the maximum and minimum polarizations.

As stated before, if the absorptions are observed for only one face, the orientation of $M_{\sim gv^o,fv'}$ cannot be determined. Rather, the molecular transition moment is assigned to the various molecular symmetry axes. Then, the polarization ratio is calculated to determine which gives the best agreement with the observed ratio, Ab_{max}/Ab_{min}.

Since molecular $Mo_2(O_2CCH_3)_4$ possesses D_{4h} point group symmetry, a line will appear in the molecular spectrum when the product of the total electronic-vibrational wave functions in equation 21, viz., $\chi_{v^o}\cdot\psi_g\cdot\psi_f\cdot\chi_{v'}$ is a basis function for A_{2u} or E_u. However, the $Mo_2(O_2CCH_3)_4$ molecule occupies a site of much lower symmetry than D_{4h}, viz. $\bar{1}$ in the crystal. The crystal fields therefore may compromise the molecular symmetry. Many more transition moments may now be non-zero. Transition moments may also be shifted in space. The degenerate transitions under D_{4h} may now be separated in energy, and the orthogonality of the two transition moments is no longer required. In such cases, crystal spectra will retain their value to the extent that the crystal field perturbations to the D_{4h} symmetry are sufficiently small. The shifts in transition energies and moments will then not be so great but that impositions of molecular symmetry can still be recognized, even though they are not absolute.

The availability of intensities for two faces of crystals has provided considerably more information about the transition moment orientation than the spectra of a single face. For the A0 peak the polarization ratios, Ab_{max}/Ab_{min}, were 9.36 and 83.1 for the 0 0 1 and the 1 0 0 faces

respectively. Since the dihedral angle between these faces is 75.8^{o}, such high polarization ratios in these two faces would not be possible for a degenerate pair of equal orthonormal transition moments. Hence, the A0 peak must be considered as due to a single transition moment. From equation 22, since $|\theta_2'|=|90^{o}-\theta_1'|$, the transition moment is required to be in a plane normal to the 0 0 1 face which cuts the 0 0 1 face at the angle, $\cot^{-1}(9.36)^{\frac{1}{2}}$ or 18.1^{o} away from the $A_{max}(0\,0\,1)$ direction. There are two such planes possible, one on each side of $A_{max}(0\,0\,1)$. From the polarization ratio of 83.1 for the 1 0 0 face, the transition moment must lie in either of two planes normal to this face which cut it at angles of 6.3^{o} away from $A_{max}(1\,0\,0)$. The intersection of the two planes normal to 0 0 1 with the two normal to 1 0 0 give four possible orientations for the A0 transition moment. A choice between these four possible orientations can be based on the relative intensities in the two faces. This ratio should be given by the ratio of the vector dot products,

$$A_{max}(1\,0\,0)\cdot L(0\,0\,1)/A_{max}(0\,0\,1)\cdot L(1\,0\,0) = \left[\hat{A}\cdot\hat{A}_{max}(1\,0\,0)/\hat{A}\cdot\hat{A}_{max}(0\,0\,1)\right]^{2} \qquad (23)$$

where $\hat{A}$ is a unit vector in the direction of the transition moment, $\hat{A}_{max}$ is a unit vector in the indicated polarization direction, and the L's are the crystal thicknesses.

Calculated values for the four possible ratios are: 1.69, 0.19, 0.049, and 4.40. The observed value, evident from Figure 13, was 1.42. Accordingly, the first vector gives by far the best agreement with the observed ratio, and has been taken as $\hat{A}$, the unit vector which defines the direction of the A0 transition moment. The projections of this vector

for both faces are shown in Figure 13, which also includes the projection of the molecular axis, $\underset{\sim}{z}$, on each face. $\hat{A}$ is oriented in space some 33.9^{o} away from $\underset{\sim}{z}$. We have concluded therefore that the A progression represents a series of single transition vibrational lines with $\underset{\sim}{z}$ polarization, for which the molecular polarization has been shifted from the molecular axis by the crystal field perturbations. If these correspond to one member of a degenerate pair, split by the crystal field, as Trogler et al. (2) proposed, it would correspond to a shift from the molecular polarization which must be 90^{o} to $\underset{\sim}{z}$.

The data from the E peak were treated similarly, on the basis of the assumption that is was due to a single non-degenerate transition. Again, the intersection of four planes yielded four possible transition moment vectors, which gave ratios between the two faces of 1.39, 14.1, .108 and 1.10. Since the experimental ratio was 1.31, the second and third vectors could be eliminated, but either first and fourth seemed feasible, although the first gave somewhat better agreement with experiment. The first vector proved to be 88.5^{o} away from the molecular $\underset{\sim}{z}$ axis and 87.0^{o} away from $\hat{A}$, whereas the fourth vector was 66.3^{o} away from the molecular $\underset{\sim}{z}$ axis and 47.7^{o} away from $\hat{A}$.

The C and the D peaks have other absorption features near them, so a quantitative least squares treatment of their absorbance vs. polarization angle was not attempted. However, it can be seen qualitatively from Figures 11 and 12, and it was still more evident from the total set of spectra that the D peaks followed the polarization of the A peaks, and the C peaks followed closely the polarization of the E peaks. Hence, if C and E each represent a single transition, normal to the molecular $\underset{\sim}{z}$ axis,

which has been split away from another member of a degenerate pair, there appear to be no other lines in the crystal spectra of comparable intensity corresponding to the other transition. Moreover, although a pair of normal transition moments for a truly degenerate transition might give a high polarization ratio for either of the 1 0 0 or 0 0 1 faces, it would then be required to yield a low polarization ratio for the other face. The low value of 1.52 for the 0 0 1 face suggests that E might therefore be due to such a pair of degnerate molecular transitions. For consideration of this possibility, a unit vector $\hat{N}$ was defined which would be perpendicular to a pair of equal and normal transition moments. For true molecular x,y polarized transitions, $\hat{N}$ would be the molecular $\underset{\sim}{z}$ axis. The polarization ratio for each face, derived from equation 22, is:

$$\frac{E_{max}}{E_{min}} = \frac{\sin^2\theta_1}{\sin^2\theta_2} = \left[\frac{\hat{N} \times \hat{E}_{max}}{\hat{N} \times \hat{E}_{min}}\right]^2 \qquad (24)$$

where $\hat{E}_{max}$ and $\hat{E}_{min}$ are unit vectors in the extinction directions.

The substitution of the polarization ratios for the E0 peak in the 1 0 0 and the 0 0 1 faces into expression 24 gave two equations involving the three components of the $\hat{N}$ vector, and the normalization requirement of $\hat{N}$ provided a third equation. The three equations were solved by reiterative numerical methods to give two unique vectors $\hat{N}_1$ and $\hat{N}_2$ which satisfied the three equations. The vectors $-\hat{N}_1$ and $-\hat{N}_2$ were also satisfactory, but did not represent different transition moments. Values of E_{max} (1 0 0)/E_{max} (0 0 1) were calculated to be 1.26 and 0.99 for $\hat{N}_1$ and $\hat{N}_2$ respectively, so although $\hat{N}_1$ appeared better, $\hat{N}_2$ was not really eliminated.

$\hat{N}_1$ was oriented at 32.3° away from the molecular $\underset{\sim}{z}$ axis and 64.2° away from $\hat{A}$. $\hat{N}_2$ on the other hand was 26.5° away from the molecular $\underset{\sim}{z}$ axis and only 10.6° away from $\hat{A}$.

It appears that the preceding observations are consistent with the proposal that the E0 peak corresponds to a pair of degenerate transitions with molecular $\underset{\sim}{x},\underset{\sim}{y}$ polarization which have not been split in energy by the crystal field. However, the direction and perhaps magnitude of the transition moments have been altered, although both transition moments appear to be normal to each other, and of approximately the same magnitude. A vector normal to each of the transition moments probably lies close to $\hat{N}_2$ and approximately 10° away from $\hat{A}$. The C peaks are also attributed to a degenerate pair of molecular $\underset{\sim}{x},\underset{\sim}{y}$ polarized transitions.

There is another transition at 21,955 cm^{-1}, only 20 cm^{-1} below the C0 peak. However, this transition is weaker in both faces than C0, and therefore is considered another transition, rather than a transition which has been split out from a degenerate pair. Although its intensity vs polarization follows the C line in the 1 0 0 face, it is quite different in the 0 0 1 face.

b. Hot bands The preceding analysis has indicated electronic excitation to discrete vibrational states for the low energy band with either molecular $\underset{\sim}{z}$ or $\underset{\sim}{x},\underset{\sim}{y}$ polarization. It is therefore possible that this band is an electric-dipole forbidden transition excited by vibronic (Herzberg-Teller) perturbations. On the other hand, the first observed absorption feature at the temperature of 5K, A0 at 21,700 cm^{-1}, is the origin of clearly the most intense progression; although it is not an order of magnitude more intense than the C or E progression. There is

the possibility that this electronic band is the dipole allowed $^1A_{1g} \rightarrow {}^1A_{2u}$ transition, which possesses such a small static electric-dipole transition moment that it only yields intensities comparable to some vibronically excited lines. To distinguish between these two options, a study of the hot bands was undertaken. These hot bands are comprised of absorptions which can be measured as the temperature is raised at longer wavelengths than the lowest energy low temperature feature. Thick crystals are required for observation of these bands, since, in order to obtain resolvable peaks, only minor population of the excited vibrational states of the electronic ground state can be allowed. The lines that might be resolved in hot bands are shown in the energy level diagram of Figure 14. If this is an allowed transition, $^1A_{1g} \rightarrow {}^1A_{2u}$, then the lowest observed absorption at helium temperatures, A0, is the 0-0 transition. The A progression arises as successive vibrational states $\bar{\nu}_1'$, $2\bar{\nu}_1'$, $3\bar{\nu}_1'$ etc. are excited, where $\bar{\nu}_1'$ is the frequency for a totally symmetric vibration (A_{1g}) in the excited electronic state. The strong progressions each have a separation of lines amounting to 370 ± 5 cm^{-1}.[1] The lower value for the excited state is consistent with the expected relaxation of the bonds. The high intensity of successive terms in the progressions based on this vibration, only one of several A_{1g} vibrations, requires a large positional deviation of the atoms in the excited electronic states from their positions in the ground state.

As the temperature of a crystal is raised, a line, broadened somewhat by thermal factors, should appear at an energy, $\bar{\nu}_1^{\circ}$ or 406 cm^{-1} below A0.

---

[1] See Table 3.

The molecular polarization of this line should be the same as A0. The intensity of the line is proportional to the population of the first excited vibrational state, and also to a Franck-Condon factor. Hence, totally symmetric vibrations with small Franck-Condon factors will not be expected to give observable hot bands. No other hot band of comparable intensity will be expected with the A molecular polarization in the spectra with a dipole allowed transition.

For a vibronically allowed transition the origin of the progression, shown as C0 in Figure 14, is at an energy of $\bar{\nu}_i$ above the 0-0 energy, and its progression corresponds to successive excitation of the $\bar{\nu}_1'$ vibration. For this line two hot bands should be developed as the crystal temperature is raised. One band will originate from the $\bar{\nu}_1^{\circ}$ energy, as shown in Figure 14, and should be at an energy $\bar{\nu}_1^{\circ}$ or 406 cm^{-1} below C0. The second band will have an energy $\bar{\nu}_i^{\circ}+\bar{\nu}_i'$ below C0, or $\bar{\nu}_i^{\circ}$ below the 0-0 line. Both hot bands should have the same molecular polarization as the C0 line.

Hot bands were recorded at various temperatures from 85 to 175K, as well as at 5K for the 0 0 1 and 1 0 0 faces at various polarizations. The greatest differences were noted between spectra recorded near the $A0_{max}$ and the $A0_{min}$ polarizations, and these spectra are shown in Figure 15 and Figure 16 for the 0 0 1 and 1 0 0 faces respectively. The spectra for the 1 0 0 face are probably more informative, because the A0 peak has such low intensity in the 25° polarization. Hence, there is little interference from it. At the polarization of 115° for the 1 0 0 face there are two peaks evident. Both undergo a small blue shift as the temperature is decreased, and both are discernible in the 85K spectrum. The lower

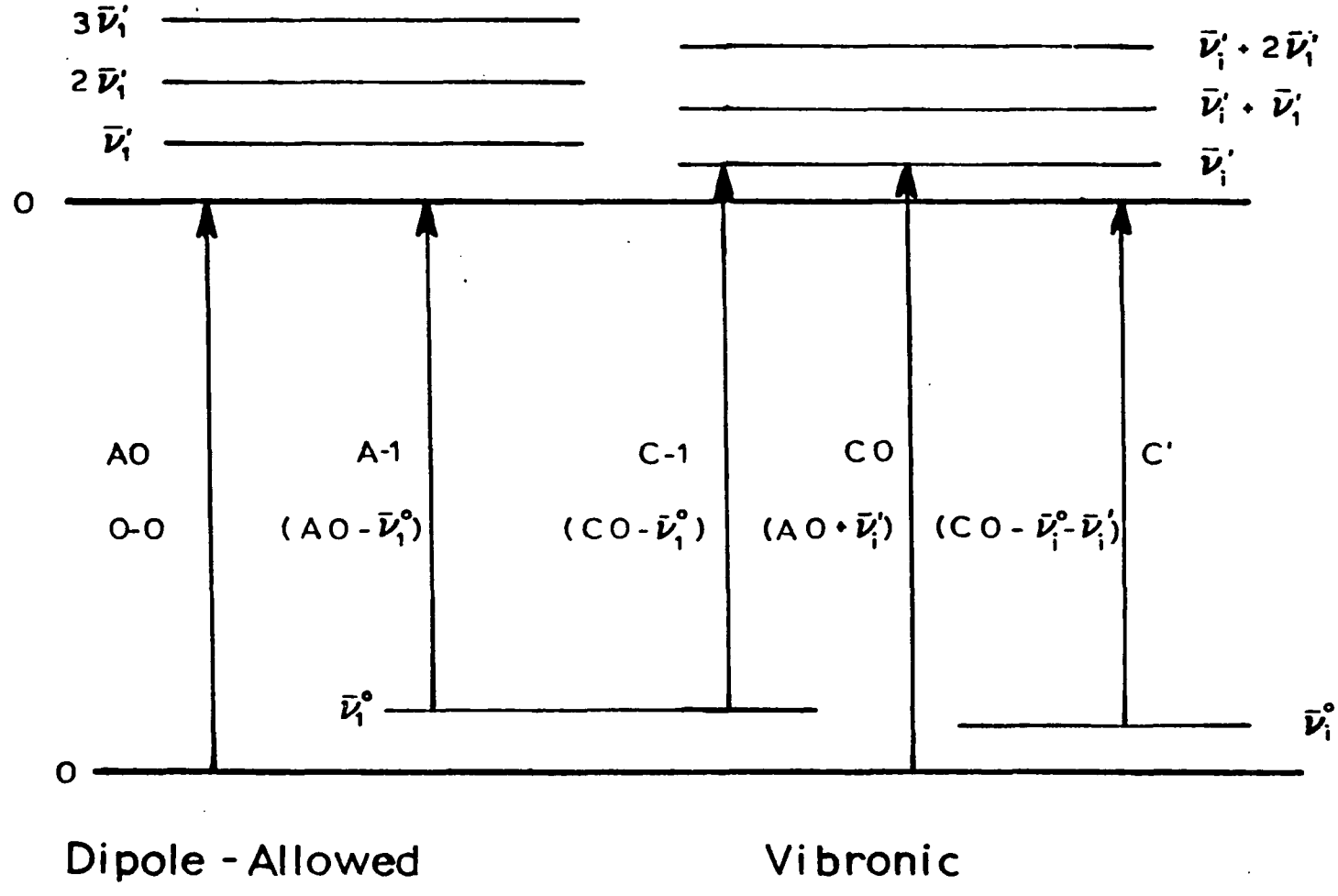

Figure 14. Vibrational lines expected in hot bands for an electric-dipole allowed and a vibronically excited electronic transition with $\bar{\nu}_1'$ the wave number for an A_{1g} vibration with a high Franck-Condon factor and with $\bar{\nu}_i'$ the wave number for an exciting vibration in a dipole forbidden vibronic (Herzberg-Teller) transition

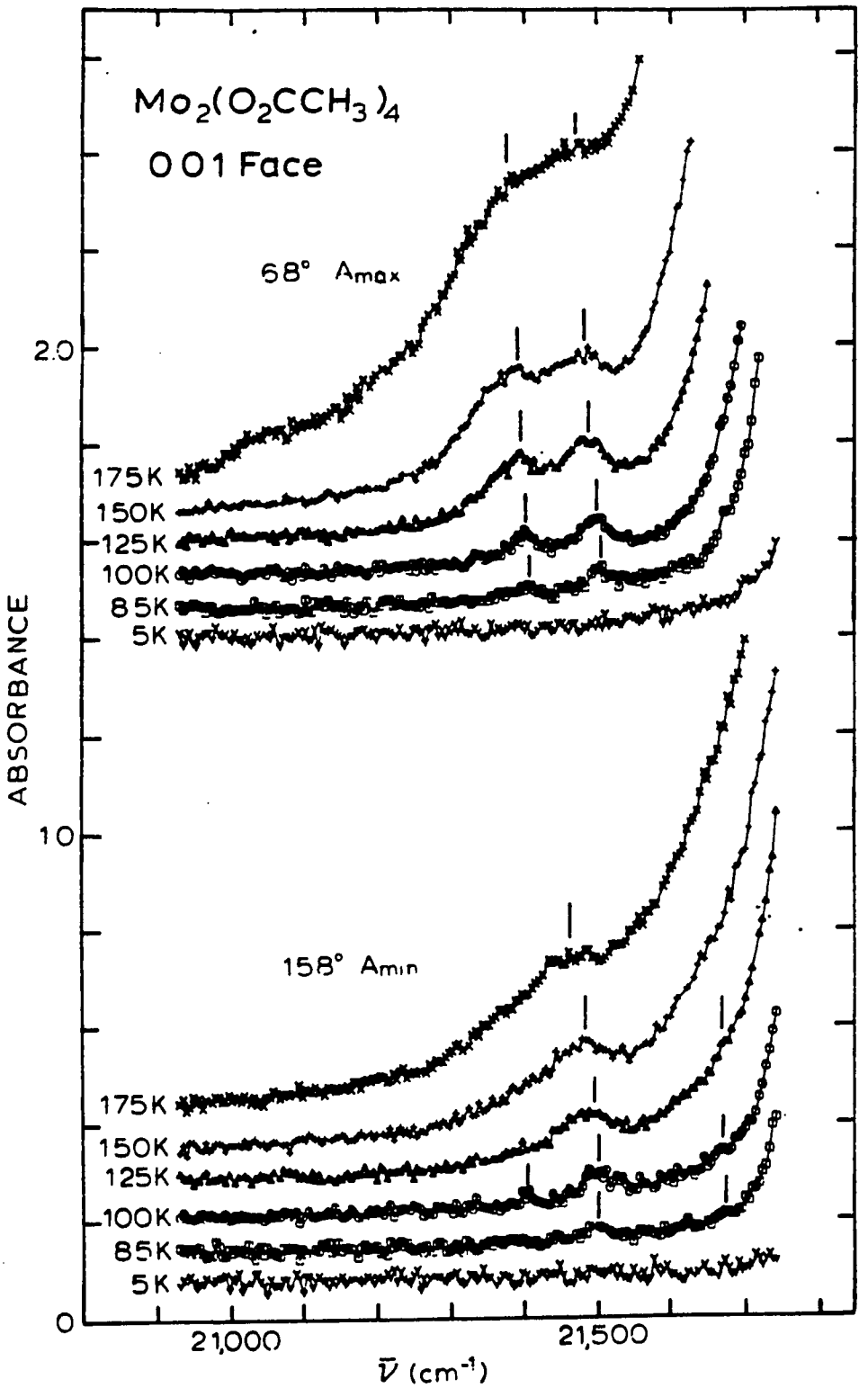

Figure 15. Hot bands recorded for the 0 0 1 face of a $Mo_2(O_2CCH_3)_4$ crystal that was 220 μ thick

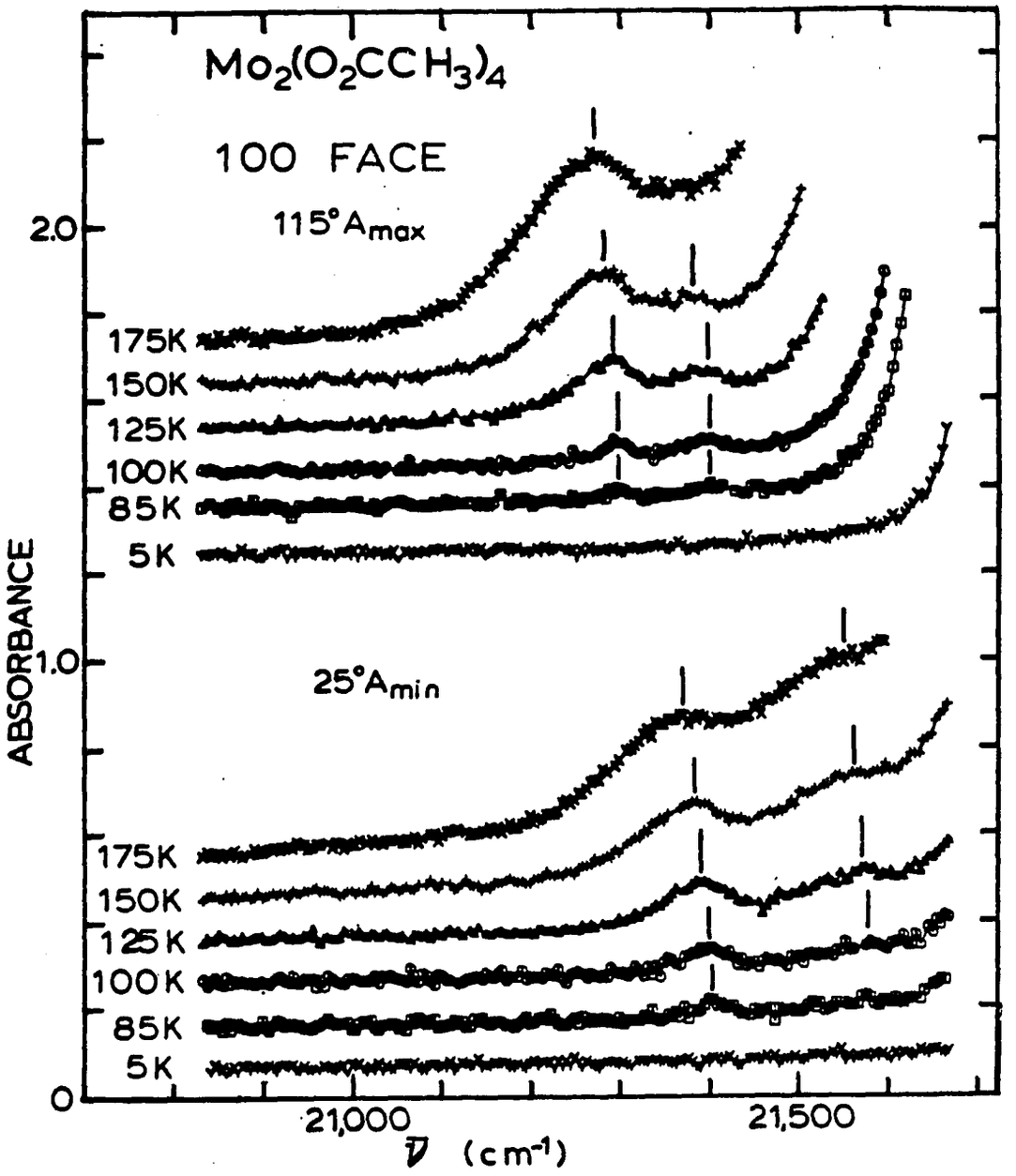

Figure 16. Hot bands recorded for the 100 face of a $Mo_2(O_2CCH_3)_4$ crystal that was 164 μ thick

energy peak at 85K is at 21,300 cm^{-1} and the other peak at 21,405 cm^{-1}. At 25° polarization the 21,300 cm^{-1} peak is absent, but the 21,405 cm^{-1} peak is more intense than at 115°. In addition, a band with a maximum at higher energy can be clearly seen at 125 and 150K. It could also be observed on the recorder chart at 100K at 21,575 cm^{-1}, although it is not definitely discernible in the computer plot of Figure 16. The 21,300 cm^{-1} and 21,405 cm^{-1} peaks are clearly evident in the 68° polarization of the 0 0 1 face in Figure 15, for the somewhat thicker crystal. The 21,300 cm^{-1} peak has a much lower intensity at 158°, but is still discernible at 100K. Since the A0 peak retains greater intensity for A_{min}, the rise in absorption masks the 21,575 cm^{-1} band somewhat; but careful inspection does reveal its presence at 125K, and perhaps somewhat clearer in the 100K spectrum.

The single hot band which follows the A polarization is just 400 cm^{-1} below A0, well within the experimental uncertainty for $\bar{\nu}_1^{\circ}$. On the other hand, two peaks are observed with follow the C-E polarization. The C0 peak is the first major feature above A0, and the hot bands from the C transitions are therefore expected to be the only ones observable at sufficiently low temperatures for adequate resolution to be retained. The 21,575 cm^{-1} peak is just 400 cm^{-1} below C0 and has been labeled C-1. The 21,405 cm^{-1} is 295 cm^{-1} below A0, and has been labeled C'. This pattern is exactly that shown in Figure 14, and provides strong evidence that this band is an electric-dipole allowed transition, $^1A_{1g} \rightarrow {}^1A_{2u}$, with a very low transition moment. In this case, the C0 vibronic origin line is excited by a molecular transition with a frequency of 275 cm^{-1} in the $^1A_{2u}$ excited state, and 295 cm^{-1} in the $^1A_{1g}$ ground state.

In Figure 16, it can be seen that the 21,300 and 21,405 cm^{-1} peaks have comparable intensities at 85K. The 21,300 cm^{-1} peak grows faster as the temperature is increased, consistent with a higher Boltzmann factor based on the higher 406 cm^{-1} vibration in comparison to 295 cm^{-1}.

A number of vibrations in the excited state may now be assigned from the spectra, in addition to the A_{1g} metal-metal stretch of 370 cm^{-1}. The 275 cm^{-1} and the 545 cm^{-1} vibrations which excite the C and E progressions are presumably E_g vibrations. Apparently, only two of the five E_g degenerate pairs of vibrations of the Mo-O-C framework interact effectively with the electronic states to give observable vibronic lines in the spectra. There is a weak 299 cm^{-1} line seen in the Raman spectrum which would correspond to the vibration exciting the C progression. This would presumably be primarily an Mo-O stretch, although Bratton et al. (63) did not place an E_g vibration in this vicinity from force field calculations of the Mo_2O_8 skeleton. There also is a very weak Raman line reported at 567 cm^{-1}, which would be the ground state value for the vibration exciting the E0 line 545 cm^{-1} above A0. This vibration is presumably a ring deformation which would involve motion of the molybdenum atoms.

The D0 peak intensity follows that of A0, as a function of polarization angle. It then could be due to the addition of an A_{1g} vibration of 320 cm^{-1} on to the 0-0 energy. This should also give a Franck-Condon (F-C) progression, but the F-C factors are so small that only the first peak above 0-0 is discernible. It was also noted that the F0 and G0 peaks fall 315 and 320 cm^{-1} above the C0 and E0 peaks, respectively, and could therefore represent the addition of this same A_{1g} energy on to those

vibronic origins. This could be associated with the 322 cm^{-1} weak line in the Raman spectrum.

Although the A0 and E0 peaks are very narrow and isolated from other features in Figures 12 and 13, both the A1 and E1 peaks have weak absorption at about 20 cm^{-1} lower energy, i.e. about 350 cm^{-1} above the origin lines. However, there is no Raman line for a $\bar{\nu}^{o}$ which might be associated with the $\bar{\nu}'$. Since there are strong IR vibrations at 338 and 350 cm^{-1}, it seems these weak features may be due to vibronic excitations, forbidden in D_{4h}, which become allowed in the lower crystal site symmetry. They would be required to have gerade symmetry, however.

It was apparent from the spectra in Figures 11 and 12 that there was an absorption feature, labeled B, at 21,875 cm^{-1}, 175 cm^{-1} above A0. Therefore, spectra for 0 0 1 and 1 0 0 faces of thick crystals were recorded as a function of polarization angle. Uncertainties in the polarizations of B_{max} were about 5^{o} for each face. Spectra close to B_{max} and B_{min} are shown in Figure 17. The B0 peak was polarized approximately, but not exactly opposite to the A0 peak, i.e., B_{max} was close to A_{min}, etc. However, the polarization ratio was large enough in the two faces that B0 cannot be assigned to a degenerate pair of transitions. The orientations of the four possible transition moment vectors were found to be 47^{o}, 56^{o}, 71^{o}, and 76^{o} away from $\underset{\sim}{z}$. It was not possible to discriminate between any of these vectors by the intensities in the two faces. Calculated ratios for B_{max} (1 0 0)/L (1 0 0) : B_{max} (0 0 1)/L (0 0 1) ranged from 0.96 to 1.24 for the four indicated possible transition moment vectors; and the observed value was 1.29. The direction of the four vectors, however, range from 72^{o} to 78^{o} away from the $\hat{A}$ transition moment vector. It seems that the

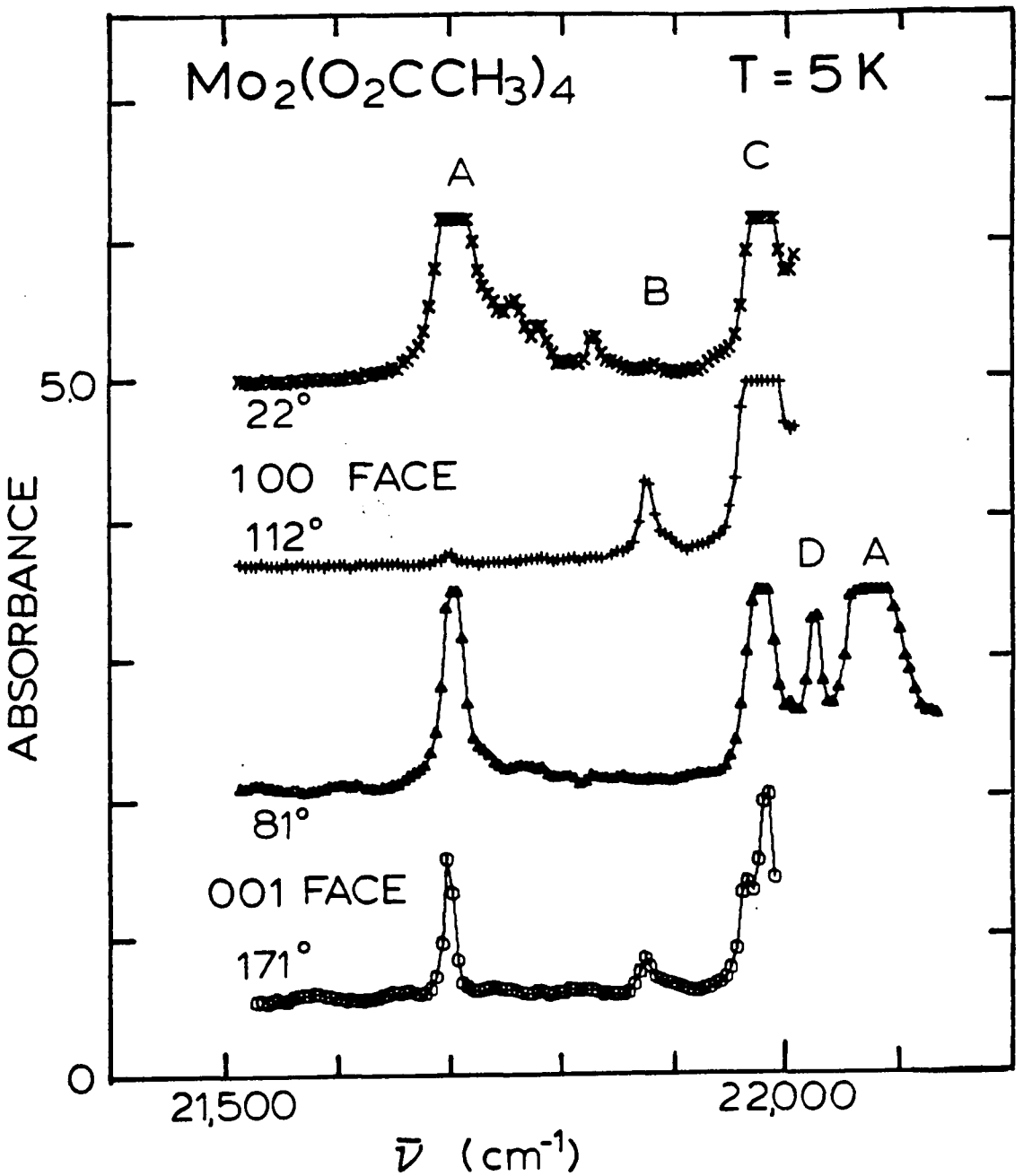

Figure 17. Spectra of thick crystals of $Mo_2(O_2CCH_3)_4$ close to B_{max} and B_{min} for the 1 0 0 face and the 0 0 1 face of thick crystals. The 1 0 0 face was for a crystal 60 μ thick so absorbances can be converted to molar absorptivities by multiplying by 32. The 0 0 1 face was for a crystal 37 μ thick so absorbances can be converted to molar absorptivities by multiplying by 53

direction of the weaker B transition moment deviates a greater amount from the molecular axis than does $\hat{A}$ for the stronger transition. Such deviation may therefore be intensity dependent, since the crystal perturbations are relatively more important for weak transitions.

Figure 17 shows the interesting feature that for the 1 0 0 face, the polarization ratio for A0 is so great that A_{min} is comparable to B_{min}, whereas for the 0 0 1 face, A_{min} is considerably greater than B_{max}. The waves in the recording of zero absorbance to the left of A0 for the 0 0 1 face in Figure 17 are the consequence of interference from multiply reflected beams between the unusually high quality optical faces of this crystal.

The 175 cm^{-1} vibration, which would be required to excite the B0 line, is in the expected region of Mo-Mo-O bending vibrations. Apparently, such vibrations are not as effective as a Mo-O stretch in the vibronic excitation process. It is a bit worrisome, but apparently only a coincidence, that the B0 peak lies exactly 370 cm^{-1}, or the value of $\bar{\nu}_1'$, below the E0 peak.

The crystal for the 1 0 0 face in Figure 17 was sufficiently thick that weak absorption features at 25, 60 and 80 cm^{-1} above A0, which follow A polarization, are clearly evident. These features likely represent phonon bands on the A0 line. The weak absorption peak at 130 cm^{-1} above A0 may or may not be a phonon feature as well.

The intensities of successive lines in the A, C, and E progressions offer additional supportive evidence that this band is a $^1A_{1g} \rightarrow {}^1A_{2u}$ transition. The crystal spectra over the entire measurable range are presented in Figure 18 for the 1 0 0 and 0 0 1 faces. The polarization

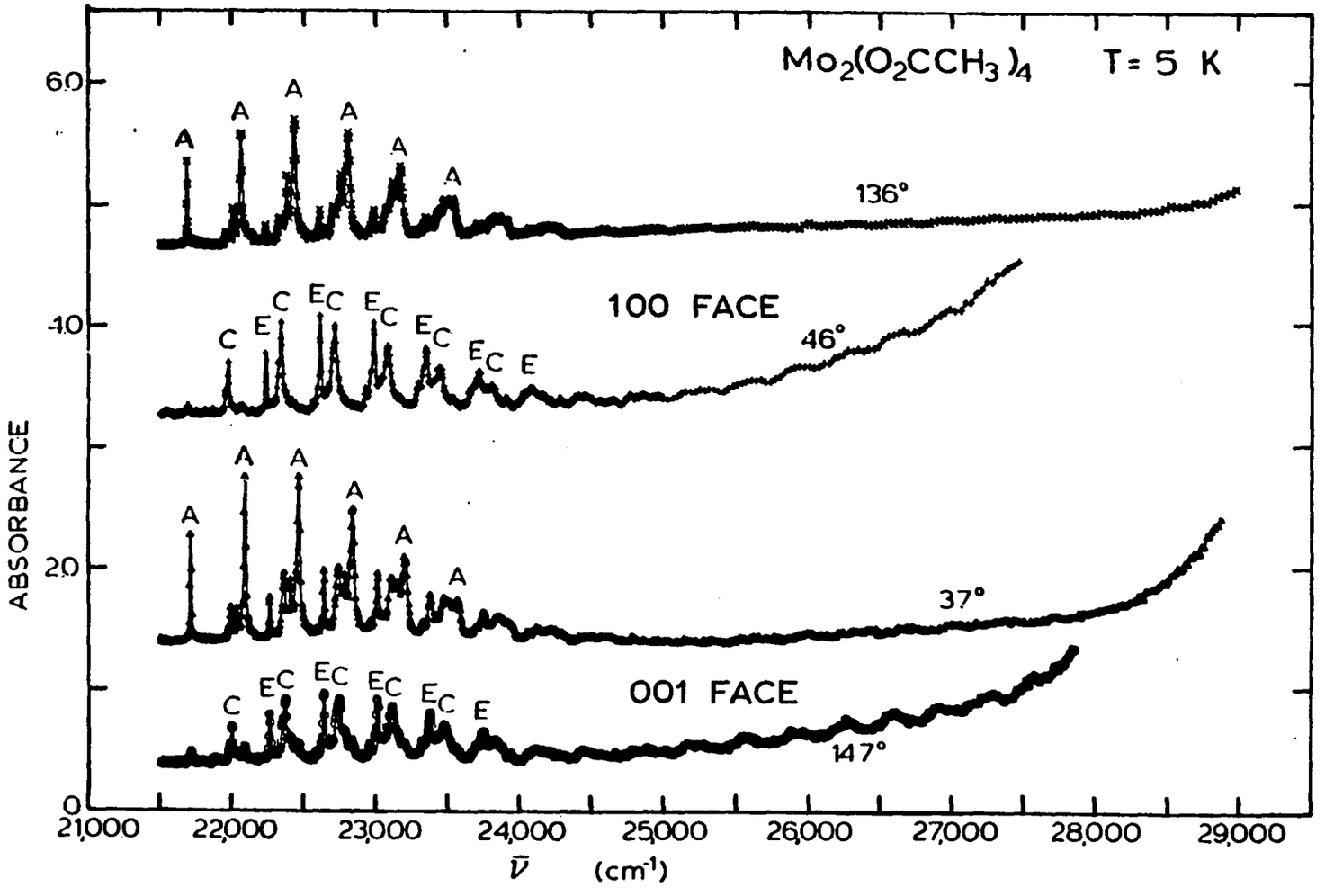

Figure 18. Crystal spectra over the measurable range for the 1 0 0 and 0 0 1 faces of $Mo_2(O_2CCH_3)_4$. The crystals were 3.8 μ thick for the 1 0 0 face and 4.1 μ thick for the 0 0 1 face. Polarizations were selected which approximately gave maximum and minimum absorbances at 26,600 cm^{-1}

angles were chosen to give maximum and minimum absorption at 26,600 cm^{-1}; however, they are not far from the A_{max} and A_{min} polarizations. Hence, for one polarization of each face, the A peaks are the major feature, and for the other polarization, the E and C peaks are dominant. In the lower spectrum for each face, the intensity of the E and C components decrease in height toward a minimum in the absorption which occurs in the region 24,000-25,000 cm^{-1}. Beyond 25,000 cm^{-1}, a series of 7 to 8 broad peaks can be seen in a region of increasing intensity. The average separation of these peaks amounts to 350 cm^{-1}. Absorption is rather low throughout this region in the upper spectrum for each face until the tail of an intense absorption band beyond 29,000 cm^{-1} becomes evident. The absorption at energies above 25,000 cm^{-1} must be due to another electronic transition. Since the origin of the transition is not apparent, it will be designated as the 26,500 cm^{-1} band, since the vibrational components appear to maximize at about this energy.

When the relative heights of the successive A peaks are examined in Figure 18, it can be seen that they follow a discernibly different pattern from the E or C peaks. Thus, the third A peak, designated A2 in Table 7, is the highest; A3 is approximately equal to A1, and greater than A0. For the E progression the second peak, E1, is the highest, whereas E2 is distinctly shorter; and E3 is comparable to E0. The C progression generally follows the E pattern. Since each progression is based on the same totally symmetric vibration, the same set of Franck-Condon parameters would normally be expected. However, in case the transition moment for an electric-dipole allowed transition becomes sufficiently small, a totally symmetric vibration can be significantly involved in the vibronic coupling.

The theory for treatment of Herzberg-Teller coupling by a totally symmetric vibration was presented by Craig and Small (64). They noted that the moment, $\underset{\sim}{M}_{gv^o,fv'}$, can be written as

$$\underset{\sim}{M}_{gv^o,fv'} = \langle \chi_v o(..Q_i..)| \, M_{g,f}(..Q_i..)|\chi_{v'}(..Q_i..)\rangle \tag{25}$$

The harmonic approximation to this quantity for a transition from the lowest vibrational level of the ground state will be:

$$\underset{\sim}{M}_{go,fv'} = \underset{\sim}{M}_{g,f}(Q_o)\langle \chi_{go}||\chi_{gv'}\rangle \equiv \underset{\sim}{M}_o\langle go||fv'\rangle \tag{26}$$

where Q_o is the equilibrium position for the ground state, $\langle go||fv'\rangle$ is the vibrational wave function overlap factor; and its square is the normal Franck-Condon factor which gives the sequence of intensities for the lines.

The molecular vibrations cause a breakdown of the harmonic approximation; and if only one normal vibration, Q_i, influences the transition moment, the deviation from the harmonic approximation is given by:

$$\underset{\sim}{M}_{g,f}(Q) = \underset{\sim}{M}_o + \underset{\sim}{m}_i Q_i . \tag{27}$$

With this value substituted in equation 25, and with the general vibrational wave functions expressed as products of harmonic oscillator wave functions for normal coordinates, the squares of the transition moments, proportional to the line intensities, become:

$$\begin{aligned}\underset{\sim}{M}^2_{go,fv_i'} = {} & [\underset{\sim}{M}_o^2\langle go||fv_i'\rangle^2 \\ & + 2\underset{\sim}{M}_o\underset{\sim}{m}_i\langle go \,||\, fv'_i\rangle \langle go|Q_i|fv_i'\rangle \\ & + \underset{\sim}{m}_i^2\langle go\,|Q_i|fv'_i\rangle^2] \prod_{j\neq i}\langle go||fv'_j\rangle^2\end{aligned} \tag{28}$$

For the usual vibronically excited transition, the first two terms vanish because M_{no} is zero. Q_i must be non-totally symmetric, and only $v_i' = 1$ will produce a non-zero value for $\langle go|Q_i|fv_i'\rangle$. The normal Franck-Condon factor is then included in the final product. However, if M_{no} is not zero and Q_i is totally symmetric, all three terms contribute to the intensity. The center term may become quite important; and as the signs of $\langle go||fv_i'\rangle$ and $\langle go|Q_i|fv_i'\rangle$ can be either positive or negative, there can be drastic alterations in the normal Franck-Condon progressions. The integrals $\langle go||fv_i'\rangle$ have been computed for totally symmetric vibrations, from the formulae presented by Hutchisson which are based on harmonic oscillator wave functions. The values of $\bar{\nu}^o = 406\ cm^{-1}$ and $\bar{\nu}' = 370\ cm^{-1}$ are fixed from the Raman and the electronic spectra. Values were obtained for a series of Δr(Å) for the reduced mass of 48 a.m.u.; and the set of integrals, which were considered subjectively to give the best fit with the experimental peak heights in the E progression, are given in Table 8. The $\langle go|Q|fv'\rangle$ integrals were evaluated from Hutchisson's formulae by the method of Yeung (65) for this value of Δr_i and a series of trial values of m_i. A set of calculated intensities in reasonable agreement with the first few terms of the A progression is also shown in Table 8. All sets were normalized to a value of 1.00 for the highest peak in the progression. The indicated increase, Δr, in the metal-metal equilibrium distance in the excited state from that in the ground state is fairly substantial, i.e., 0.11 Å. The indicated value for $m_i \Delta r/M_o$ was 0.30, so a fairly modest value of m_i can result in the type of difference observed between the A and the C or E progressions. The calculated bands appear to be somewhat narrower than the observed band. Part of this effect may be due to the

Table 8. Calculation of intensities from the Franck-Condon and the Herzberg-Teller factors

Transition	Intensity E progression		Intensity A progression	
	Obsd. peak height	Calcd.[a] Franck-Condon only	Obsd. peak height	Calcd.[a,b] Franck-Condon and Herzberg-Teller
0-0	.61	.30	.67	.26
0-1	1.00	1.00	.97	.97
0-2	.94	.94	1.00	1.00
0-3	.61	.38	.75	.48
0-4	.35	.09	.44	.13

[a] $\bar{\nu}^{o} = 406\ cm^{-1}$; $\bar{\nu}' = 370\ cm^{-1}$; $\mu = 48$ AMU; $r'-r_o = 0.11$ Å.

[b] $m_i = 2.77\ Å^{-1}\ M_o$.

fact that the origin peaks were so narrow. Thus, their peak height alone does not give an accurate measure of intensity, because of the breadth of the higher peaks. Even so, the calculated progressions fall off more rapidly than the experimental peaks. Perhaps this is not too surprising, in view of the simplicity of the model. Hutchisson notes that even a small asymmetry in the vibrational potential energy function can modify the calculations considerably.

The preceding analysis of vibrational intensities at low temperatures and in the hot bands has presented strong evidence that the band which maximizes at 23,000 cm^{-1} for $Mo_2(O_2CCH_3)_4$ is an electric-dipole allowed transition, $^1A_{1g} \rightarrow {}^1A_{2u}$, with an inordinately low transition moment, so that Herzberg-Teller vibronic excitations provide some comparable intensities, even at helium temperature. The value of 4.32×10^{-9} cm-$M\int\varepsilon\partial\bar{\nu}$ for an A_{max} spectrum at 300K was about 1×10^{-3}, which is comparable to the oscillator strength that Trogler et al. (2) gave for a solution spectrum of $Mo_2(O_2CCF_3)_4$. As a Mo-Mo $\delta \rightarrow$ Mo-Mo δ^* transition, it attains intensity by the electron transfer from the d_{xy} orbital of one Mo atom into the d_{xy} orbital of the other. The d_{xy} orbitals have their greatest extension in a plane normal to the metal-metal axis; therefore, none of the $\delta \rightarrow \delta^*$ transitions are particularly intense. It is recognized that for the alkyl carboxylates, the lowest unoccupied orbital is the π^* orbital involving carbon and oxygen p orbitals. One symmetry adapted linear combination of the carboxylate π^* orbitals, shown in Figure 19, is a basis for the b_{2g} irreducible representation. It is possible, therefore, that this orbital mixes with the Mo-Mo δ orbital somewhat. In fact, the relatively high transition energy of the first band for the carboxylate

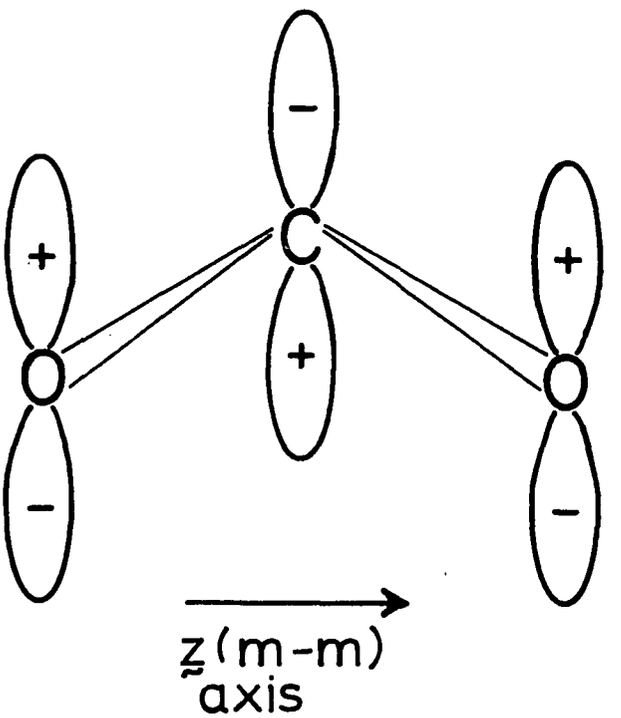

Figure 19. π-antibonding linear combination of p-orbitals for the carboxylate ligand with the proper symmetry to interact with the metal-metal (m-m) delta-bond in $Mo_2(O_2CR)_4$ complexes

complexes might result from this stabilization of the δ orbital; for there is no b_{1u} linear combination for the carboxylate π^* orbitals. Involvement of the carboxylate orbitals would result in withdrawal of electron population from the vicinity of the metal-metal bond, where the overlap required for the transition dipole moment occurs. The low intensity for this band may therefore result from such a reduction in the transition dipole moment. Also, the crystal field perturbations may affect the band intensity in some way.

Xα-scattered wave calculations, performed for the molybdenum(II) tetraformate molecule by Norman and coworkers (15), have predicted that the lowest spin-allowed transition should be the $\delta \rightarrow \delta^*$. To this extent the present results are in agreement with the calculation. However, the original theoretical transition energy was only 14,700 cm^{-1}. The application of the Xα-VB model for this compound would most likely raise the calculated transition energy to a value much nearer the observed energy, as was the case in the Xα-VB calculation for $Mo_2Cl_8^{4-}$ (19).

It is possible that the 26,500 cm^{-1} band observed for $Mo_2(O_2CCH_3)_4$ is the dipole forbidden $^1A_{1g} \rightarrow {}^1E_g$ ($\delta \rightarrow \pi^*$) transition. Norman et al. calculated this transition to be 25,600 cm^{-1}, which would be rather close agreement with experiment. It is the only other spin-allowed transition placed below 37,000 cm^{-1} by the theory. It is also possible that it could be a spin-forbidden transition, corresponding to the intense band seen in solution at about 33,000 cm^{-1}.

The greatest pattern of similarity between the high resolution spectra of the dimolybdenum alkylcarboxylates is the presence of the three strong vibrational progressions for the band in the vicinity of 23,000 cm^{-1},

corresponding to the A, C, and E progressions of $Mo_2(O_2CCH_3)_4$. The energies of the A origin peaks, and distances of the C and E origins above A0, are given for four carboxylate complexes in Table 9. The formate

Table 9. Energies of the origins of corresponding intense vibrational progressions in the crystal spectra of the carboxylate complexes of molybdenum(II)

Complex	A0 cm^{-1}	C0-A0 cm^{-1}	E0-A0 cm^{-1}	A1-A0 cm^{-1}
$Mo_2(O_2CCH_3)_4$	21,700	275	545	375
$Mo_2(O_2CH)_4$	21,870	400	790	350
$Mo_2(O_2CCF_3)_4$	22,070	255	511	360
$Mo_2(O_2CCH_2NH_3)_4(SO_4)_2 \cdot 4H_2O$	21,510	280	420	350

has the highest metal-metal stretching frequency (ν_1'); and the acetate and trifluoroacetate have fairly similar values for the vibrational frequencies leading to the C and E origins. Although the glycine complex has a similar frequency for the C0 peak as the acetate, the frequency for the E0 peak is considerably smaller than that for the acetate complex. The formate has considerably higher vibrational frequencies for the C and E origins, implying a stiffer ring structure for this complex.

Other differences between the carboxylate complex spectra are noted as well. The formate spectra (3) were obtained for the 0 0 1 face of an orthorhombic crystal, so there was no complication of the direction for the transmitted plane-polarized light waves changing with wavelength. With only one face available, the orientation in space of transition moments for

individual lines could not be established. Qualitatively, the polarizations of all peaks were opposite to that expected for exactly $\underset{\sim}{z}$-polarized lines.

Crystals of $Mo_2(O_2CCH_2NH_3)_4(SO_4)_2 \cdot 4H_2O$ provided the first polarized spectra of a carboxylate compound; and they are especially important, because crystals of this compound are tetragonal (18). The metal-metal axis is aligned with the $\underset{\sim}{c}$ axis, so crystal spectra provided directly the molecular polarizations. Unfortunately, vibrational details were not as well resolved as with the other compounds; but these three intense progressions (A, C, and E) are clearly seen. The A progression whose origin is listed in Table 9 is clearly $\underset{\sim}{z}$-polarized, and the C and E progressions are both $\underset{\sim}{x},\underset{\sim}{y}$-polarized. However, for this crystal there is a weak, $\underset{\sim}{z}$-polarized progression, ca. 10% of the intensity of A, with an origin 940 cm^{-1} below the A origin. At that time, it was proposed that the transition was forbidden in D_{4h}, but dipole allowed in the site symmetry, S_4. The A progression was then thought to be vibronically excited by a 940 cm^{-1} vibration. In view of the present results, this seems no longer tenable. Rather, we now believe that the A0 peak is the origin for a majority component, and the lower energy progression may be the consequence of a minority or defect component. In this crystal the $-NH_3$ groups of the glycine hydrogen bond to neighboring sulfate oxygens. It is suggested that the defects may arise from transfer of a small fraction of such protons to the sulfate across the hydrogen bond. It is recognized that spectra and polarizations for defect components in a host crystal may be modified somewhat (66).

The interpretation of this weak low energy progression as due to a defect component has been verified by Bino et al. in their study of the polarized spectra of $Mo_2(L\text{-leucine})_4^{4+}$ (67). The origin for the intense $\underset{\sim}{z}$-polarized progression in this compound was reported as 21,594 cm^{-1}, within 100 cm^{-1} of the intense $\underset{\sim}{z}$-polarized band in the glycinate (see Figure 4). The remaining $\underset{\sim}{x},\underset{\sim}{y}$ polarized bands were also similar for the two complexes, but no other $\underset{\sim}{z}$-polarized band was ever observed, even for very thick crystals. The authors claimed that this result proved that the weak, low energy $\underset{\sim}{z}$-polarized band in the glycine complex is due to a defect component (67).

As in the case of the formate complex, the study of the polarized spectra of $Mo_2(O_2CCF_3)_4$ yielded polarization ratios opposite to what was expected for a $\underset{\sim}{z}$-polarized transition. Crystal spectra for a crystal $\sim 4 \pm 1$ μm thick, recorded at 300K and 5K, are shown in Figure 20. The lowest energy band maximizes at $\sim$23,000 cm^{-1} at room temperature. The band is more intense in the 170° polarization than at 80°, and some vibrational structure can be seen in the more intense polarization. Also, there is a second band observed at $\sim$27,000 cm^{-1} in the 300K spectra, and it appears to be polarized opposite to the first band at 300K, being more intense in the 80° polarization. This band lies on the tail of an intense absorption centered beyond 30,000 cm^{-1}. At 5K, the low energy band exhibits rich vibrational structure in both polarizations, reminiscent of the acetate spectra. The second band undergoes an observable blue shift from 300-5K, and appears to maximize at $\sim$27,600 cm^{-1} in the low temperature spectra.

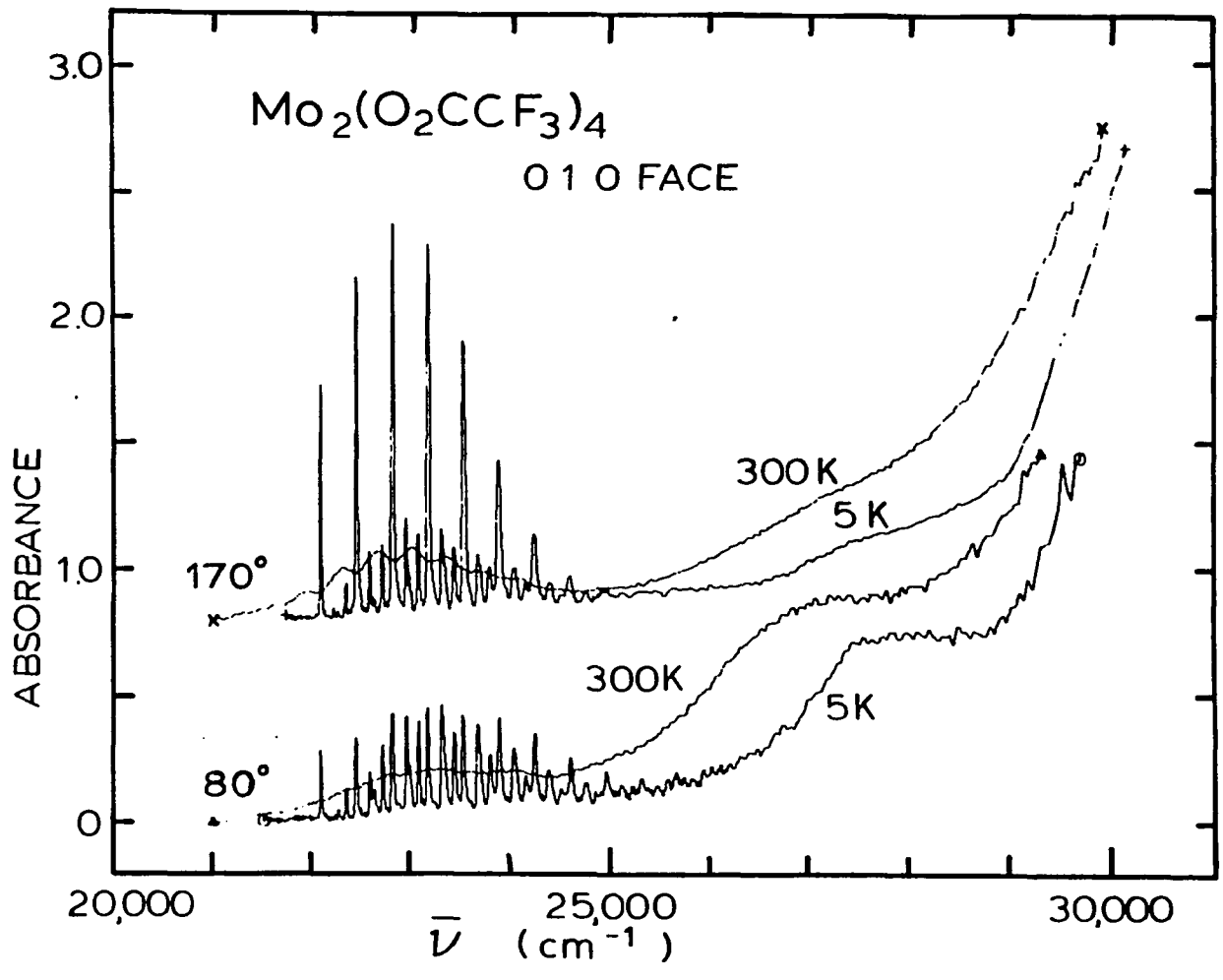

Figure 20. Single-crystal polarized absorption spectra over the entire measurable range for $Mo_2(O_2CCF_3)_4$. The crystal was ∿ 4 μm thick

An expanded plot of the low energy region of the first band is shown in Figure 21, in which the remarkable resolution of vibrational detail for this band at 5K is evident. Frequencies for the individual lines, as well as the frequency spacing from the previous progression line, are listed in Table 10. (Several of the weak features in Figure 21 are not listed.)

The A peak maximized and minimized within $\sim 5^{o}$ of the extinctions observed under the polarizing microscope, in contrast to the marked deviation from the observed extinction for the A peak in spectra of $Mo_2(O_2CCH_3)_4$. The C and E lines did not exhibit a large polarization ratio, but $I_{A0}\ (170^{o})/I_{A0}\ (80^{o}) = 3.4$, where I represents peak height. The ordering of the A, B, C, and E progressions follows the sequence established in the description of the 5K spectra of $Mo_2(O_2CCH_4)_4$. The similarity between the 5K spectra of the $R = CF_3$[1] and $R = CH_3$[2] carboxylate complexes favors an assignment of the A0 peak in $Mo_2(O_2CCF_3)_4$ as the origin of the dipole allowed $\delta \rightarrow \delta^{*}$ transition. However, in spectra for a polycrystalline sample of $Mo_2(O_2CCF_3)_4$, Trogler et al. (2) observed weak absorption features at lower energy than the A_o line. Therefore, spectra were recorded for a crystal ca. 105 μm thick at 5K, as shown in Figure 22. Three weak lines are observed at lower energy than the A0 line at 5K. Trogler et al. observed the lines at 29,060 cm^{-1} and 21,990 cm^{-1}, but did not resolve the line at 22,030 cm^{-1} for their polycrystalline sample. However, no evidence was found, even with thicker crystals, for the line

---

[1] See Figure 20.

[2] See Figure 18.

Table 10. Vibrational details in the low energy absorption band of $Mo_2(O_2CCF_3)_4$ at 5K.

Progression line	$\bar{\nu}$, cm^{-1}	$\Delta\bar{\nu}$,[a] cm^{-1}
	21,960 (w)	(-120)[b]
	21,990 (w)	(-90)[b]
	22,030 (w)	(-50)[b]
A_o	22,080	--
B_o	22,210 (w)	(130)
D_o	22,260 (w)	(180)
C_o	22,340	(260)
A_1	22,450	370
B_1-E_o	22,580	370-(500)
C_1	22,700	360
A_2	22,810	360
B_2-E_1	22,940	360
C_2	23,060	360
A_3	23,160	350
B_3-E_2	23,300	360
C_3	23,420	360
A_4	23,520	360
B_4-E_3	23,650	350

[a]Values in parentheses give the difference, $\Delta\bar{\nu}$, from the A_o line. Values without parentheses give the $\Delta\bar{\nu}$ values from the preceding line in a progression.

[b]Considered due to a defect, or decomposition.

Table 10. Continued

Progression line	$\bar{\nu}$, cm^{-1}	$\Delta\bar{\nu}$,[a] cm^{-1}
C_4	23,780	360
A_5	23,870	360
B_5E_4	24,020	370
C_5	24,140	360
A_6	24,220	350
B_6-E_5	24,370	350
C_6	24,490	350
A_7	24,560	340
B_7-E_6	24,730	350
C_7	24,840	350
A_8	24,900	340
B_8-E_7	25,070	360
C_8	24,840	350
A_9	25,240	340
B_9E_8	25,330	360
C_9-X	25,540	360
A_{10}	25,600	360

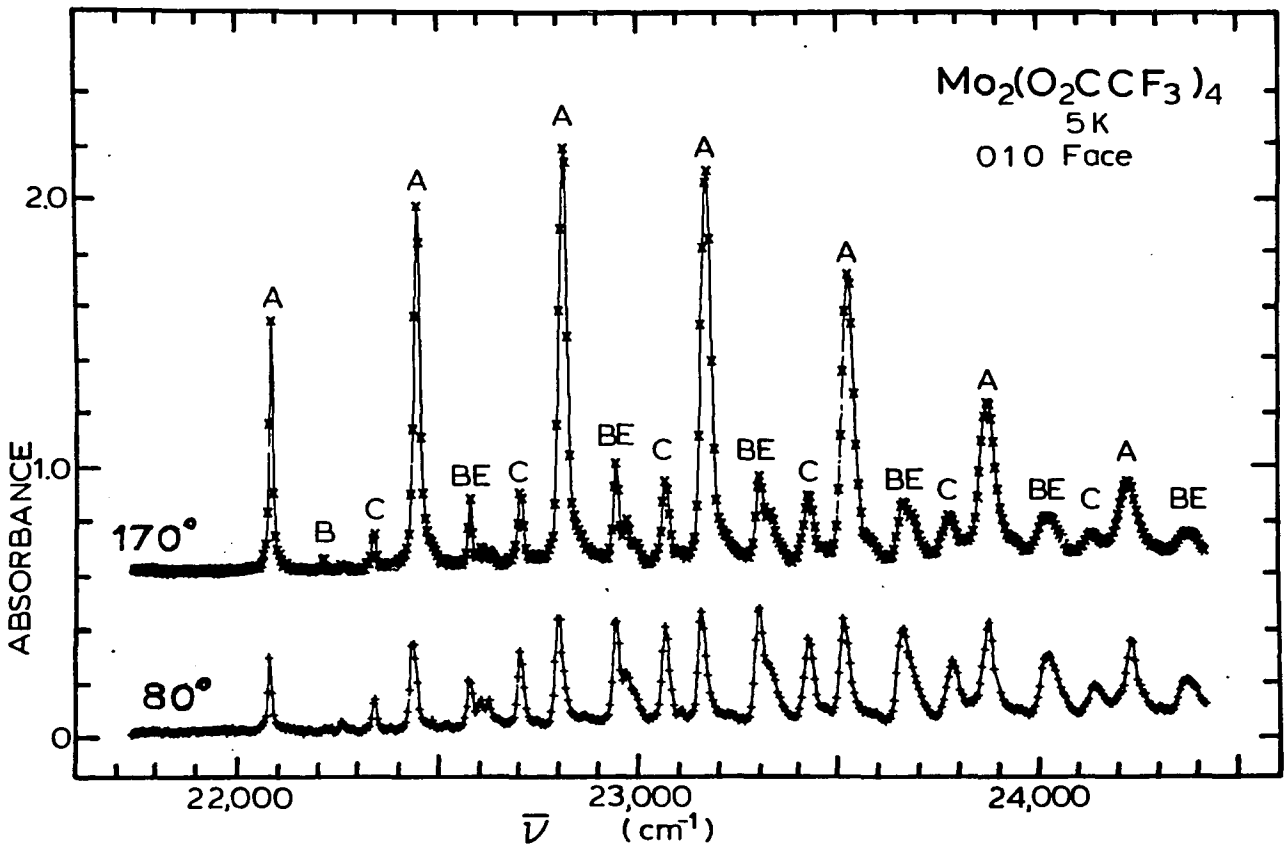

Figure 21. Single-crystal polarized absorption spectra for $Mo_2(O_2CCF_3)_4$ at 5K, expanded along the $\bar{\nu}$ axis. The crystal was ∿4 μm thick

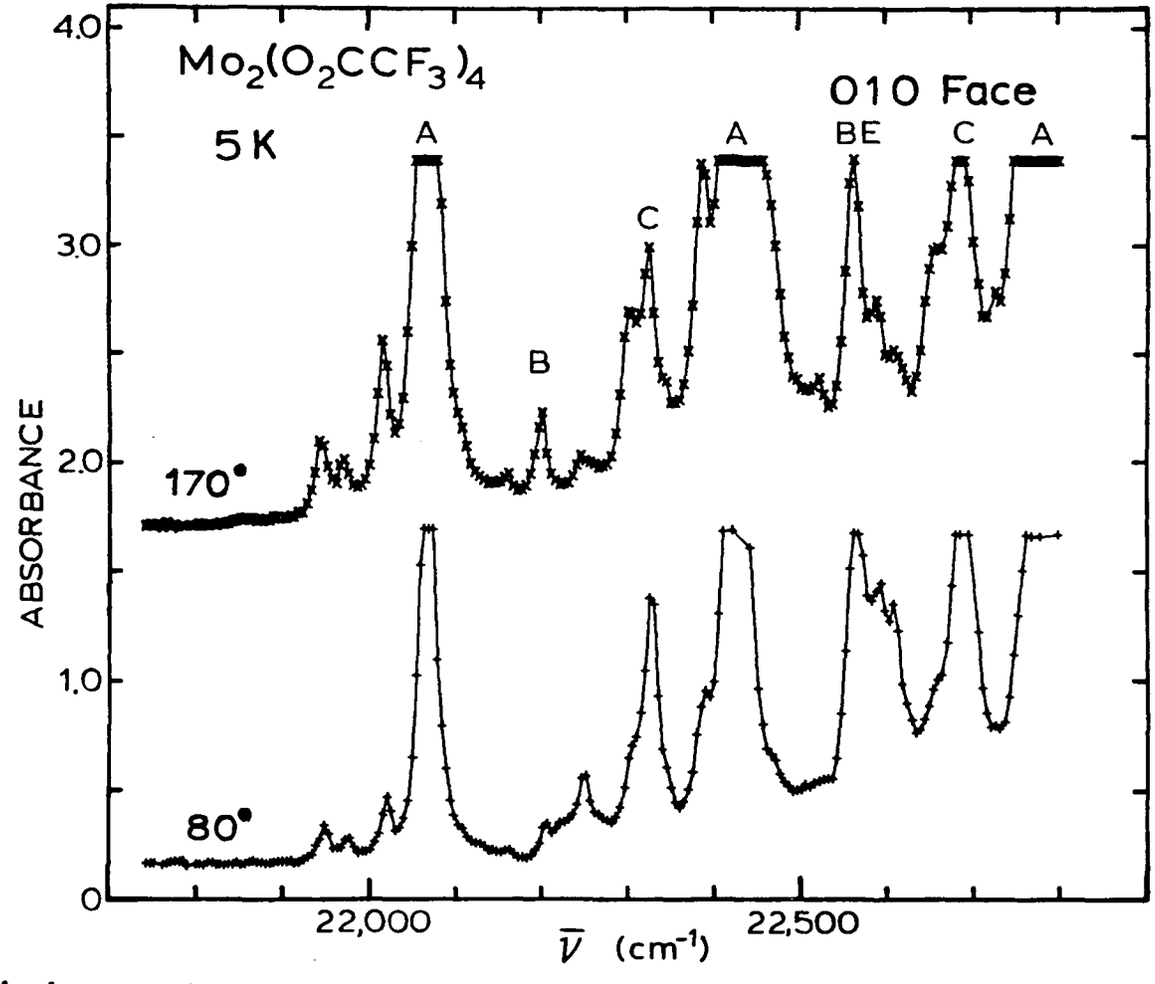

Figure 22. Single-crystal polarized absorption spectra in the low energy region for a thick crystal of $Mo_2(O_2CCF_3)_4$. The crystal was ∿105 μm thick

at 21,860 cm^{-1}, which was assigned as the 0-0 line for the low-energy band by Trogler et al. (2).

These three peaks are of such low intensity that it is impossible to compare them with the intensities of other peaks in the low energy band. As shown in Figure 22, for a crystal which yields acceptable intensities for these weak features, the majority of the remaining features of the band are too intense to be measurable. The spectra shown in Figures 20 and 21 were for a crystal which was freshly prepared by sublimation prior to spectral examination. The low energy portion (primarily the A_o peak) of the 170° polarization from the 5K spectra for this crystal is compared in Figure 23 with that for a crystal of comparable thickness, obtained from a preparation several months old. The three weak features, especially the line at 22,030 cm^{-1}, are obviously present for the older crystal, but are unobserved in the lower spectrum from the freshly prepared sample. On the basis of this evidence, it has been concluded that these weak features are due to a decomposition and/or defect component.

Since no line was observed at 21,860 cm^{-1}, even for very thick (ca. 1 mm) crystals of $Mo_2(O_2CCF_3)_4$, we believe this feature in the spectra of Trogler et al. must also be due to additional decomposition/defects, or to an impurity in their preparation.

Although the observed polarization ratio of 3.4/1 for the trifluoroacetate complex grossly disagrees with the calculated ratio of .63/1 for a molecular $\underset{\sim}{z}$-polarized transition, we were convinced that the same phenomenon was being observed here that was observed for $Mo_2(O_2CCH_3)_4$,

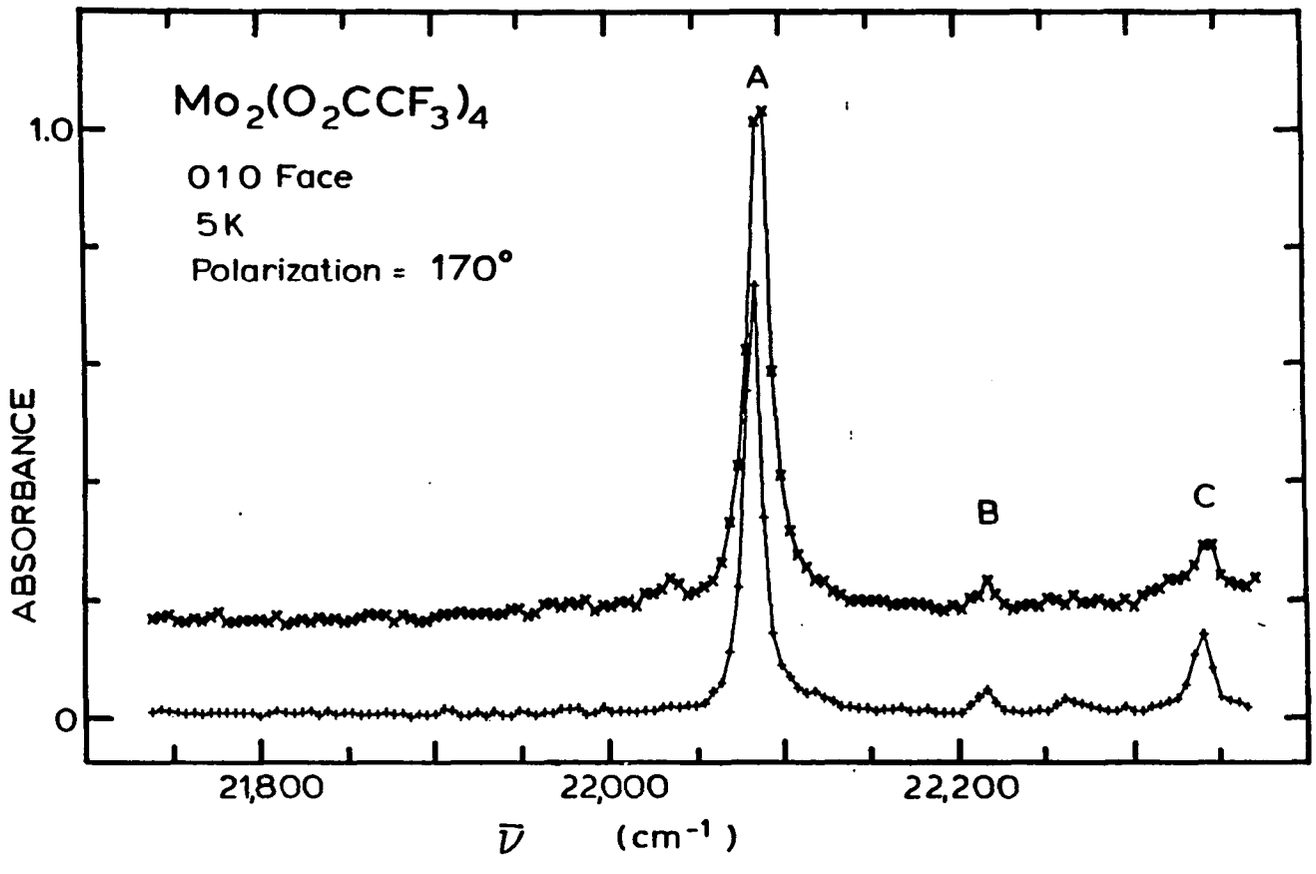

Figure 23. Single-crystal polarized spectra for the low energy region of the first absorption band of $Mo_2(O_2CCF_3)_4$ at 5K. The polarization at which A was at a maximum was chosen. The upper plot is for an older crystal; the lower plot for a freshly prepared one

namely, the distortion of the transition moment vector away from the molecular $\underset{\sim}{z}$ axis. However, since it was possible to obtain spectra for only one crystal face, the location of the transition moment could not be restricted at all.

The next best approach was to compare some structural similarities of $Mo_2(O_2CCH_3)_4$ and $Mo_2(O_2CCF_3)_4$, as well as $Mo_2(O_2CH)_4$. Figure 24 is an illustration of the molecular plane which contains the intermolecular axially-coordinating oxygens of the $Mo_2(O_2CR)_4$ molecules. The orientation of the molecules in this plane is remarkably similar for the R = CH_3:CF_3:H complexes. A comparison of the stacking axes, stacking angles, metal-metal bond lengths, and metal-axial oxygen distances is shown in Table 11. Also shown in Figure 24 is the orientation of the transition moment, $\hat{A}$[1], for the A0 peak of $Mo_2(O_2CCH_3)_4$.

It was possible to calculate transition moment vectors for the R = CF_3 and R = H $Mo_2(O_2CR)_4$ dimers which had orientations similar to $\hat{A}$ with respect to their unit cells[2], and accounted for the experimentally observed polarization ratios. This was accomplished by working in reverse order, starting with the observed polarization ratio. By taking the $\cot^{\frac{1}{2}}$ of this observed ratio, a value was obtained which defined the angle between the maximum absorption extinction and the projection of the transition moment in the crystal face. Two planes perpendicular to the

---

[1]For a symbol $\hat{S}$, "$\hat{}$" indicates a unit vector, or a vector whose magnitude is 1.

[2]See Figure 24.

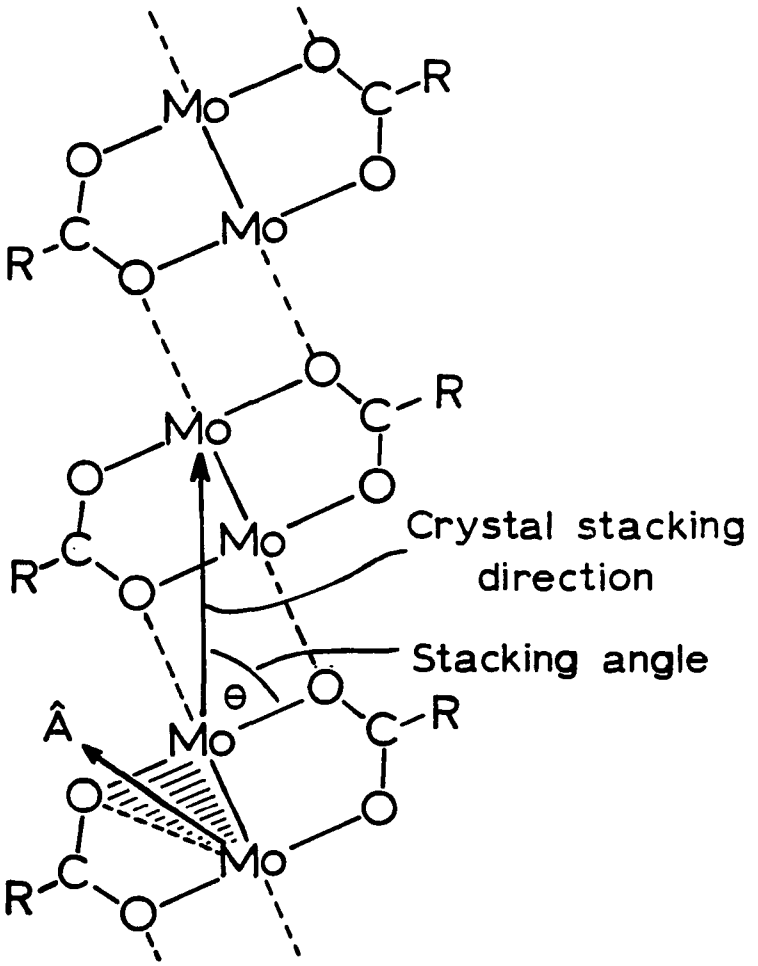

Figure 24. A diagram of the plane containing the Mo-Mo bond and the axially coordinating carboxylate oxygens for the R = CF_3, CH_3, and H[1] molybdenum carboxylate dimers. $\hat{A}$ represents the transition moment vector found for $Mo_2(O_2CCH_3)_4$

[1]For $Mo_2(O_2CH)_4$, the molecule does not have $\bar{1}$ symmetry, so some of the carboxylate oxygens deviate from this plane, by $<1^o$.

Table 11. A comparison of some structural properties for $Mo_2(O_2CR)_4$ compounds

Compound	Stacking axis	Stacking axis length	Stacking angle, θ	M-M distance	M-O[a] distance
$Mo_2(O_2CCH_3)_4$	$\underset{\sim}{b}$	5.500(1)Å	56°	2.093(1)Å	2.645(4)Å
$Mo_2(O_2CCF_3)_4$	$\underset{\sim}{c}$	5.568(5)Å	56.3°	2.090(4)Å	2.72(1)Å
$Mo_2(O_2CH)_4$	$\underset{\sim}{c}$	5.500(1)Å	56.6°	2.091(2)Å	2.644(4)Å

[a]Metal-axial oxygen distance (closest intermolecular distance).

crystal face could be defined for this angle, on either side of the absorption maximum. The plane which was oriented closest to the $\underset{\sim}{z}$ axis was chosen, consistent with the acetate result. The closest possible transition moment to the $\underset{\sim}{z}$ axis was then found which was also in this plane.

A comparison of the calculated transition moment vectors with the acetate $\hat{A}$ vector is given in Table 12. There appears to be a trend in the angles which are used to describe the orientation for the transition moments. For the sequence R = CF_3:CH_3:H, the angle between $\hat{N}$ and $\hat{A}$ decreases, the angle between $\hat{z}$ and $\hat{A}$ increases, and the angle between $\hat{S}$ and $\hat{A}$ increases. Perhaps this trend is related to some property of the R-group.

Table 12. Comparison of transition moment vectors for the lowest energy transition of some $Mo_2(O_2CR)_4$ compounds

Compound	Angles[a] $\hat{N}$-$\hat{A}$	$\hat{z}$-$\hat{A}$	$\hat{S}$-$\hat{A}$
$Mo_2(O_2CCF_3)_4$	81.5°	22.2°	54.0°
$Mo_2(O_2CCH_3)_4$	80.6°	34.0°	66.7°
$Mo_2(O_2CH)_4$	76.9°	36.8°	69.4°

[a] $\hat{N}$ is a vector perpendicular to the Mo-Mo-O plane shown in Figure 24, $\hat{z}$ is the Mo-Mo axis, $\hat{S}$ is the stacking axis, and $\hat{A}$ is the transition moment vector.

Clearly, the orientations of the three transition moments are not identical, but they are not expected to be identical, because the shift of the transition moment for the A peak in the three complexes is due to the crystal field perturbations on the complexes in the solid state. Obviously, while these perturbations are expected to be related, due to the similarities of the structures (see Table 11), they should not be exactly the same for the different complexes.

On the basis of the trend observed in Table 12, and the similarities in the vibrational structure observed for the first band in 5K spectra of the three complexes[1], we have concluded that the A peak in the 5K spectra for the R = CF_3 and R = H complexes is the origin of the $\delta \rightarrow \delta^*$, $^1A_{1g} \rightarrow {}^1A_{2u}$, $\underset{\sim}{z}$-polarized, electric-dipole allowed transition, in agreement with the assignment for the spectra of $Mo_2(O_2CCH_3)_4$. In all three cases, the transition has a sufficiently low oscillator strength that vibronically excited lines are observable for molecular $\underset{\sim}{x},\underset{\sim}{y}$-polarization that are not orders of magnitude less intense than the electric-dipole allowed, $\underset{\sim}{z}$-polarized A lines.

Additional support for this assignment is seen in the more recent results for the spectra of $Mo_2[(CH_2)_2P(CH_3)_2]_4$, reported by Cotton and Fanwick (68). The authors claimed that they observed the same unusual phenomenon which we have concluded is occurring for the molybdenum carboxylates, i.e., the excitation of a dipole-allowed transition of low oscillator strength in the same energy region ($\sim$20,000 cm^{-1}) as we have

---

[1]See Table 10.

observed, and vibronic progressions with intensities of nearly the same magnitude as the allowed transition.

The average spacing between successive lines in the Franck-Condon progressions observed for $Mo_2(O_2CCF_3)_4$ is 356 ± 8 cm^{-1}. This corresponds to the frequency of the totally symmetric metal-metal stretching vibration in the excited state, which has been found to have a frequency of 397 cm^{-1} in the ground state.[1]

Further vibrational details in the 5K spectra of $Mo_2(O_2CCF_3)_4$ are evident upon careful examination of the higher energy portion of the first band, shown in Figure 25. At frequencies above A_7, the lines in the A progression for the 80° polarization are not aligned with the lines in the 170° polarization. Furthermore, the lines for 80° polarization are narrower and higher than the lines for 170°, whereas for the earlier members in the progression, the 170° A lines are clearly more intense (see Figure 21). Therefore, the new 80° lines must represent another progression that begins perhaps at 24,240 cm^{-1} (under A_6). Further evidence for new progressions is found in the behavior of the C peaks. For the 80° polarization, C_7 is clearly less intense than C_6, but there is an increase in intensity for C_8, and perhaps also for C_9, which has been designated as a new progression, labeled X.

Finally, there is another progression, labeled Y, which is first clearly observable at 25,350 cm^{-1}. It does not seem reasonable to assign these as vibronically excited lines, as they would require vibrations of 2000-3000 cm^{-1}, which is not a reasonable energy range for normal

---

[1] See Table 3.

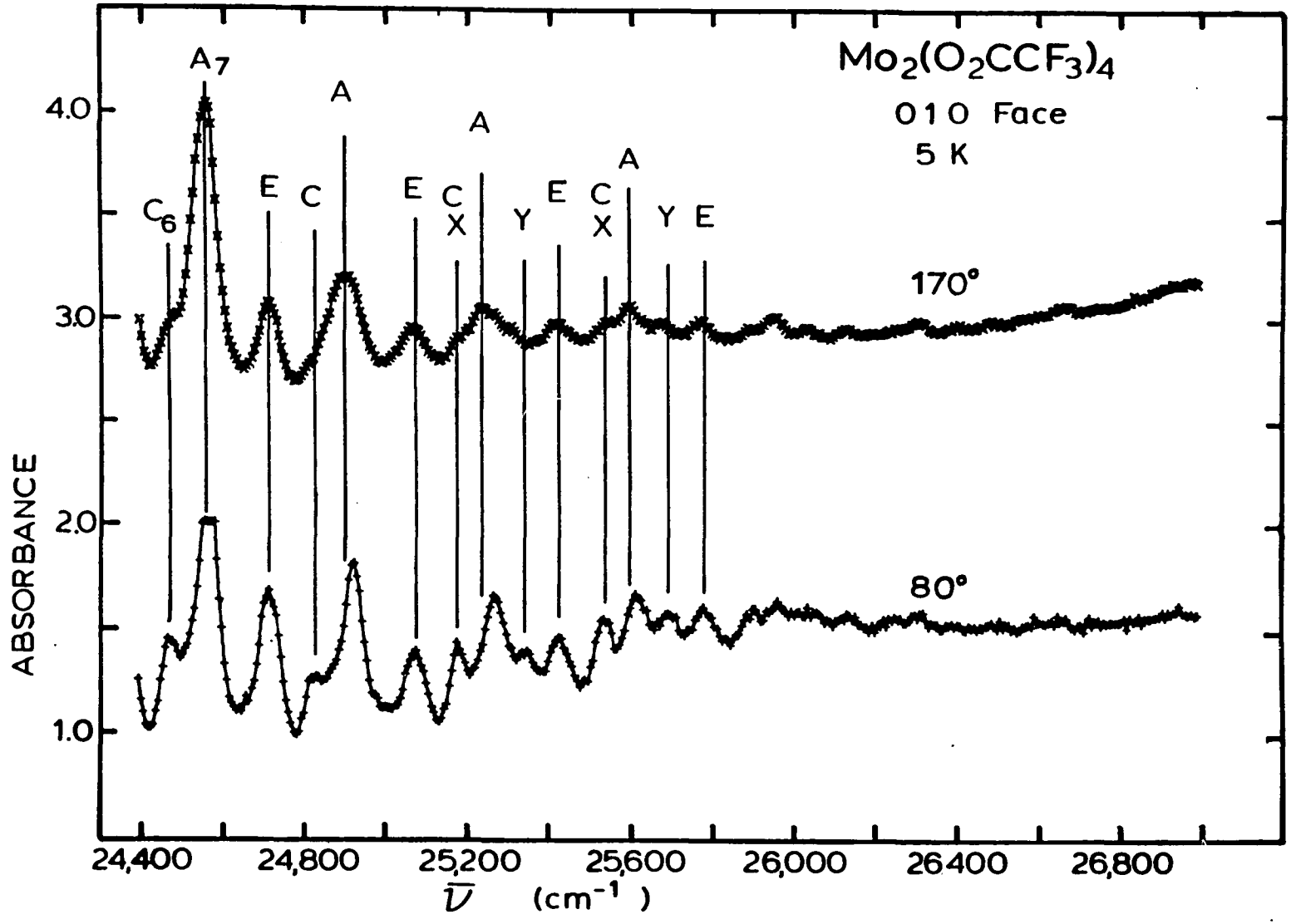

Figure 25. Single-crystal polarized spectra for the high-energy region of the first band of $Mo_2(O_2CCF_3)_4$ at 5K

vibrations associated with the $Mo_2(O_2CCF_3)_4$ molecule, which does not contain any hydrogens.

It has therefore been concluded that there is another band in this region that is somewhat weaker than the $\delta \rightarrow \delta^*$ transition. There is also the possibility of a defect component, but the intensities of these lines seems rather high for such a possibility. Perhaps this band is due to a spin-forbidden singlet-triplet transition which gains intensity due to its proximity to the $\delta \rightarrow \delta^*$ transition. The corresponding spin-allowed transition would then presumably lie under the intense absorption above 30,000 cm^{-1}.

Since the 27,500 cm^{-1} band, evident in Figure 20, falls on the tail of a more intense band at higher energy, the temperature dependence of this band is not clear. It is most likely the same transition observed for $Mo_2(O_2CCH_3)_4$ at $\sim$26,500 cm^{-1}, for which an assignment as the $\delta \rightarrow \pi^*$, $^1A_{1g} \rightarrow {}^1E_g$ transition has been proposed.

B. $K_2[Pt_2(SO_4)_4 \cdot 2H_2O]$

No wavelength-dependence for the extinctions was observable for crystals of $K_2[Pt_2(SO_4)_4 \cdot 2H_2O]$ between crossed polarizers of a polarizing microscope. Room temperature and 6K spectra, measured for the optically observed extinctions, are shown in Figures 26 and 27. The maximum polarization angle was checked at 300K for the 27,000 cm^{-1} band by rotating the polarizer first 10^o, then 20^o in both directions, and then measuring the absorption. No increase in absorption was observed for this band at 300K for other polarization angles.

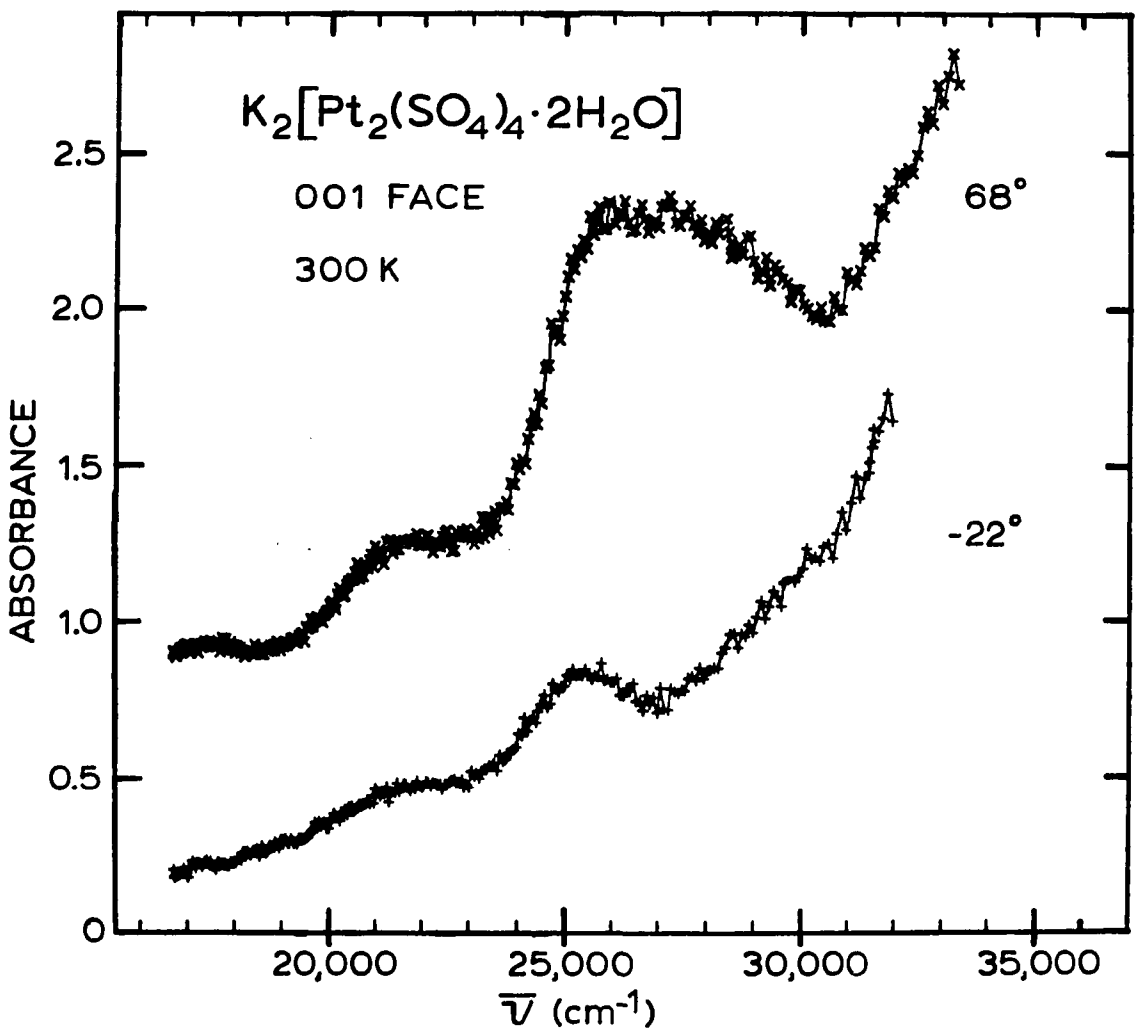

Figure 26. Single-crystal polarized absorption spectra for $K_2[Pt_2(SO_4)_4 \cdot 2H_2O]$ over the measurable range above 17,000 cm^{-1}. The small waves in the spectra from ∿17,000-18,000 cm^{-1} are due to inconsistencies in the baseline

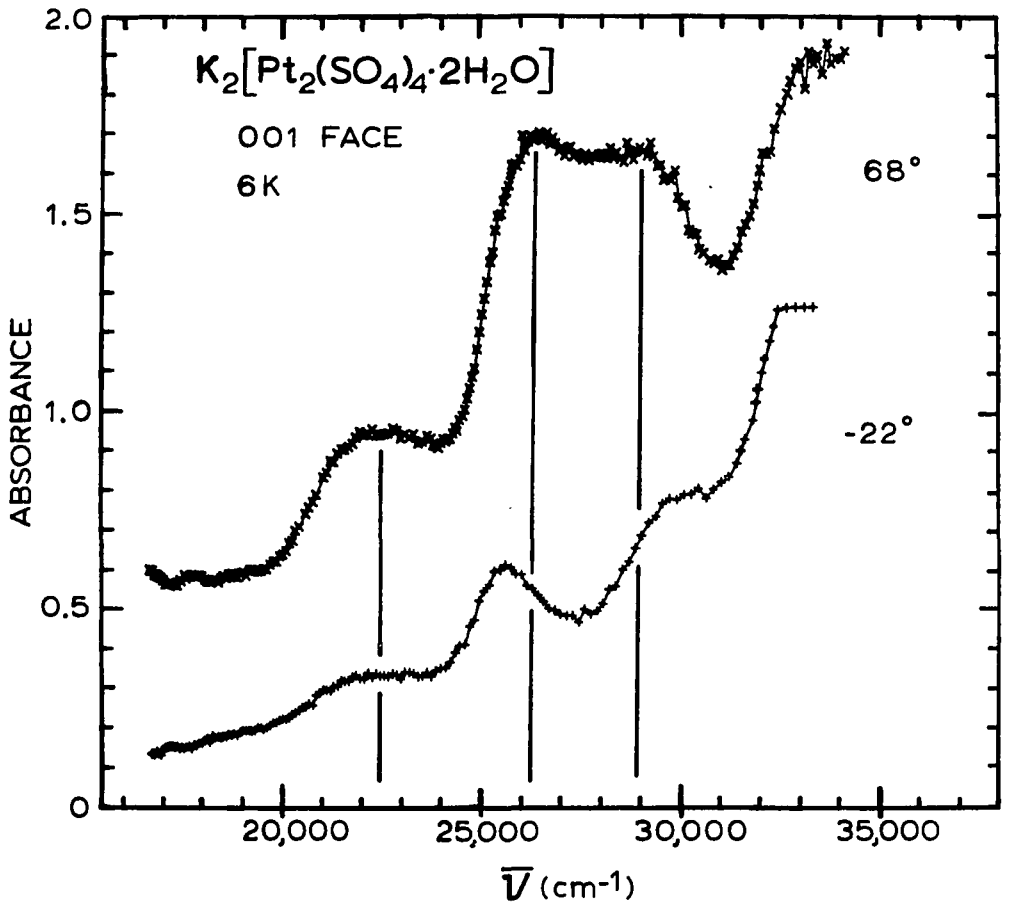

Figure 27. Single-crystal polarized spectra over the entire measurable range above 17,000 cm^{-1}. Note the peak at ca. 25,600 cm^{-1} in the -22° spectrum. The small waves from ∿17,000-18,000 cm^{-1} in the spectra are due to baseline inconsistencies

Originally it was believed that the polarizations of the low energy transitions of $K_2[Pt_2(SO_4)_4 \cdot 2H_2O]$ would follow those observed for $Rh_2(O_2CCH_3)_4 \cdot 2H_2O$, since both compounds have a d^7 electron configuration for the metal. Of the three lowest transitions observed in the spectroscopically accessible region for $Rh_2(O_2CCH_3)_4 \cdot 2H_2O$, two, including the lowest, were $\underset{\sim}{x},\underset{\sim}{y}$-polarized, and one was $\underset{\sim}{z}$-polarized.

The calculated polarization ratio for a molecular z-polarized transition in the 0 0 1 crystal face of the tetra-μ-sulfatodiplatinum(III) complex is $I_{68^o}/I_{-22^o} = 6.3/1$; for a molecular $\underset{\sim}{x},\underset{\sim}{y}$-polarized transition, $I_{68^o}/I_{-22^o} = 1/1.6$. We can see from Figures 26 and 27 that for all of the observed bands, the polarizations are considerably >1, so the transitions appear to be $\underset{\sim}{z}$-polarized.

However, careful examination of the 6K spectra later revealed a weak band in the -22^o spectrum at ca. 25,600 cm^{-1}, which is believed to correspond to an $\underset{\sim}{x},\underset{\sim}{y}$-polarized transition. While the three bands at 22,400 cm^{-1}, 26,300 cm^{-1}, and 29,100 cm^{-1} are all clearly $\underset{\sim}{z}$-polarized, it was not discovered until later, as shown in Figure 28, that the two higher energy bands did not maximize in the 68^o polarization at 6K. The 26,300 cm^{-1} band maximized at 58^o, and the 29,100 cm^{-1} band was a maximum at a polarization of 78^o. The peak seen at ~29,000-30,000 cm^{-1} for -22^o polarization in Figure 27 does not necessarily indicate a separate $\underset{\sim}{x},\underset{\sim}{y}$-polarized transition. Although it is not absolutely clear from Figure 27, this may correspond to the $\underset{\sim}{z}$-polarized band at 29,100 cm^{-1}. The apparent wavelength shift between these peaks for -22^o and 68^o spectra is likely due to baseline anomalies in this region for the two polarizations.

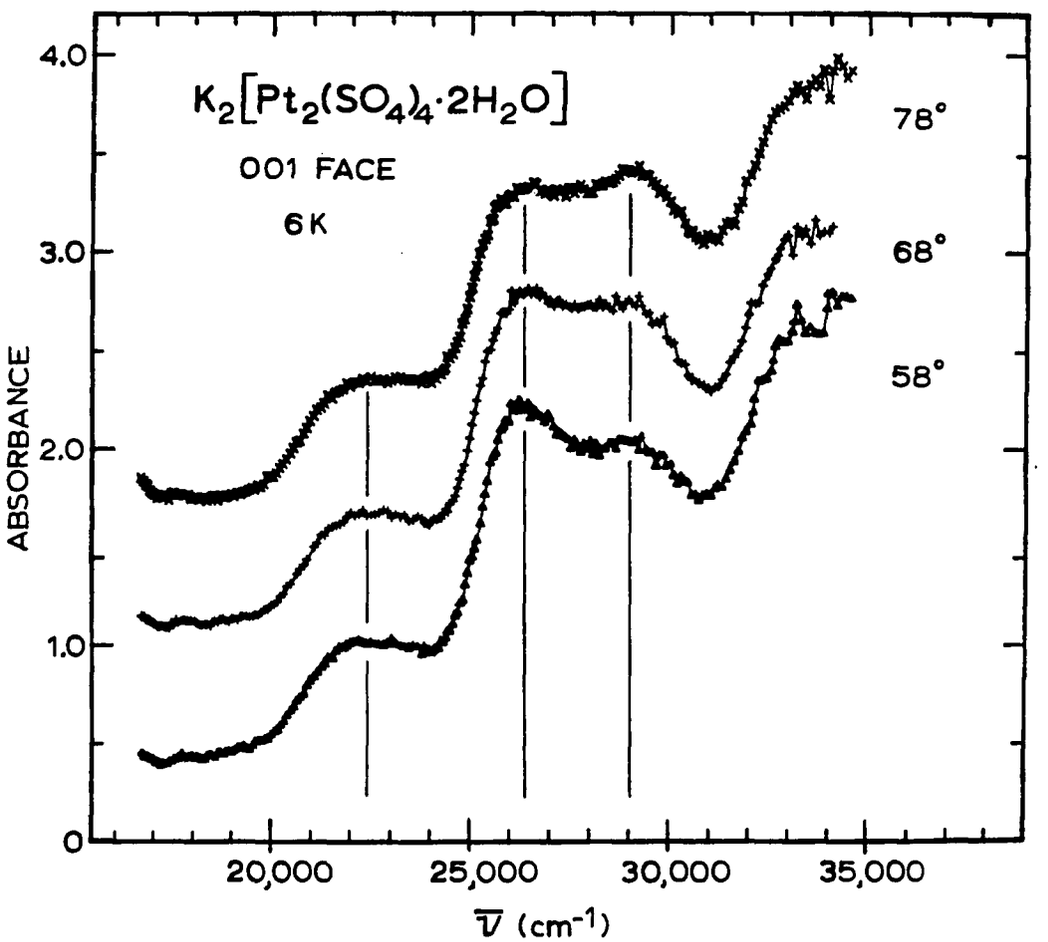

Figure 28. Single-crystal polarized absorption spectra over the measurable range above 17,000 cm^{-1} for $K_2[Pt_2(SO_4)_4 \cdot 2H_2O]$ at 6K. The small waves from ~17,000-18,000 cm^{-1} in the spectra are due to baseline inconsistencies

The observed results for the 6K polarized spectra, along with molar absorbtivities (ε) for the various maxima, are summarized in Table 13.

Table 13. Observed absorption maxima and molar absorptivities for $[K_2Pt_2(SO_4)_4 \cdot 2H_2O]$

Transition, cm^{-1}	Maximum polarization	ε value, $cm^{-1}M^{-1}$
22,400	58^o $(\underset{\sim}{z})$	∿145
25,600	-22^o $(\underset{\sim}{x},\underset{\sim}{y})$[a]	∿180
26,300	58^o $(\underset{\sim}{z})$	∿430
29,100	78^o $(\underset{\sim}{z})$	∿410

[a]Indeterminable due to the proximity of an intense absorption (see Figure 27).

The discrepancies between these results and those observed for $Rh_2(O_2CCH_3)_4 \cdot 2H_2O$ clearly indicate that some substantial shifts exist in molecular orbital energies between $Rh_2(O_2CCH_3)_4 \cdot 2H_2O$ and $K_2[Pt_2(SO_4)_4 \cdot 2H_2O]$. The primary difference in the 6K spectra appears to be the absence of the two intense $\underset{\sim}{x},\underset{\sim}{y}$-polarized bands observed for diaquo-tetra-μ-acetatodirhodium(II). Also, three $\underset{\sim}{z}$-polarized bands were observed, all of which exhibit the temperature-independent intensity properties of dipole allowed transitions. From the molecular orbital energy diagram derived from the Xα calculation for $Rh_2(O_2CH)_4 \cdot 2H_2O$ (see Figure 6), there are no $\underset{\sim}{z}$-polarized transitions accessible to account for more than two $\underset{\sim}{z}$-polarized bands in this region.

The following rationalization for the discrepancies between the polarized spectra of $Rh_2(O_2CCH_3)_4 \cdot 2H_2O$ and $K_2[Pt_2(SO_4)_4 \cdot 2H_2O]$ is offered, based on the assumption of ideal D_{2h} molecular symmetry for the $Pt_2(SO_4)_4 \cdot 2H_2O^{2-}$ anion. From earlier discussion, it is well-recognized that this may be an invalid assumption, since $Pt_2(SO_4)_4 \cdot 2H_2O^{2-}$ is only required to have $\bar{1}$ symmetry in the solid state. However, in a case where spectra are available for only one crystal face, the assignment of the transition moments as aligned with the molecular axes, which implies idealized molecular symmetry, is necessary in order to interpret the polarized spectra.

Some relevant bond distances for $Rh_2(O_2CCH_3)_4 \cdot 2H_2O$ and $Pt_2(SO_4)_4 \cdot 2H_2O^{2-}$ are given below:

Bond	M = Rh	M = Pt
M-M	2.3855Å	2.466Å
M-O_b [1]	2.039Å	1.988Å [2]
M-OH_2	2.310Å	2.12Å

The metal-metal bonding in the platinum complex should be stronger than for rhodium, even though the M-M distance is ∿0.08Å longer, since the larger 5d orbitals of platinum will have greater overlap than the 4d orbitals of rhodium. While the M-O_b distance is shorter for platinum, this is likely due to greater ionic bonding, as platinum forms notoriously

---

[1] O_b = oxygen of bridging ligand.

[2] Average value.

poor covalent bonds to small, "hard" ligands such as oxygen. However, the much shorter ($\sim$0.2Å) M-OH_2 distance for the platinum complex indicates that the axial waters are interacting more with the metal p_z orbitals than in the rhodium complex. Another difference, caused by the change in bridging ligands from carboxylates to sulfates, is the fact that the sulfate ligand has empty p-π^* molecular orbitals which can interact with the metal-metal π^* orbital, whereas the carboxylate has no unfilled molecular orbitals capable of interacting with this orbital. Also, and perhaps more important, the platinum p_x and p_y orbitals, which are only weakly covalently bonding to the oxygens of the bridging ligands, are thus released for greater mixing with the π and π^* orbitals of the platinum metal-metal bond.

Both of these interactions would have an energy-lowering effect on the normal π and π^* orbitals, formed from the $5d_{xz}$ and $5d_{yz}$ orbitals of platinum.

The postulated results of all these effects are shown in Figure 29. The lowering in energy of the M-Oσ^* orbitals in the diagram is due to the weaker covalent bonding expected between platinum and the sulfate oxygens. The b_{1g}, M-Oσ^* is shifted much lower than the a_u, M-Oσ^* because it has bonding symmetry with respect to the metal-metal axis, while the latter has metal-metal antibonding symmetry. The increase in energy of the M-M, M-$OH_2\sigma^*$ and M-Mδ^* orbitals is due to the stronger M-M and M-OH_2 bonding in the platinum compound. These effects result in the δ^* orbital being unoccupied in the platinum sulfate complex, and the b_{1g}, M-Oσ^* becoming the highest occupied orbital.

The $\pi(b_{2u},b_{3u})$ and $\pi^*(b_{2g},b_{3g})$ orbitals have not been labeled, since they have been shifted to lower energy. The same axis system as noted for Figure 6 has been used (see page 24).

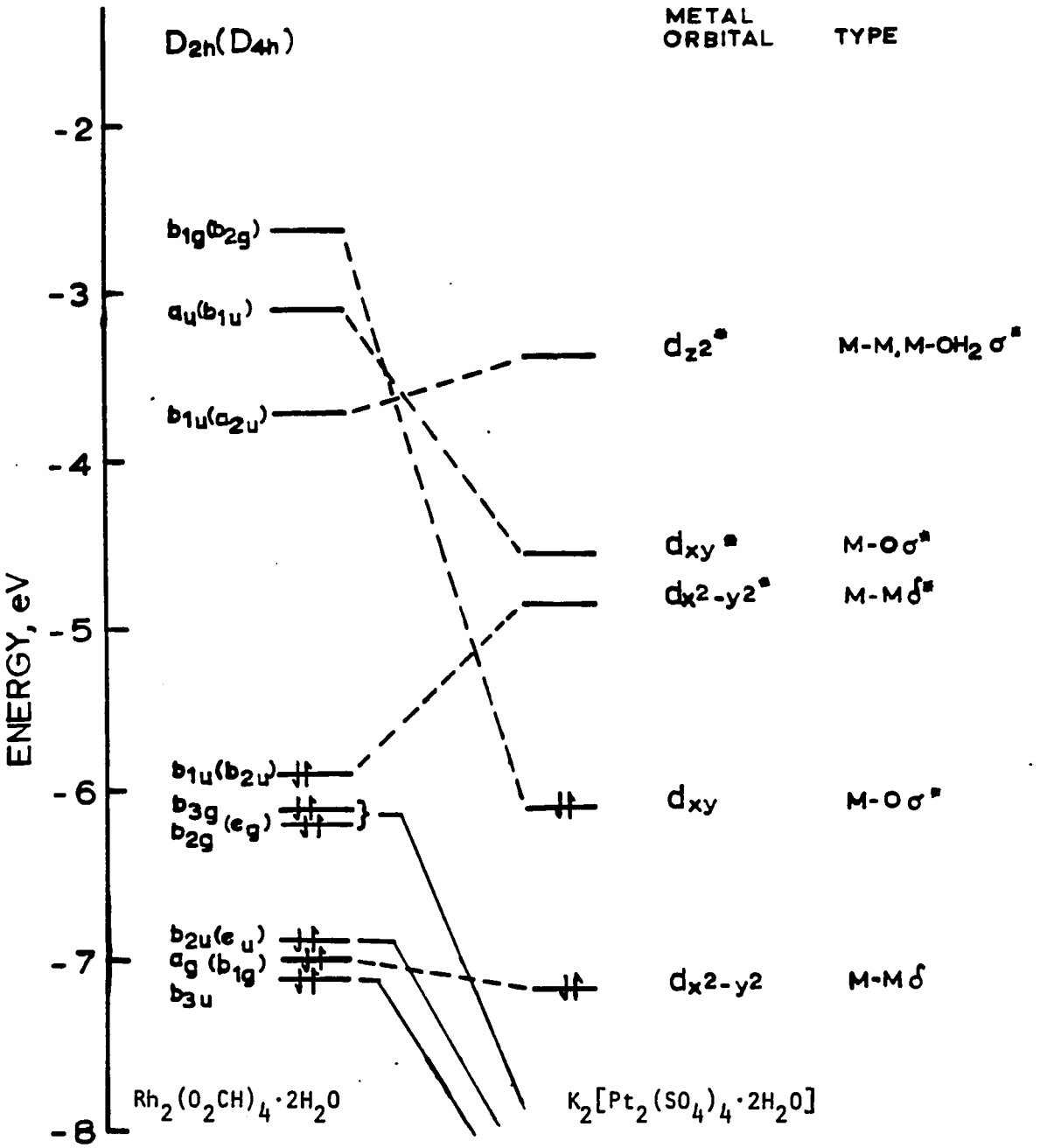

Figure 29. Proposed partial MO diagram for $K_2[Pt_2(SO_4)_4\cdot 2H_2O]$, relative to the orbital energies calculated for $Rh_2(O_2CH)_4\cdot 2H_2O$ by the SCF-Xα-SW method (34)

A molecular orbital ordering of this type can account for the observed spectra for the platinum sulfate complex. From Figure 29 under D_{2h} symmetry, the selection rules predict the following electric-dipole allowed transitions, all $\underset{\sim}{z}$-polarized:

(1) $M\text{-}O\sigma^* \rightarrow M\text{-}O\sigma^*$, $^1b_{1g} \rightarrow {}^1a_u$

(2) $M\text{-}M\delta \rightarrow M\text{-}M\delta^*$, $^1a_g \rightarrow {}^1b_{1u}$

(3) $M\text{-}M\delta \rightarrow M\text{-}M$, $M\text{-}OH_2\sigma^*$, $^1a_g \rightarrow {}^1b_{1u}$

- plus higher energy $\underset{\sim}{x},\underset{\sim}{y}$-polarized transitions.

The first transition is assumed to be due to the $M\text{-}O\sigma^* \rightarrow M\text{-}O\sigma^*$, $^1b_{1g} \rightarrow {}^1a_u$. Presumably, the intensity is somewhat reduced because the σ^* orbitals place some of the electron density on the ligands, thus reducing the overlap between the metal atoms which provides the transition moment. The second and third transitions are then assigned as the two intense maxima at 26,300 and 29,100 cm^{-1}.

The weak feature at 25,600 cm^{-1} mentioned previously is assigned as a separate x,y-polarized transition, but not just on the basis of the $\sim$700 cm^{-1} difference in the wavelength of the two maxima for the 58° and -22° polarizations. The predicted polarization ratio for a $\underset{\sim}{z}$-polarized transition is $I_{58°}/I_{-32°} = \sim 23/1$. The absorption at -32° polarization was not significantly different from that at -22°. From Figure 27, it is obvious that the observed polarization ratio cannot be that high, and in fact was measured as $\sim$3/1. The absorbance predicted for -32°, from the maximum in the 58° spectrum at 26,300 cm^{-1}, is less than 0.1. It has therefore been concluded that the 25,600 cm^{-1} $\underset{\sim}{x},\underset{\sim}{y}$-polarized band could be the spin forbidden transition, i.e., singlet-triplet, for either the

$M\text{-}M\delta \rightarrow M\text{-}M$, $M\text{-}OH_2\sigma^*$ or $M\text{-}M\delta \rightarrow M\text{-}M\delta^*$, both of which would be $^1a_g \rightarrow {}^3b_{1u}$. It would be expected to be at lower energy than the corresponding spin allowed transition, and be $\underset{\sim}{x},\underset{\sim}{y}$-polarized.[1] If this assignment is correct, one would then expect to see a spin forbidden transition associated with the remaining two $\underset{\sim}{z}$-polarized bands.

Under close examination, the region from ca. 18,000-21,000 cm^{-1} in Figures 26 and 27 appears to show a small amount of absorption for the -22^o polarization. However, baseline inconsistencies in this region prevent an unambiguous conclusion that an absorption is present.

Still, if there is in fact a weak absorption present, it could then be assigned as the $M\text{-}O\sigma^* \rightarrow M\text{-}O\sigma^*$, $^1b_{1g} \rightarrow {}^3a_u$ triplet transition associated with the 22,400 cm^{-1} band, due to its very low absorption. This then would indicate that the 25,600 cm^{-1} triplet transition is the $M\text{-}M\delta \rightarrow M\text{-}M\sigma^*$, $^1a_g \rightarrow {}^3b_{1u}$, $\sim$3500 cm^{-1} below the intense singlet transition. This spacing of $\sim$3500 cm^{-1} would then place the $^1b_{1g} \rightarrow {}^3a_u$ transition at $\sim$19,000 cm^{-1}, and the third triplet, $^1a_g \rightarrow {}^3b_{1u}$, should then be seen at $\sim$22,800 cm^{-1}. A spacing of 3500 cm^{-1} between the related singlet and triplet transitions is reasonable, based on previous proposals for platinum(II) compounds (69, 70).

While the proposed orbital energy diagram and spectroscopic assignments can adequately account for our experimental observations, there clearly is no concrete evidence to verify these conclusions. Other

---

[1] Selection rules for spin forbidden transitions in D_{2h} state that any spin allowed transition in one molecular polarization has a corresponding spin forbidden transition which is dipole allowed in the remaining two molecular polarizations.

assignments based on the $Rh_2(O_2CH)_4 \cdot 2H_2O$ orbital energy diagram might also yield a plausible interpretation of the observed polarized spectra.

It is believed the analysis presented above is quite reasonable, based on the data presently available for this complex, and the results obtained by the research group for other platinum complexes previously studied (69, 70). In order to verify or refute this analysis, more studies of the $Pt_2(SO_4)_4^{2-}$ dimeric complex are necessary. Other $Pt_2(SO_4)_4X_2^{4-}$ and $Pt_2(SO_4)_4XY^{4-}$ species[1] have been synthesized and characterized (39), though no crystal structures have been reported. Perhaps single-crystal spectral examinations of these compounds could clarify the experimental results obtained for $K_2[Pt_2(SO_4)_4 \cdot 2H_2O]$.

C. $Mo_2(O_2CCH_3)_4 \cdot KCl$

An ORTEP (71) drawing of the $Mo_2(O_2CCH_3)_4 \cdot KCl$ unit cell is shown in Figure 30. Only the crystallographically unique atoms have been labeled. The final positional and thermal parameters for the labeled atoms have been listed previously in Table 5. The potassium atoms lie on two-fold axes parallel to $\underset{\sim}{b}$, and the chlorine atoms occupy inversion centers. The The $Mo_2(O_2CCH_3)_4$ molecular unit has $\bar{1}$ symmetry, which results from the combination of $\underset{\sim}{C}$-centering and the centers of inversion. Distances and angles are listed in Tables 14 and 15, respectively.

The Mo-O1 and Mo-O2 distances of 2.127(2)Å and 2.137(2)Å are significantly longer (0.013-0.027Å) than the Mo-O3 (2.114(2)Å) and Mo-O4 (2.110(2)Å) distances. This is caused by the ionic interactions of O1

---

[1] X or Y = Cl^-, Br^-, OH^-, NO_2^-.

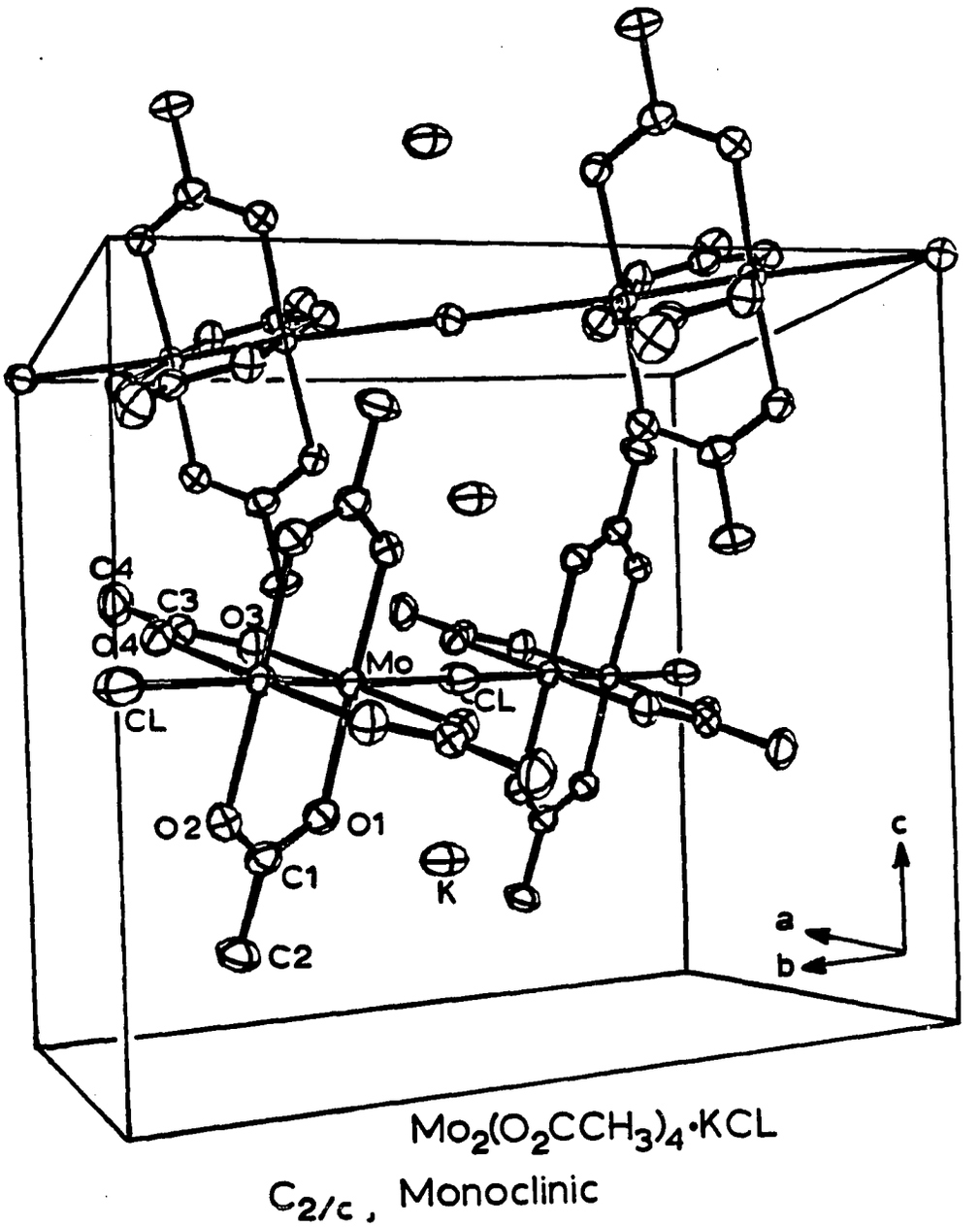

Figure 30. An ORTEP drawing of the unit cell of $Mo_2(O_2CCH_3)_4 \cdot KCl$. Note that some atoms have been added to clarify the structure, and the carboxylate ligands which would normally be at the bottom of the unit cell as shown have been moved to the top, in order to show complete molecules

Table 14. Interatomic distances and their estimated standard deviations[a] for $Mo_2(O_2CCH_3)_4 \cdot KCl$

	Distance, Å
	distances <3.0Å
Mo-Cl	2.9507(5)
Mo-Mo'	2.1019(6)
Mo-O1	2.127(2)
Mo-O2	2.137(2)
Mo-O3	2.114(2)
Mo-O4	2.110(2)
C1-O1	1.272(4)
C1-O2	1.274(4)
C1-C2	1.504(5)
C3-O3	1.265(4)
C3-O4	1.280(4)
C3-C4	1.510(5)
	distances >3.0Å
K-Cl	3.0078(6)
K-O1	3.083(3)Å
K-O2	3.022(2)Å
C2-O3	3.344(4)Å

[a] In parentheses for the least significant figure.

Table 15. Selected bond angles and their estimated standard deviations[a] for $Mo_2(O_2CCH_3)_4 \cdot KCl$

	Angle, degrees
Cl-Mo-Mo'[b]	176.20(2)
Cl-Mo-O1	90.75(7)
Cl-Mo-O2'	85.91(6)
Cl-Mo-O3	85.49(7)
Cl-Mo-O4'	91.23(6)
O1-Mo-O3	88.29(9)
O1-Mo-O4'	90.75(9)
O1-Mo-O2'	176.64(9)
O2'-Mo-O3	92.10(9)
O2'-Mo-O4'	88.67(9)
O3-Mo-O4'	176.56(9)
Mo-O1-C1	117.4(2)
Mo-O2'-C1'	117.3(2)
Mo-O3-C3	117.5(2)
Mo-O4'-C3'	117.2(2)
O1-C1-C2	119.5(3)
O2-C1-C2	118.6(3)
O3-C3-C4	119.8(3)
O4-C3-C4	118.3(3)

[a] In parentheses for the least significant figure.

[b] Primes refer to inversion-related atoms within the $Mo_2(O_2CCH_3)_4$ molecule.

and O2 with the potassium atoms, which result in a weakening of the Mo-O bond. O2 is 0.06Å closer to potassium than O1, and this closer contact is reflected in the 0.01Å longer Mo-O2 bond. The ionic attraction of the potassium also appears to determine the degree of rotation of the carboxylate "paddles" around the chain axes in the solid state (see Figure 30).

The Mo-Mo-O angles are all within 0.5° of one another, which indicates that there is little distortion within $Mo_2(O_2CCH_3)_4$ molecule in the chain axis direction. However, the Mo-Mo-Cl, Cl-Mo-O2' and Cl-Mo-O3 angles reveal that the $Mo_2(O_2CCH_3)_4$ molecule is tilted with respect to the chain axis, such that O3 and O2' are nearer to the chlorine than O1 or O4'. The chlorine atom is more than 2.95Å from the molybdenum atoms, which is approaching the chlorine-potassium ionic bonding distance of 3.0078(6)Å. This observation, plus comparison with other Mo-Cl distances (44), suggests that the Mo-Cl interaction is primarily of an ionic type. However, the Mo-Mo distance of 2.1019(6) is ∿0.009Å longer than in $Mo_2(O_2CCH_3)_4$, an indication of some electron donation from chlorine into the metal-metal σ^* orbital. It appears that the Mo-Cl and K-O interaction, combined with the normal K-Cl ionic bonding, determine the orientation of the $Mo_2(O_2CCH_3)_4$ molecules in the unit cell. The alternating chains, which extend along the two $\underset{\sim}{ab}$ diagonals, are not perpendicular to one another. Figure 31 shows an ORTEP view for several unit cells along the $\underset{\sim}{c}$ axis. The shift of the potassium atoms away from the center of the 0 0 1 plane is more obvious from this view. The acute angle between successive chains, which is bisected by $\underset{\sim}{b}$, is 74.62(2)°.

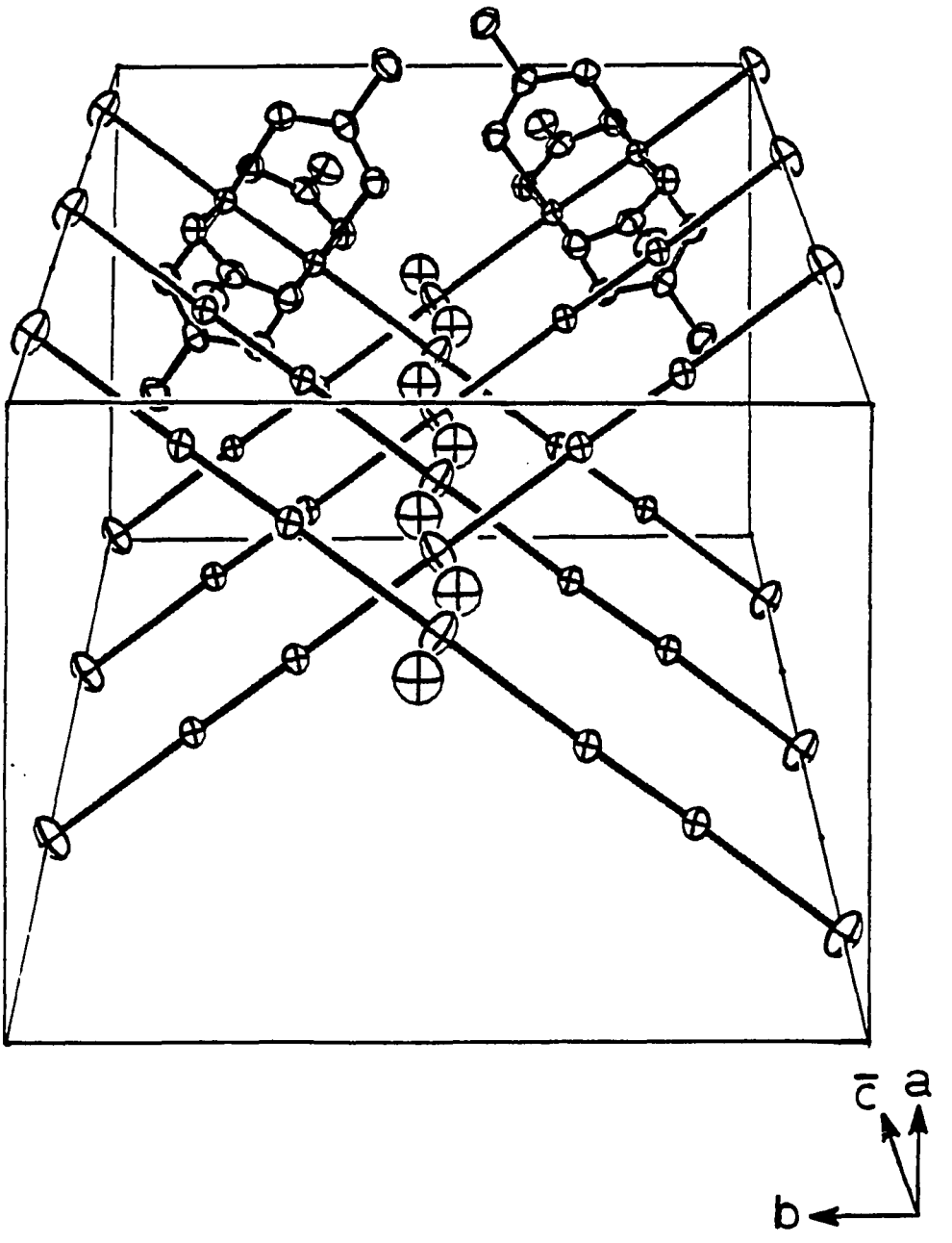

Figure 31. An alternate ORTEP view showing several unit cells along the $\bar{c}$ axis for $Mo_2(O_2CCH_3)_4 \cdot KCl$. The carboxylate ligands have been omitted for all except two of the Mo-Mo units for the purpose of clarity

The closest intermolecular contact appears to be between the atom crystallographically equivalent to C2, almost directly above O3 in Figure 30. The C2-O3 distance of 3.344(4)Å appears long, but the distortion of the O4-C3-O3 framework indicates an interaction is occurring between the C2 methyl hydrogens and O3, since the C3-O3 distance of 1.265(4)Å is significantly shorter than the O4-C3 distance of 1.280(4)Å, and the C4-C3-O3 angle of 119.8(3)° is ca. 1.5° larger than the C4-C3-O4 angle. Some distortion also occurs for the O1-C1-C2 (119.5(3)°) and O2-C1-C2 (118.6(3)°) angles. The angular distortions caused by this interaction indicate it is of a repulsive type, although the cause of the C3-O4 bond lengthening, which is on the borderline of statistical significance, is unclear. While there is no distortion of the metal dimer molecules along the chain axes, the O1-Mo-O2' and O3-Mo-O4' angles of 176.64(9)° and 176.56(9)°, respectively, indicate some distortion approximately along the directions perpendicular to each chain. The angle O3-Mo-O2' is the largest, at 92.10(9)°, between the ideally perpendicular oxygens of the two adjacent carboxylates. In Figure 30, it appears that this distortion is also due to the proximity of the C2 methyl group from the metal dimer in the upper chain.

The underlying purpose of the synthesis and characterization of this compound was to obtain a crystal containing the $Mo_2(O_2CCH_3)_4$ molecule in a different environment than in the simple acetate. It was hoped that this compound would yield more information about the bonding and energy levels of the $Mo_2(O_2CCH_3)_4$ molecule, by recording and analyzing its single-crystal polarized spectra. However, in this case, the crystals are not plate-like, and are generally of a form unsuitable for the recording

of high quality solid-state spectra. However, perhaps the synthesis and characterization of this compound will lead to the preparation of similar compounds which will be of a form more suitable for single-crystal spectroscopy.

IV. BIBLIOGRAPHY

1. Dubicki, L.; Martin, R. L. Aust. J. Chem. 1969, 22, 1571.

2. Trogler, W. C.; Solomon, E. I.; Trajberg, I.; Ballhausen, C. J.; Gray, H. B. Inorg. Chem. 1977, 16, 828.

3. Cotton, F. A.; Martin, D. S.; Fanwick, P. E.; Peters, T. J.; Webb, T. R. J. Am. Chem. Soc. 1976, 98, 4681.

4. Erwin, D. K.; Geoffroy, G. L.; Gray, H. B.; Hammond, G. S.; Solomon, E. I.; Trogler, W. C.; Zagars, A. A. J. Am. Chem. Soc. 1977, 99, 3620.

5. Fanwick, P. E.; Martin, D. S.; Cotton, F. A.; Webb, T. R. Inorg. Chem. 1977, 16, 2103.

6. Clark, R. J. H.; D'Urso, N. R. J. Am. Chem. Soc. 1978, 100, 3088.

7. Muraveiskaya, G. S.; Kukina, G. A.; Orlova, V. S.; Estaf'eva, O. N.; Porai-Koshits, M. A. Dokl. Akad. Nauk SSSR (Engl. Transl.) 1976, 226, No. 3, 596.

8. Martin, D. S.; Webb, T. R.; Robbins, G. A.; Fanwick, P. E. Inorg. Chem. 1979, 18, 475.

9. Cotton, F. A. Inorg. Chem. 1965, 4, 334.

10. Cotton, F. A.; Harris, C. B. Inorg. Chem. 1965, 4, 330.

11. Cotton, F. A.; Harris, C. B. Inorg. Chem. 1967, 6, 924.

12. Mortola, A. P.; Moskowitz, J. W.; Rosch, N.; Cowman, C. D.; Gray, H. B. Chem. Phys. Lett. 1975, 32, 283.

13. Norman, J. G.; Kolari, H. J. J. Chem. Soc., Chem. Commun. 1974, 303; J. Am. Chem. Soc. 1975, 97. 33.

14. Norman, J. G.; Kolari, H. J. J. Chem. Soc., Chem. Commun. 1975, 649.

15. Norman, J. G.; Kolari, H. J.; Gray, H. B.; Trogler, W. C. Inorg. Chem. 1977, 16, 987.

16. Gray, H. B.; Trogler, W. C. Accts. Chem. Res. 1978, 11, 232.

17. Cotton, F. A.; Kalbacher, B. J. Inorg. Chem. 1977, 16, 2386.

18. Cotton, F. A.; Fanwick, P. E.; Gage, L. D.; Kalbacher, B. J.; Martin, D. S. J. Am. Chem. Soc. 1977, 99, 5642.

19. Noodleman, L.; Norman, J. G. J. Chem. Phys. 1979, 70 (11), 4903.

20. Cotton, F. A.; Curtis, N. F.; Johnson, B. F. G.; Robinson, W. R. Inorg. Chem. 1965, 4, 326.

21. Cowman, C. D.; Gray, H. B. J. Am. Chem. Soc. 1973, 95, 8177.

22. Trogler, W. C.; Cowman, C. D.; Gray, H. B.; Cotton, F. A. J. Am. Chem. Soc. 1977, 99, 2993.

23. Clark, R. J. H.; Franks, M. L. J. Am. Chem. Soc. 1976, 98, 2763.

24. Piper, T. S. J. Chem. Phys. 1961, 35 (4), 1240.

25. Cotton, F. A.; Frenz, B. A.; Stults, B. R.; Webb, T. R.; J. Am. Chem. Soc. 1976, 98 (10), 2768.

26. Templeton, J. L. Prog. Inorg. Chem. 1979, 26, 211.

27. Cowman, C. D.; Trogler, W. C.; Gray, H. B. Israel J. Chem. 1977, 15, 308.

28. Cotton, F. A.; Martin, D. S.; Webb, T. R.; Peters, T. J. Inorg. Chem. 1976, 15, 1199.

29. Cotton, F. A.; Webb, T. R. Inorg. Chem 1976, 15, 68.

30. Schwachan, K.; Hedwig, K.; Schenk, H. J.; Greis, O. Inorg. Nucl. Chem. Lett. 1977, 13, 77.

31. Loewenschuss, A.; Shamir, J.; Ardon, M. Inorg. Chem. 1976, 15, 238.

32. Fanwick, P. E.; Martin, D. S.; Webb, T. R.; Robbins, G. A.; Newman, R. A. Inorg. Chem. 1978, 17, 2723.

33. Clark, R. J. H.; Franks, M. L. J. Am. Chem. Soc. 1975, 97, 2691.

34. Norman, J. G.; Kolari, H. J. J. Am. Chem. Soc. 1978, 100, 791.

35. Cotton, F. A.; Deboer, B. G.; Laprade, M. D.; Pipal, J. R.; Ucko, D. A. Acta Cryst. 1971, B27, 1664.

36. Johnson, S. A.; Hunt, H. R.; Neuman, H. M. Inorg. Chem. 1963, 2, 960.

37. Dubicki, L.; Martin, R. L. Inorg. Chem. 1970, 9, 673.

38. Cotton, F. A.; Norman, J. G. J. Am. Chem. Soc. 1971, 93, 80.

39. Orlova, V. A.; Muraveiskaya, G. S.; Evstaf'eva, O. N. Russ. J. Inorg. Chem., Translated from Zh. Neorg. Khim. 1975, 20, 1340.

40. Cotton, F. A.; Norman, J. G. J. Am. Chem. Soc. 1972, 94, 5697.

41. Ricard, L.; Karagiannidis, P.; Weiss, R. Inorg. Chem. 1973, 12, 2179.

42. Collins, D. M.; Cotton, F. A.; Murillo, C. A. Inorg. Chem. 1976, 15, 2950.

43. Cotton, F. A.; Frenz, B. A.; Pedersen, E.; Webb, T. R. Inorg. Chem. 1975, 14, 391.

44. Robbins, G. A. M.S. Thesis, Iowa State University, Ames, Iowa, 1978, and references cited therein.

45. Pancharatnam, S. Proc. Indian Acad. Sci., Sec. A 1955, 42, 86.

46. Bloss, F. D. "An Introduction to the Methods of Optical Crystallography"; Holt, Rinehart and Winston: New York, 1961; Chapter 5, pp. 50-53.

47. Bloss, F. D.; ibid., Chapter 8, p. 144.

48. Jacobson, R. A. "An Algorithm For Automatic Indexing and Bravais Lattice Selection: the programs BLIND and ALICE", Ames Laboratory - USAEC Report IS-3469, Iowa State University, Ames, Iowa, 1974.

49. "Crystal Data Determinative Tables", 2nd Ed.; American Cryst. Assoc., Williams and Heinz Map Corp.: Washington, D.C., 1963; pp. 2, 3.

50. Cotton, F. A.; Mester, E. C.; Webb, T. R. Acta Cryst. 1974, B30, 2768.

51. Cotton, F. A.; Norman, J. G. J. Coord. Chem. 1971, 1, 161.

52. Muraveiskaya, G. S.; Orlova, V. S.; Evstaf'eva, O. N. Russ. J. Chem., Translated from Zh. Neorg. Khim. 1974, 19, 1030.

53. Lawton, S. L.; Jacobson, R. A. Inorg. Chem. 1968, 7, 2124.

54. Takusagawa, F. Ames Laboratory USDOE, Iowa State University, Ames, Iowa, unpublished.

55. Howells, E. R.; Phillips, D. C.; Rogers, D. Acta Cryst. 1950, 3, 210.

56. Powell, D. R.; Jacobson, R. A. "FOUR: A Generalized Crystallographic Fourier Program", Ames Laboratory-DOE Report IS-4737, Iowa State University, Ames, Iowa, 1980.

57. Takusagawa, F. Ames Laboratory, USDOE, Iowa State University, Ames, Iowa, unpublished.

58. Karcher, B. A. Ph.D. Dissertation, Iowa State University, Ames, Iowa, 1981.

59. Cruickshank, D. W. J.; Pilling, D. E. "Computing Methods and the Phase Problem in X-ray Crystal Analysis", Pepinsky, R.; Roberts, J. M.; Speakmen, J. C., Editors; Pergamon Press: New York, N.Y., 1961; p. 45.

60. Hanson, H. P.; Herman, F.; Lea, J. D.; Skillman, S. Acta Cryst. 1960, 17, 1040.

61. Templeton, D. H. "International Tables for X-ray Crystallography"; The Kynoch Press: Birmingham, England, 1962; Vol. III, Table 3.3.2c, pp. 215, 216.

62. Stewart, R. F.; Davidson, N. J. Chem. Phys. 1963, 39, 255.

63. Bratton, W. K.; Cotton, F. A.; DeBeau, M. J. Coord. Chem. 1971, 1, 121.

64. Craig, D. P.; Small, G. J. J. Chem. Phys. 1969, 50, 3827.

65. Yeung, E. S. J. Mol. Spectrosc. 1973, 45, 142.

66. Craig, D. P.; Walmsley, S. H. "Excitons in Molecular Crystals", W. A. Benjamin, Inc.: New York, 1968; Chapter 6.

67. Bino, A.; Cotton, F. A.; Fanwick, P. E. Inorg. Chem. 1980, 19, 1215.

68. Cotton, F. A.; Fanwick, P. E. J. Am. Chem. Soc. 1979, 18, 5252.

69. Martin, D. S.; Tucker, M. A.; Kassman, A. J. Inorg. Chem. 1965, 4, 1682.

70. Kroening, R. F.; Rush, R. M.; Martin, D. S.; Clardy, J. C. Inorg. Chem. 1974, 13, 1366.

71. Johnson, C. K. AEC Report ORNL-3794, Oak Ridge Tenn., March 1971 (second revision).

V. ACKNOWLEDGEMENTS

The author wishes to express his gratitude to Dr. R. A. Jacobson and members of his X-ray Crystallography group, for all their advice and assistance with the countless crystallographic problems encountered during the course of this research, and also especially thanks Jim Richardson, for his invaluable assistance in the solution of the crystal structure reported herein. He also gratefully acknowledges the diligent effort of Linda Deaton in performing the nearly impossible task of interpreting the author's almost illegible handwriting and typing the manuscript.

The author also wishes to thank the members of Radiochemistry Group II, for their assistance and advice in the course of the research, and for the many interesting discussions which created a stimulating atmosphere in which to work.

The author wishes to specially acknowledge his wife, Sigrid, without whose patience, support and understanding, this work would never have been accomplished. He also wishes to thank his parents for their continued support and encouragement throughout his academic career.

Finally, and most importantly, the author wishes to thank Dr. Don S. Martin for all the advice, encouragement and assistance rendered during the course of his graduate career, and for the many stimulating discussions which nurtured his curiosity and interest in the field of spectroscopy.

VI. APPENDIX: FINAL OBSERVED AND CALCULATED STRUCTURE FACTORS FOR $Mo_2(O_2CCH_3)_4 \cdot KCl$

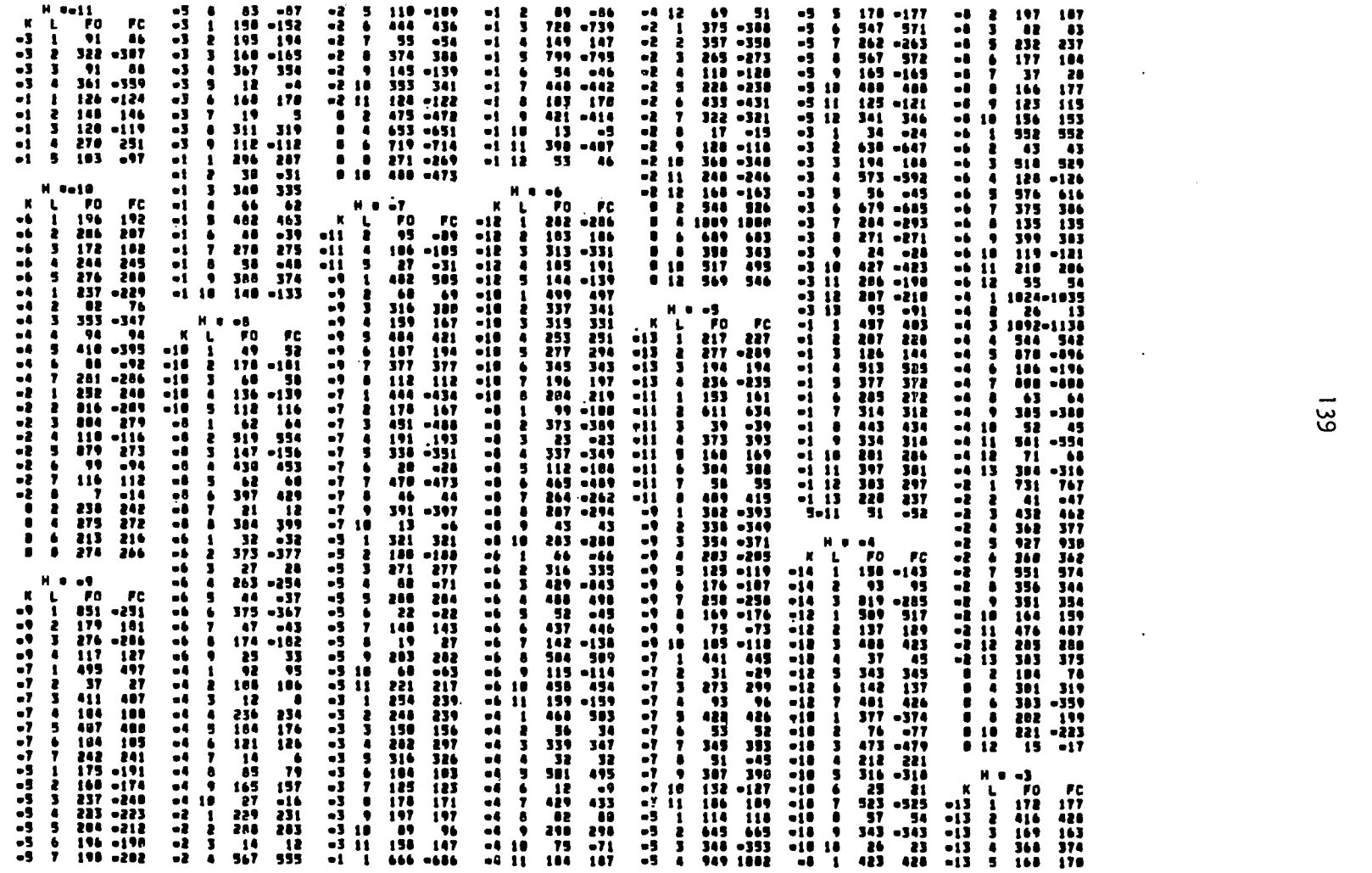

-13	6	373	389	-1	2	384	-378	-6	8	187	-187	-11	9	15	10	-1	11	403	-411	8	3	318	311	3	8	188	188
-11	1	18	8	-1	3	69	78	-6	9	148	-136	-9	1	633	654	-1	12	291	286	8	4	679	-652	3	9	208	196
-11	2	486	-505	-1	4	39	30	-6	10	148	-143	-9	2	138	-134	-1	13	285	-298	8	5	209	-211	3	10	131	-131
-11	3	26	38	-1	5	335	325	-6	11	328	-313	-9	3	938	933	-1	14	69	66	8	6	656	-660	3	11	177	178
-11	4	485	-497	-1	6	354	-367	-6	12	99	-103	-9	4	188	-118	15	-2	169	166	8	7	257	258	3	12	142	141
-11	5	149	148	-1	7	44	40	-6	13	254	-259	-9	5	942	955					8	8	538	-543	3	13	95	108
-11	6	397	-408	-1	8	64	-60	-4	1	898	949	-9	6	26	18		M =	0		8	9	118	-109	5	0	945	954
-11	7	84	-86	-1	9	258	253	-4	2	447	478	-9	7	161	173	K	L	FO	FC	8	10	418	-433	5	1	438	416
-11	8	521	-536	-1	10	369	-361	-4	3	553	605	-9	8	26	-28	-8	12	227	-243	8	11	95	-93	5	2	244	293
-11	9	66	62	-1	11	61	51	-4	4	287	327	-9	9	498	496	8	4	1326	1361	10	0	504	482	5	3	719	703
-9	1	48	-48	-1	12	87	-89	-4	5	858	894	-9	10	138	-133	8	6	1879	1874	10	1	143	-139	5	4	674	674
-9	2	569	593	-1	13	18	11	-4	6	279	269	-9	11	218	228	8	8	767	769	10	2	437	440	5	5	415	416
-9	3	434	-451	-1	14	188	-182	-4	7	524	513	-7	1	476	-485	8	10	496	501	10	3	184	184	5	6	328	336
-9	4	532	547	7	-9	234	-248	-4	8	239	239	-7	2	117	-99	8	12	798	826	10	4	508	489	5	7	564	559
-9	5	162	-164					-4	9	508	503	-7	3	756	-796	8	14	463	423	10	5	43	-42	5	8	129	116
-9	6	362	345		M =	-2		-4	10	218	-199	-7	4	194	208	2	8	985	-1078	10	6	316	326	5	9	316	312
-9	7	62	-38	K	L	FO	FC	-4	11	557	559	-7	5	476	-511	2	1	76	-88	10	7	77	78	5	10	178	165
-9	8	464	457	-14	1	169	181	-4	12	163	169	-7	6	83	-89	2	2	789	-795	10	8	335	333	5	11	289	295
-9	9	15	-30	-14	2	458	451	-4	13	509	485	-7	7	638	-658	2	3	565	-558	10	9	98	88	5	12	146	131
-9	10	338	344	-14	3	211	198	-2	1	193	-186	-7	8	60	-58	2	4	349	-378	10	10	285	293	5	13	95	97
-9	11	58	-11	-14	4	242	250	-2	2	112	71	-7	9	508	-528	2	5	536	-492	12	0	256	249	7	0	261	258
-7	1	412	429	-14	5	144	156	-2	3	287	-281	-7	10	63	50	2	6	829	-832	12	1	23	-23	7	1	1068	-1032
-7	2	298	323	-12	1	316	-321	-2	4	959	986	-7	11	433	-449	2	7	187	189	12	2	361	355	7	2	281	251
-7	3	210	204	-12	2	108	-112	-2	5	833	-820	-7	12	46	-43	2	8	58	-46	12	3	45	49	7	3	927	-918
-7	4	338	337	-12	3	615	-614	-2	6	427	444	-5	1	693	732	2	9	46	-51	12	4	281	281	7	4	83	88
-7	5	336	353	-12	4	27	-18	-2	7	789	-798	-5	2	681	688	2	10	386	-373	12	5	74	-69	7	5	1029	-1028
-7	6	218	216	-12	5	332	-345	-2	8	651	657	-5	3	174	182	2	11	74	-63	12	6	288	282	7	6	19	18
-7	7	22	-19	-12	6	64	-59	-2	9	489	-399	-5	4	365	376	2	12	286	-287	12	7	51	-41	7	7	588	-581
-7	8	281	285	-12	7	397	-408	-2	10	338	327	-5	5	413	438	2	13	79	-88	12	8	173	177	7	8	258	241
-7	9	185	184	-12	8	43	-44	-2	11	493	-488	-5	6	279	288	4	0	148	121	14	0	291	-284	7	9	691	-688
-7	10	114	109	-10	1	526	554	-2	12	336	348	-5	7	270	275	4	1	584	-648	14	1	89	-89	7	10	169	-165
-7	11	41	24	-10	2	146	-146	-2	13	217	-215	-5	8	723	741	4	2	86	-128	14	2	388	-395	7	11	304	-299
-7	12	175	178	-10	3	479	488	-0	14	86	86	-5	9	318	318	4	3	168	206	14	3	13	4	7	12	34	37
-5	1	137	-139	-10	4	278	-275	0	2	351	-379	-5	10	297	301	4	4	485	491	14	4	418	-426	9	0	111	-78
-5	2	964	-962	-10	5	562	554	0	4	517	-502	-5	11	148	146	4	5	72	61	14	5	83	-68	9	1	568	558
-5	3	198	-191	-10	6	37	29	0	6	1122	-1123	-5	12	494	483	4	6	75	-69					9	2	244	-249
-5	4	538	-565	-10	7	361	359	0	8	169	-163	-5	13	877	288	4	7	285	271		M =	1		9	3	846	814
-5	6	612	-626	-10	8	0	-5	0	10	208	-195	-3	1	150	167	4	8	153	151	K	L	FO	FC	9	4	45	-46
-5	7	304	-318	-10	9	425	427	0	12	91	-68	-3	2	442	-428	4	9	81	55	1	0	385	444	9	5	497	484
-5	8	314	-316	-10	10	56	-56	0	14	186	-178	-3	3	62	-39	4	10	60	-56	1	2	48	18	9	6	188	95
-5	9	75	60	-8	1	60	38					-3	4	158	-171	4	11	203	211	1	3	346	-315	9	7	443	446
-5	10	337	-332	-8	2	603	617		M =	-1		-3	5	715	709	4	12	4	-2	1	4	567	565	9	9	339	354
-5	11	83	-73	-8	3	299	-308	K	L	FO	FC	-3	6	581	-607	4	13	148	141	1	5	871	-887	9	10	65	64
-5	12	898	-294	-8	4	658	697	-15	1	348	364	-3	7	861	862	6	0	1831	1816	1	6	165	166	9	11	337	341
-5	13	38	26	-8	5	113	-118	-15	2	29	27	-3	8	267	-258	6	1	323	-317	1	7	717	-718	11	0	317	323
-3	1	461	437	-8	6	367	378	-13	1	267	-258	-3	9	333	355	6	2	642	663	1	8	422	434	11	1	237	-237
-3	2	878	938	-8	7	23	-26	-13	2	158	-158	-3	10	291	-282	6	3	84	79	1	9	648	-654	11	2	346	338
-3	3	117	-117	-8	8	363	394	-13	3	448	-455	-3	11	98	89	6	4	1075	1068	1	10	114	111	11	3	54	56
-3	4	1269	1302	-8	9	23	-13	-13	4	117	-118	-3	12	154	-148	6	5	44	35	1	11	599	-598	11	4	261	254
-3	5	116	104	-8	10	287	291	-13	5	176	-188	-3	13	67	62	6	6	892	905	1	12	192	184	11	5	148	-136
-3	6	784	817	-8	11	169	-171	-13	6	18	-14	-1	0	36	27	6	7	198	-184	1	13	526	-507	11	6	131	126
-3	7	838	283	-8	12	251	263	-13	7	246	-251	-1	3	1334	-1406	6	8	798	779	3	0	235	234	11	7	10	4
-3	8	866	888	-6	1	458	-465	-11	1	33	33	-1	4	1132	1138	6	9	224	-224	3	1	561	483	11	8	95	102
-3	9	47	-42	-6	2	514	-561	-11	2	588	517	-1	5	1435	-1384	6	10	512	516	3	2	165	-226	11	9	185	-185
-3	10	585	597	-6	3	518	-547	-11	3	28	-22	-1	6	417	446	6	11	54	51	3	3	331	358	13	0	181	-173
-3	11	157	-165	-6	4	46	47	-11	4	379	407	-1	7	555	-573	6	12	495	515	3	4	177	170	13	1	344	-337
-3	12	668	687	-6	5	75	-84	-11	6	289	284	-1	8	495	493	8	0	658	-647	3	5	194	187	13	2	102	-99
-3	13	14	-23	-6	6	306	-315	-11	7	59	-62	-1	9	421	-408	8	1	167	168	3	6	451	-458	13	3	402	-399
-1	1	51	53	-6	7	502	-497	-11	8	337	347	-1	10	77	75	8	2	627	-642	3	7	352	372	13	4	49	-46

K	L	FO	FC
13	5	238	-236
13	6	3	-9
13	7	163	-162
15	0	56	58
15	1	363	351

M = 2

K	L	FO	FC
0	0	615	-601
0	2	356	-375
0	4	83	-100
0	6	1095	-1083
0	8	382	-397
0	10	663	-644
0	12	343	-349
2	0	1172	1248
2	1	1121	-1204
2	2	278	321
2	3	208	-252
2	4	849	911
2	5	688	-588
2	6	793	881
2	7	632	-634
2	8	733	717
2	9	228	-223
2	10	342	325
2	11	115	-111
2	12	448	444
2	13	161	-169
4	0	777	726
4	1	1198	1112
4	2	156	-134
4	3	813	807
4	4	434	449
4	5	623	611
4	6	184	188
4	7	558	559
4	8	145	156
4	9	88	85
4	10	89	79
4	11	345	348
4	12	181	188
4	13	168	171
6	0	549	-552
6	1	632	-612
6	2	397	-399
6	3	118	-114
6	4	524	-538
6	5	534	-533
6	6	613	-624
6	7	123	-117
6	8	134	-118
6	9	216	-213
6	10	238	-244
6	11	173	-167
6	12	166	-171
8	0	918	918
8	1	387	-379
8	2	832	828
8	3	89	-65
8	4	771	736
8	6	469	468
8	7	61	61
8	8	495	501
8	9	74	-71
8	10	467	478
8	11	69	78
10	0	229	-219
10	1	322	307
10	2	219	-218
10	3	396	388
10	4	60	-63
10	5	134	135
10	6	46	-39
10	7	368	375
10	8	134	-143
10	9	250	253
10	10	149	-158
12	0	44	-41
12	1	328	-303
12	2	33	-29
12	3	247	-243
12	4	64	-58
12	5	295	-298
12	6	41	38
12	7	188	-176
12	8	61	-60
14	0	383	317
14	1	161	153
14	2	393	368
14	3	168	169
14	4	359	358

M = 3

K	L	FO	FC
1	0	152	85
1	1	788	734
1	2	478	-498
1	3	428	435
1	4	31	-28
1	5	551	555
1	6	484	-492
1	7	683	568
1	8	13	18
1	9	389	318
1	10	148	-138
1	11	285	218
1	12	18	-28
1	13	232	235
3	0	1528	1676
3	1	639	-627
3	2	1278	1228
3	3	436	-418
3	4	972	981
3	5	246	-238
3	6	743	754
3	7	67	-58
3	8	683	677
3	10	484	418
3	11	16	35
3	12	487	491
5	0	761	-747
5	1	265	-247
5	2	872	-885
5	3	62	-57
5	4	258	-258
5	5	384	-366
5	6	518	-507
5	7	34	38
5	8	168	-176
5	9	133	-137
5	10	364	-371
5	11	136	-138
5	12	189	-197
7	0	298	308
7	1	365	358
7	2	159	151
7	3	477	468
7	4	392	389
7	5	228	208
7	6	366	362
7	7	339	338
7	8	133	134
7	10	95	96
7	11	274	288
9	0	388	374
9	1	388	-388
9	2	428	406
9	3	52	43
9	4	516	508
9	5	161	-151
9	6	295	291
9	7	197	-186
9	8	375	376
9	9	375	-377
9	10	289	294
11	0	201	-196
11	1	4	1
11	2	364	-354
11	3	79	74
11	4	585	-587
11	5	26	-21
11	6	397	-393
11	7	68	49
11	8	358	-365
13	0	316	314
13	1	95	43
13	2	448	428
13	3	188	183
13	4	338	322
13	5	68	61

M = 4

K	L	FO	FC
0	0	428	445
0	2	46	-51
0	4	561	545
0	6	189	114
0	8	139	146
0	10	172	175
0	12	252	251
2	0	98	119
2	1	1146	1184
2	2	328	-384
2	3	593	627
2	4	276	277
2	5	558	565
2	6	54	36
2	7	702	723
2	8	218	211
2	9	383	384
2	10	52	-58
2	11	396	393
2	12	98	91
4	0	345	344
4	1	1249	-1245
4	2	386	392
4	3	383	-396
4	4	159	143
4	5	724	-725
4	6	109	-112
4	7	743	-733
4	8	211	203
4	9	447	-468
4	10	93	-98
4	11	458	-464
4	12	24	11
6	0	427	417
6	1	478	496
6	2	39	-38
6	3	555	563
6	4	253	251
6	5	298	289
6	6	113	128
6	7	435	437
6	8	121	115
6	9	188	187
6	10	171	172
6	11	332	342
8	0	309	317
8	1	95	92
8	2	135	138
8	3	161	158
8	4	51	49
8	5	79	84
8	6	75	-78
8	7	201	191
8	8	27	-24
8	9	92	89
8	10	106	-99
10	0	92	-98
10	1	576	-558
10	2	78	74
10	3	611	-586
10	4	53	44
10	5	607	-594
10	6	137	148
10	7	292	-298
10	8	189	192
12	0	6	8
12	1	461	422
12	2	16	18
12	3	652	642
12	4	125	117
12	5	515	496
12	6	118	109
12	8	49	44
14	1	186	-173

M = 5

K	L	FO	FC
1	0	769	778
1	1	325	327
1	2	424	432
1	3	454	448
1	4	497	508
1	5	279	298
1	6	386	392
1	7	288	285
1	8	491	488
1	9	14	-3
1	10	105	111
1	11	32	36
3	0	397	-413
3	1	126	-138
3	2	856	-868
3	3	52	-58
3	4	329	-348
3	5	263	-278
3	6	738	-737
3	7	95	-101
3	8	449	-463
3	9	68	-71
3	10	388	-382
3	11	28	4
5	0	627	638
5	1	228	-288
5	2	748	756
5	3	134	-118
5	4	614	626
5	5	19	-12
5	6	548	546
5	7	27	22
5	8	643	637
5	9	122	-128
5	10	429	446
7	0	73	65
7	1	78	78
7	2	228	-220
7	3	317	316
7	4	68	62
7	5	111	98
7	6	82	-72
7	7	185	196
7	8	29	-32
7	9	83	79
7	10	39	-23
9	0	292	-293
9	1	149	-145
9	2	254	-241
9	3	13	-4
9	4	259	-265
9	5	126	-123
9	6	168	-167
9	7	41	37
9	8	164	-166
11	0	576	575
11	1	17	9
11	2	701	655
11	3	77	78
11	4	631	598
11	5	49	-42
11	6	366	385
13	0	231	-233
13	1	95	86
13	2	279	-271
13	3	116	119

M = 6

K	L	FO	FC
0	0	1288	1214
0	2	885	823
0	4	496	491
0	6	858	839
0	8	423	434
0	10	132	133
2	0	393	-415
2	1	592	-588
2	2	435	-493
2	3	423	-422
2	4	87	-89
2	5	497	-503
2	6	296	-291
2	7	345	-339
2	8	68	-68
2	9	121	-129
2	10	18	-17
4	0	219	233
4	1	534	537
4	3	557	568
4	4	234	231
4	5	429	419
4	6	66	67
4	7	689	651
4	8	43	32
4	9	326	328
4	10	53	-52
6	0	453	481
6	1	292	-298
6	2	432	420
6	3	384	-388
6	4	441	435
6	6	211	-212
6	6	364	371
6	7	254	-244
6	8	377	382
6	9	238	-258
8	0	268	-265
8	1	72	-73
8	2	263	-254
8	3	154	159
8	4	282	-281
8	5	190	-189
8	6	245	-246
8	7	14	-17
8	8	288	-289
10	0	265	265
10	1	253	245
10	2	148	129
10	3	339	348
10	4	218	209
10	5	309	299
10	6	161	168
12	0	135	124
12	1	304	-291
12	2	145	158
12	3	237	-238

M = 7

K	L	FO	FC
1	0	44	-45
1	1	648	-651
1	2	248	-257
1	3	408	-395
1	4	118	107
1	5	278	-266
1	6	39	-24
1	7	416	-423
1	8	53	49
1	9	388	-373
3	0	455	451
3	1	175	178
3	2	411	414
3	3	282	293
3	4	328	334
3	5	145	148
3	6	248	239
3	7	117	115
3	8	326	316
3	9	29	32
3	0	132	132
5	1	278	266
5	2	275	-265
5	3	432	425
5	4	95	-101
5	5	207	214
5	6	211	-205
5	7	235	243
5	8	102	-102
5	9	162	166
7	0	47	42
7	1	506	-514
7	2	237	239

K	L	FO	FC
7	3	534	-545
7	4	108	106
7	5	477	-486
7	6	58	-35
7	7	282	-285
9	0	169	166
9	1	282	269
9	2	120	117
9	3	407	415
9	4	180	181
9	5	325	323
9	6	195	206
11	0	79	-74
11	1	40	-36
11	2	108	-105
11	3	32	-28

H = 8

K	L	FO	FC
0	0	362	-361
0	2	439	-443
0	4	347	-389
0	6	562	-556
0	8	451	-473
2	0	554	546
2	1	40	-37
2	2	402	401
2	3	71	-71
2	4	410	415
2	5	43	-37
2	6	300	310
2	7	51	52
2	8	404	436
4	0	210	204
4	1	72	67
4	2	57	58
4	3	61	-59
4	4	114	113
4	5	47	-41
4	6	109	108
4	7	16	-14
4	8	113	113
6	0	483	-487
6	1	111	-114
6	2	460	-455
6	3	150	146
6	4	267	-278
6	5	61	-62
6	6	289	-291
6	7	77	83
8	0	551	575
8	1	45	40
8	2	477	471
8	3	39	36
8	4	500	533
8	5	126	118
10	0	144	-151
10	1	10	-15
10	2	143	-135

H = 9

K	L	FO	FC
1	0	10	-19
1	1	436	438
1	2	147	-142
1	3	511	529
1	4	12	4
1	5	383	384
1	6	21	-31
1	7	395	412
3	0	331	332
3	1	172	-169
3	2	235	234
3	3	172	-167
3	4	254	251
3	5	123	-131
3	6	86	92
5	0	160	-155
5	1	245	-236
5	2	77	-71
5	3	140	-125
5	4	23	-22
5	5	177	-169
7	0	244	233
7	1	369	371
7	2	53	54
7	3	403	415
7	4	59	49
9	0	74	69
9	1	224	-237

H = 10

K	L	FO	FC
0	0	484	469
0	2	362	340
0	4	389	400
2	0	163	-167
2	1	330	319
2	2	226	-230
2	3	219	218
2	4	155	-166
4	0	20	22
4	1	376	-380
4	2	6	3
4	3	154	-157
4	4	43	43
6	0	299	303
6	1	187	175
6	2	204	208

H = 11

K	L	FO	FC
1	0	198	199
1	1	129	-126
3	0	235	-237